

DIG FILE COPY

REPORT DOCUMENTATION PAGE

Form Approved  
OMB No. 0704-0188

Public reporting burden for this collection of information is estimated to average 1 hour per response, including the time for reviewing instructions, searching existing data sources, gathering and maintaining the data needed, and completing and reviewing the collection of information. Send comments regarding this burden estimate or any other aspect of this collection of information, including suggestions for reducing this burden to Washington Headquarters Services, Directorate for Information Operations and Reports, 1215 Jefferson Davis Highway, Suite 1204, Arlington, VA 22202-4302, and to the Office of Management and Budget, Paperwork Reduction Project (0704-0188), Washington, DC 20503.

1. AGENCY USE ONLY (Leave blank) 2. REPORT DATE August 1990 3. REPORT TYPE AND DATES COVERED Thesis/Dissertation

4. TITLE AND SUBTITLE EQCM Mmeasurements: Redox-Induced Changes in Solvent and ION Content in Anchored Redox Monolayers of Organosulfur Compounds and their Electrocatalysis on Gold Electrodes  
6. AUTHOR(S) Hugh C. De Long

5. FUNDING NUMBERS

7. PERFORMING ORGANIZATION NAME(S) AND ADDRESS(ES) AFIT Student at: University of Wyoming

8. PERFORMING ORGANIZATION REPORT NUMBER AFIT/CI/CIA -90-019D

9. SPONSORING/MONITORING AGENCY NAME(S) AND ADDRESS(ES) AFIT/CI Wright-Ptatterson AFB OH 45433

10. SPONSORING/MONITORING AGENCY REPORT NUMBER

11. SUPPLEMENTARY NOTES

12a. DISTRIBUTION/AVAILABILITY STATEMENT Approved for Public Release IAW AFR 190-1 Distribution Unlimited ERNEST A. HAYGOOD, 1st Lt, USAF Executive Officer, Civilian Institution Programs

12b. DISTRIBUTION CODE

13. ABSTRACT (Maximum 200 words)

DTIC ELECTE AUGO 1 1990 S B D

14. SUBJECT TERMS

15. NUMBER OF PAGES 161  
16. PRICE CODE

17. SECURITY CLASSIFICATION OF REPORT UNCLASSIFIED

18. SECURITY CLASSIFICATION OF THIS PAGE

19. SECURITY CLASSIFICATION OF ABSTRACT

20. LIMITATION OF ABSTRACT

AD-A224 679

EQCM MEASUREMENTS: REDOX-INDUCED CHANGES IN SOLVENT AND ION  
CONTENT IN ANCHORED REDOX MONOLAYERS OF ORGANOSULFUR  
COMPOUNDS AND THEIR ELECTROCATALYSIS ON GOLD ELECTRODES.

by  
HUGH C. DE LONG, Captain, USAF

A dissertation  
submitted to  
The Department of Chemistry and  
The Graduate School of the University of Wyoming  
in partial Fulfillment of Requirements  
for the Degree of

DOCTOR OF PHILOSOPHY  
in  
CHEMISTRY

Laramie, Wyoming  
August, 1990  
161 pages

De Long, Hugh C. EQCM Measurements: Redox-Induced Changes in Solvent and Ion Content in Anchored Redox Monolayers of Organosulfur Compounds and their Electrocatalysis on Gold Electrodes, Ph.D., Department of Chemistry, August, 1990.

↓  
This project involved the use of the Electrochemical Quartz Crystal Microbalance (EQCM) to detect redox-induced changes in ion and solvent content in disulfide and thiol anchored monolayers. The EQCM will also be used to detect the monolayers' electrocatalytic effects on various organometallic cations. The EQCM simultaneously measures the current response to changes in potential with the corresponding frequency response induced by those changes. Use is made of organosulfur compounds as precursors for attachment of organometallic and organic redox couples. Several organometallic disulfides (e.g. cobalticinium and ferrocene derivatives) and organic amphiphilic thiols (e.g. viologen derivatives) have been synthesized and chemisorbed onto gold EQCMs. The viologen derivatives are inverse bilayer in structure where the charged part is in the middle and the alkane chains are extended on either side of the monolayer. All these self-assembling monolayers are strongly bound and very robust. When the redox couple for the

adsorbed molecule involves changes in the charge of the group (e.g. as is the case for adsorbed viologens), then changes in the ion and solvent content of the adsorbate monolayer may occur making the viologen derivatives good models for monitoring transport across a bilayer. Trends in the extent of these changes in content along with structural features of the adsorbates and how these structural changes effect electrocatalysis will be investigated.

Accession For	
NTIS GRA&I	<input checked="" type="checkbox"/>
DTIC TAB	<input type="checkbox"/>
Unannounced	<input type="checkbox"/>
Justification	
By _____	
Distribution/	
Availability Codes	
Dist	Avail and/or Special
A-1	



EQCM MEASUREMENTS: REDOX-INDUCED CHANGES IN SOLVENT AND ION  
CONTENT IN ANCHORED REDOX MONOLAYERS OF ORGANOSULFUR  
COMPOUNDS AND THEIR ELECTROCATALYSIS ON GOLD ELECTRODES.

by  
Hugh C. De Long

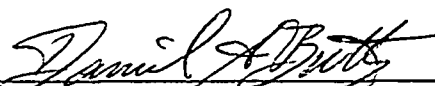
A dissertation  
submitted to  
The Department of Chemistry and  
The Graduate School of the University of Wyoming  
in partial Fulfillment of Requirements  
for the Degree of

DOCTOR OF PHILOSOPHY  
in  
CHEMISTRY

Laramie, Wyoming  
August, 1990

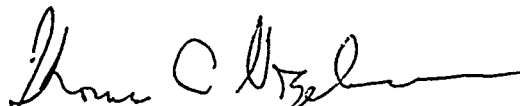
TO THE OFFICE OF THE GRADUATE SCHOOL:

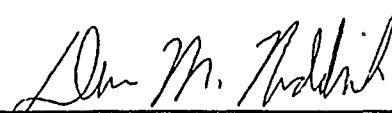
The members of the committee approve the dissertation  
of Hugh C. De Long presented on June 25, 1990.

  
\_\_\_\_\_  
Dr. Daniel A. Buttry, Chairman

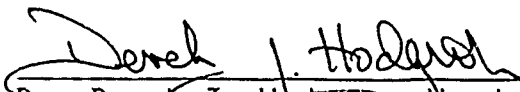
  
\_\_\_\_\_  
Dr. Vernon S. Archer

  
\_\_\_\_\_  
Dr. Keith T. Carron

  
\_\_\_\_\_  
Dr. Thomas C. Vogelmann

  
\_\_\_\_\_  
Dr. Dean M. Roddick

APPROVED:

  
\_\_\_\_\_  
Dr. Derek J. Hodgson, Head, Department of Chemistry

  
\_\_\_\_\_  
Dr. Thomas G. Dunn, Dean of Graduate Studies and Research

To my wife, Beth, and family.

## Acknowledgements

The author would like to thank the following people for their help and guidance in making this work a success:

Dr. Daniel A. Buttry, who was this author's advisor and research director, is thanked for the guidance he provided in all phases of this work.

Dr. Ricardo E. Borjas was helpful in many aspects concerning the electrochemistry performed in this research effort.

Dr. Bruce A. Barner, Dr. Dean M. Roddick and Dr. John J. Donohue are thanked for the help they provided in the synthetic aspects of this work.

We are grateful for the generous support of this work by a grant from the Office of Naval Research and support of the Air Force Institute of Technology Civilian Institute Program, Wright-Patterson AFB, OH.

## TABLE OF CONTENTS

CHAPTER	PAGE
I.	INTRODUCTION.....1
II.	ELECTROCHEMICAL AND QUARTZ CRYSTAL MICROBALANCE: Theory and Instrumentation.....6
	Introduction.....6
	Experimentation.....12
III.	ELECTROCHEMICAL AND QUARTZ CRYSTAL MICROBALANCE STUDIES OF FERROCENE AND COBALTICINIUM DERIVATIVES: ION AND SOLVENT TRANSPORT PROPERTIES.....15
	Introduction.....15
	Experimentation.....19
	Results and Discussion.....23
	Conclusions.....42
IV.	ELECTROCHEMICAL AND QUARTZ CRYSTAL MICROBALANCE STUDIES OF VIOLOGEN DERIVATIVES: ION AND SOLVENT TRANSPORT PROPERTIES.....44
	Introduction.....44
	Experimentation.....46
	Results and Discussion.....52
	Conclusions.....110
V.	ELECTROCHEMICAL AND QUARTZ CRYSTAL MICROBALANCE STUDIES OF VIOLOGEN DERIVATIVES: ELECTRON-MEDIATED EVENTS.....114
	Introduction.....114
	Experimentation.....118
	Results and Discussion.....119
	Conclusions.....135

REFERENCES.....137

LIST OF TABLES

	PAGE
Table 3.1	Demonstration of changes in mass sensed by the crystal from changes in the surface coverage of Ferrocenamide phenyl disulfide in .1M NaCl supporting electrolyte.....29
Table 4.1	Effects of varing surface coverage of the monolayer in 0.1M NaCl.....62
Table 4.2	Effects of varying temperature on the monolayer in 0.1M NaClO <sub>4</sub> and in relation to the E <sub>f<sub>whh</sub></sub> of the current peak .....69
Table 4.3	Effects of differing the anion used as the supporting electrolyte with C10VC10SH.....72
Table 4.4	Anion effects on various viologen monolayers in 0.1M NaCl and 0.1M NaClO <sub>4</sub> changing anions on all viologen derivatives synthesized.....111

## LIST OF FIGURES

	PAGE
Figure 2.1	a) Piezoelectric effect caused by applied pressure producing a polarization b) Converse piezoelectric effect (structural deformation) caused by applying a potential across the crystal.....7
Figure 2.2	Example of the fundamental thickness shear mode.....9
Figure 2.3	EQCM setup for data collection.....13
Figure 2.4	Examples of the AT cut crystals used by this laboratory. Shown are various views of a crystal.....14
Figure 3.1	I= Ferrocenamide phenyl disulfide, II=Ferrocene ester phenyl disulfide, III=Cobalticinamide phenyl disulfide.....20
Figure 3.2	Ferrocenamide phenyl disulfide in 1M HClO <sub>4</sub> with a scan rate of 100mV per second versus SSCE.....24
Figure 3.3	Ferrocene ester phenyl disulfide in 1M HClO <sub>4</sub> with a scan rate of 100mV per second versus SSCE.....26
Figure 3.4	Graphic explanation of results depicted in Table 3.1. Shown is Ferrocenamide phenyl disulfide bound to the surface in varying

	coverages.....	30
Figure 3.5	Voltammograms of Ferrocenamide phenyl disulfide and Ferrocene ester phenyl disulfide from two different coatings are superimposed on each other. Both were done in 1M HClO <sub>4</sub> versus SSCE.....	32
Figure 3.6	Voltammogram of Ferrocenamide phenyl disulfide in: A) 1M HClO <sub>4</sub> , B) 1M HNO <sub>3</sub> , and C) 1M H <sub>2</sub> SO <sub>4</sub> versus SSCE.....	34
Figure 3.7	Study of hydrolysis of the ester bond. Voltammograms of Ferrocene ester phenyl disulfide in 0.1M HClO <sub>4</sub> versus SSCE.....	37
Figure 3.8	Voltammogram of Cobalticinamide phenyl disulfide in 0.1M NaClO <sub>4</sub> /Acetonitrile versus silver as a pseudo reference electrode.....	40
Figure 4.1	I=N-(n-Decyl)-N'-(10-Mercaptodecyl)-4,4'-Bipyridinium (C10VC10SH) II=N-(n-Octadecyl)-N'-(10-Mercaptodecyl)-4,4'-Bipyridinium (C18VC10SH) III=N-(10-Heneicosyl)-N'-(10-Mercaptodecyl)-4,4'-Bipyridinium (C9C11VC10SH) IV=N-(n-Decyl)-N'-(16-Mercaptohexadecyl)-4,4'-Bipyridinium (C10VC16SH) V=N-(n-Decyl)-N'-(3-Mercaptopropyl)-4,4'-Bipyridinium (C10VC3SH) VI=N-methyl-N'-(12-Mercaptododecyl)-4,4'-Bipyridinium (C1VC12SH).....	47
Figure 4.2	Voltammogram of N-(n-Decyl)-N'-(10-Mercaptodecyl)-4,4'-Bipyridinium Dichloride (C10VC10SH) in 0.1M NaF with a scan rate of 100mV/sec versus SSCE.....	53
Figure 4.3	Graphic depiction of solvent-separated ion pair of C10VC01SH in NaF supporting electrolyte.....	55
Figure 4.4	Voltammogram of N-(n-Decyl)-N'-(10-Mercapto-	

	decyl)-4,4'-Bipyridinium Dichloride (C10VC10SH) in 0.1M NaCl with a scan rate of 100mV/sec versus SSCE.....	57
Figure 4.5	Graphic depiction of intercalation of second layer into the monolayer to form a stable bilayer.....	63
Figure 4.6	Voltammogram of N-(n-Decyl)-N'-(10-Mercapto- decyl)-4,4'-Bipyridinium Dichloride (C10VC10SH) in 0.1M NaClO <sub>4</sub> with a scan rate of 100mV/sec versus SSCE.....	65
Figure 4.7	Graphic depiction of contact ion pair of C10VC10SH in NaClO <sub>4</sub> supporting electrolyte..	68
Figure 4.8	Voltammogram of N-(n-Decyl)-N'-(10-Mercapto- decyl)-4,4'-Bipyridinium Dichloride (C10VC10SH) in all the 0.1M supporting electrolytes with a scan rate of 100mV/sec versus SSCE.....	74
Figure 4.9	Voltammogram of N-(n-Decyl)-N'-(10-Mercapto- decyl)-4,4'-Bipyridinium Dichloride (C10VC10SH) in 0.1M NaClO <sub>4</sub> or 0.1M TEAPF <sub>6</sub> in acetonitrile with a scan rate of 100mV/sec versus SSCE.....	77
Figure 4.10	Voltammogram of N-(n-Octadecyl)-N'- (10-Mercaptodecyl)-4,4'-Bipyridinium Dichloride (C18VC10SH) in 0.1M NaCl with a scan rate of 100mV/sec versus SSCE.....	80
Figure 4.11	Voltammogram of N-(n-Octadecyl)-N'- (10-Mercaptodecyl)-4,4'-Bipyridinium Dichloride (C18VC10SH) in 0.1M NaClO <sub>4</sub> with a scan rate of 100mV/sec versus SSCE.....	83
Figure 4.12	Voltammogram of N-(10-Heneicosyl)-N'- (10-Mercaptodecyl)-4,4'-Bipyridinium Dichloride (C9C11VC10SH) in 0.1M NaCl with a scan rate of 100mV/sec versus SSCE.....	87

Figure 4.13	Voltammogram of N-(10-Heneicosyl)-N'-(10-Mercaptododecyl)-4,4'-Bipyridinium Dichloride (C9C11VC10SH) in 0.1M NaClO <sub>4</sub> with a scan rate of 100mV/sec versus SSCE.....	90
Figure 4.14	Voltammogram of N-(n-Decyl)-N'-(3-Mercaptopropyl)-4,4'-Bipyridinium Dichloride (C10VC3SH) in 0.1M NaCl with a scan rate of 100mV/sec versus SSCE.....	93
Figure 4.15	Voltammogram of N-(n-Decyl)-N'-(3-Mercaptopropyl)-4,4'-Bipyridinium Dichloride (C10VC3SH) in 0.1M NaClO <sub>4</sub> with a scan rate of 100mV/sec versus SSCE.....	96
Figure 4.16	Voltammogram of N-Methyl-N'-(12-Mercaptododecyl)-4,4'-Bipyridinium Dichloride (C1VC12SH) in 0.1M NaCl with a scan rate of 100mV/sec versus SSCE.....	99
Figure 4.17	Voltammogram of N-Methyl-N'-(12-Mercaptododecyl)-4,4'-Bipyridinium Dichloride (C1VC12SH) in 0.1M NaClO <sub>4</sub> with a scan rate of 100mV/sec versus SSCE.....	102
Figure 4.18	Voltammogram of N-(10-Henicosyl)-N'-(10-Mercaptododecyl)-4,4'-Bipyridinium Dichloride (C9C11VC10SH) in a) 0.1M NaCl and in b) 0.1M NaI with a scan rate of 100mV/sec versus SSCE.....	105
Figure 4.19	Voltammogram of N-(10-Henicosyl)-N'-(10-Mercaptododecyl)-4,4'-Bipyridinium Dichloride (C9C11VC10SH) in .1M NaCl with 0.1mM tetrakis(p-sulfonatophenyl)porphrin with a scan rate of 100mV/sec versus SSCE.....	107
Figure 5.1	Voltammogram of C10VC10SH in 0.1M NaCl with 0.5mM Ru(NH <sub>3</sub> ) <sub>6</sub> Cl <sub>3</sub> ; scan rate is 100mV/sec versus SSCE.....	121

Figure 5.2	Voltammogram of C9C11VC10SH in 0.1M NaCl with 0.75mM Ru(NH <sub>3</sub> ) <sub>6</sub> Cl <sub>3</sub> ; scan rate is 100mV/sec versus SSCE.....	122
Figure 5.3	Voltammogram of C1VC12SH in 0.1M NaCl with 1.0mM Ru(NH <sub>3</sub> ) <sub>6</sub> Cl <sub>3</sub> ; scan rate is 100mV/sec versus SSCE.....	124
Figure 5.4	Voltammogram of C10VC10SH in 0.1M NaCl with 0.5mM Co(NH <sub>3</sub> ) <sub>6</sub> Cl <sub>3</sub> ; scan rate is 100mV/sec versus SSCE.....	126
Figure 5.5	Voltammogram of C9C11VC10SH in 0.1M NaCl with 0.75mM Co(NH <sub>3</sub> ) <sub>6</sub> Cl <sub>3</sub> ; scan rate is 100mV/sec versus SSCE.....	127
Figure 5.6	Voltammogram of C1VC12SH in 0.1M NaCl with 1.0mM Co(NH <sub>3</sub> ) <sub>6</sub> Cl <sub>3</sub> ; scan rate is 100mV/sec versus SSCE.....	129
Figure 5.7	Voltammogram of C10VC10SH in 0.1M NaCl with 0.5mM CoSepCl <sub>3</sub> ; scan rate is 100mV/sec versus SSCE.....	130
Figure 5.8	Voltammogram of C9C11VC10SH in 0.1M NaClO <sub>4</sub> with 0.75mM CoSepCl <sub>3</sub> ; scan rate is 100mV/sec versus SSCE.....	132
Figure 5.9	Voltammogram of C10VC10SH in 0.1M NaCl with added dimethylaminomethylferrocene; scan rate is 100mV/sec versus SSCE.....	134

## CHAPTER I

### Introduction

There is considerable interest in modifying electrode surfaces at the monolayer level for their use in detailed studies of either structure, function, or both, at the solid-liquid interface. Our interest lies in probing the influence of synthesized, and therefore known, structural changes in monolayers at this interface and their effect on the electrochemical processes which are known to occur there. Two distinct areas which show the most interest are the use of alkyltrichlorosilanes<sup>1</sup> on silicon or glass and the use of organosulfur compounds on gold<sup>2</sup> and silver<sup>3</sup>. The bulk of the work in attaching redox couples to surfaces has been with alkyl n-chlorosilanes<sup>1b,4,15</sup> and alkoxy silanes<sup>5</sup> on metal oxides, especially silicon dioxide. However, our interest lies in the formation of monolayers using alkyl sulfur compounds on the Electrochemical and Quartz Crystal Microbalance (EQCM) gold electrode.

There are two common means of forming a monolayer: The Langmuir-Blodgett technique and the self-assembling mechanism. Comparison of both techniques shows that the

Langmuir-Blodgett films<sup>6</sup> have several drawbacks; to mention some: they are weakly bound to the surface, can only use compounds that form a Langmuir-Blodgett film on water, are limited to planar surfaces, and they can undergo structural transformation during the transfer process, where the latter disadvantage brings about irreproducible formation of films. On the other hand, films prepared by the self-assembling mechanism<sup>1b,2,7,8</sup> have the advantage of being either chemically bound or strongly adsorbed (by means of a physical process, i.e., hydrophobicity) to the surface. This mechanism introduces better reproducibility on the film formation, stronger binding to the surface, and it can be formed on any surface, perhaps, with certain limitations for the case of the chemically bound ones since the surface and the adsorbate must react to form the bond.

It is clear from the preceding paragraph that the self assembling technique uses two distinct processes for the formation of the monolayer: chemisorption and physisorption. In the first one, the adsorbate forms a chemical bond, i.e., thiols on gold form a Au-S bond, whereas in the second one, the adsorbate is on the surface due to electrostatic forces or by incompatibility with the solution (hydrophobicity), i.e., surfactants.<sup>9,10</sup>

There are several examples of chemisorption that will be mentioned. Wrighton and coworkers<sup>4,5a,11</sup> affixed a ferrocene to metal/metal oxides by way of chlorosilanes and

alkoxysilanes. Murray and coworkers<sup>12</sup> and, Majda and coworkers<sup>13</sup> affixed dialkylviologens to metal/oxides by way of an alkoxysilane. Wrighton and coworkers<sup>5b-c,14</sup> also affixed dialkylviologens to metal/metal oxides by way of alkoxysilanes but attached both ends instead of just one. Others such as Ghosh and coworkers,<sup>15</sup> Murray and coworkers,<sup>16</sup> and Anson and coworkers<sup>17</sup> affixed pentaamineruthenium chloride through complexation to nitrogens in amines and pyridyls that were attached to the electrode by way of trichlorosilanes on metal oxide or by acid chloride chemistry on carbon electrodes. Donohue<sup>18</sup> initiated studies on viologens similar to Majda's but anchored with thiols to gold to study electron transfer in a monolayer. Weaver and coworkers<sup>19</sup> looked at binding of cobalt compounds to mercury and gold electrodes through attachment with sulfides. Finklea and coworkers<sup>20</sup> looked at coadsorption of viologen surfactants and alkylmercaptans on gold electrodes. Finally, there is the work of Regen and coworkers<sup>21</sup> who chemisorbed phosphatidylcholine molecules ( both thiols and sulfides ) to gold surfaces by way of self assembling monolayers.

Extensive studies have been done with alkyl thiols on gold surfaces to elucidate their binding structure,<sup>2</sup> that is to say, their mode of attachment to the gold surface and their association between each other. Nuzzo, Whitesides, and others<sup>2</sup> exhaustively examined how the sulfur was attached to

the gold and how these monolayers are assembled. They determined that the sulfur, be it a disulfide or a thiol, binds as a thiolate to gold. Also determined was that in order to get the proper association between molecules and proper Au-S bond angle, that the chains of these thiolates had to be tilted  $30^\circ$  from normal to the electrode surface.<sup>38</sup> Use is made of thiols as a head group on gold due to the stability of these thiols and their potential for chemical modification.

A number of laboratories has studied redox attachment to electrodes through different means ( amines on graphite,<sup>17b,22</sup> silanes,<sup>1b,16,23</sup> nitriles on platinum<sup>24</sup>, etc. ) but one of the major drawbacks to these methods is that the surface coverage is not that high. These monolayers depend on the existence of specific binding sites (such as hydroxides or acids, etc.) on the electrode surface (except nitriles, which bind by adsorption through the triple bond). These sites do not allow for the possibility of lateral transport of molecules across the surface, since there are a fixed number formed and binding can only take place at these sites. Therefore, higher packing densities can not be attained. Thiols and disulfides, on the other hand, form high surface coverages which allow for tightly packed monolayers. This may be due to rapid lateral transport<sup>1f,41</sup> on the surface enabling more molecules to get to the surface to bind. Reported herein is a way to take advantage of this

high packing density and affix redox couples to a gold electrode surface.

The EQCM is a valuable tool to use in understanding solvent and anion transport. This is a problem of great importance because knowledge of such transport leads to the understanding of the kinetic factors which affect the electrochemistry of the redox moieties of the monolayer. Use is made of the EQCM for data collection due to its unique ability to simultaneously collect both charge and mass combination of data. As will be discussed in the experimental section, the charge and mass data can be used to get surface coverages and grams per mole mass changes which are sensed by the quartz crystal. This is in addition to the usual electrochemical data obtained from cyclic voltammetry.

## CHAPTER II

# ELECTROCHEMICAL AND QUARTZ CRYSTAL MICROBALANCE: Theory and Instrumentation

### Introduction

To thoroughly comprehend the system used for these experiments, it becomes necessary to understand some of the fundamentals of the Electrochemical Quartz Crystal Microbalance (EQCM) which give rise to the mass detection process, namely, the piezoelectric effect. The piezoelectric effect is defined as the electric polarization caused by applying some sort of pressure to the crystal in use<sup>25,44</sup>. The converse effect can be achieved by applying a voltage across the crystal which causes a deformation of its' structure(see figure 2.1). If this voltage alternates at the proper frequency, one can achieve a vibration which is quite stable under predetermined conditions, i.e., temperature, crystal cut, and the nature of the surrounding medium.

Alpha quartz is used to make the quartz crystals for the microbalance because it is inexpensive and has a relatively high piezoelectric coefficient<sup>26</sup>. Various cuts can be obtained, but AT cut crystals (Valpey-Fisher

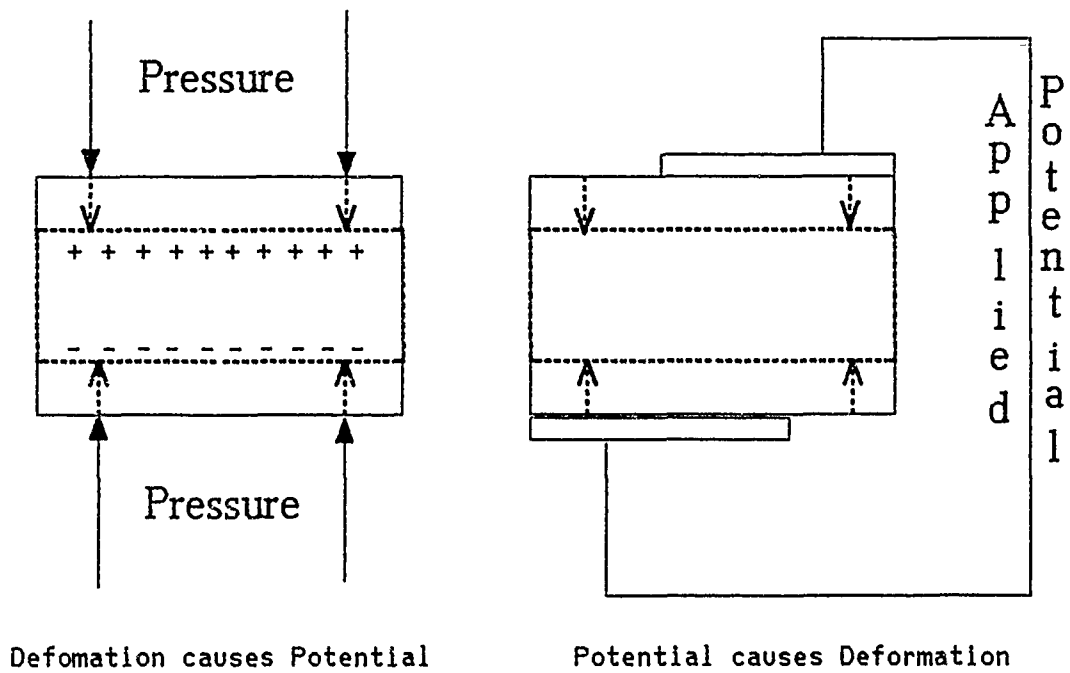


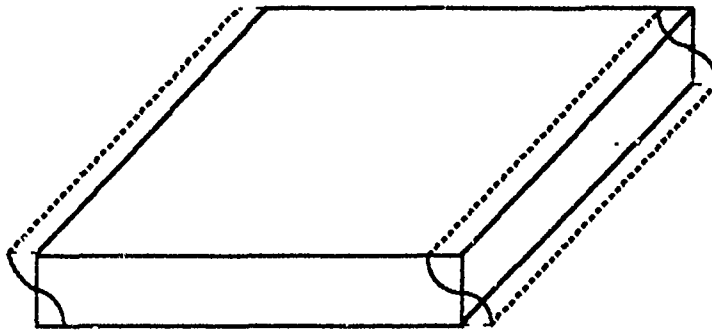
Figure 2.1 A) Piezoelectric effect caused by applied pressure producing a polarization. B) Converse piezoelectric effect (structural deformation) caused by applying a potential across the crystal.

Corporation, Hopkinton, Massachusetts) are used in this laboratory. This is because the AT cut is temperature insensitive around room temperature<sup>27</sup>. The crystal oscillates in the thickness shear mode, as shown in figure 2.2. Since the AT cut crystals vibrate in the thickness shear mode, the thickness of the crystal determines the resonance frequency. The thicker the crystal is, the lower the resonance frequency and vice versa. This means that a 10MHz crystal operated at the fundamental mode is thinner than a 5MHz crystal in the fundamental mode.

The quartz crystals are used to detect mass changes at the surface of the crystal. This is possible because as the mass is increased or decreased on the crystal a change in the resonance frequency of that crystal occurs. The data obtained are the changes in the frequency, or  $\Delta f$ , experienced by the crystal over the time of the experiment. To utilize these frequency data to obtain useful information, they must be related to mass changes. This is done through the use of the Sauerbrey equation<sup>28</sup>.

$$\Delta f = \frac{-2 \Delta m n f_o^2}{A \sqrt{\mu_q \rho_q}} = - C_f \frac{\Delta m}{A}$$

The change in the resonance frequency is equal to minus the



Fundamental Thickness-Shear Mode

Figure 2.2 Example of the fundamental thickness shear mode.

change in mass at the crystal surface per unit area (or areal mass change) times a constant,  $C_f$ . The constant is the overtone number ( $n$ ), times the frequency of the fundamental mode of the QCM ( $f_0$ ) squared, divided by the density of the quartz ( $\rho_q = 2.648 \text{ g cm}^{-3}$ )<sup>27</sup> and the shear modulus of the quartz ( $\mu_q = 2.947 \times 10^{11} \text{ g cm}^{-1} \text{ s}^{-2}$ )<sup>27</sup>. Therefore, the change in frequency is inversely proportional to the mass gained or lost. This gives a mass sensitivity of  $56.6 \text{ Hz cm}^2 \mu\text{g}^{-1}$  for the 5MHz crystals used in our laboratories.

Notice in the above equation that properties of the deposited layer are not taken into account. This is because they are unimportant as long as the deposit is thin enough so there is a less than 2% change in the resonance frequency from the addition of the film on the electrode surface. This is the thin film limit<sup>45</sup>, and the above equation is only valid within this limit. This is because the film does not experience shear deformation so all of the mass is present at the antinode of the standing wave. This is not true when the above limit is exceeded. If this happens then the properties of the film are important. They must be taken into consideration, and a different treatment is used<sup>46</sup>.

Another problem is viscous damping of the shear wave within the film. This damping is from the attenuation of the shear wave within a viscous material<sup>47</sup>. The more viscous a material is, then the more damping is experienced by the shear wave. This damping typically causes large changes in

frequency. The Sauerbrey equation is only valid for rigid layers where viscosity is zero (totally elastic). This is the rigid layer approximation<sup>47,48</sup>. Monolayers act as rigid layers which are totally elastic and therefore the rigid layer approximation holds<sup>9,29,31,32</sup>.

Extensive work has been done on using the quartz crystal microbalance as a modified electrode<sup>9,29-32</sup> to study surface processes in a controlled fashion. This enables one to monitor, simultaneously, the mass changes which occur during the electrochemical event. The data are in the form of a voltammogram and a frequency versus potential plot. By combining these two data formats, a wealth of information about transport processes can be obtained.

### Experimental

The experimental setup is shown in figure 2.3. This consists of a standard H-cell where the quartz crystal is held in place with clamped o-rings and used as a working electrode. The crystal oscillation is driven by the oscillation board and monitored with a Philips 6654 frequency counter. A BAS CV27 potentiostat was used as a true analogue ramp generator. An IBM PC with a Data Translation DT2801-A board and the Asyst programming environment were used for the control and collection of data. All potentials are reported with respect to a sodium chloride saturated calomel reference electrode (SSCE).

The EQCM working electrode is an AT cut 5MHz quartz crystal about one inch in diameter which has had 50Å of chromium followed by 2000Å of gold vapor deposited using a mask (see figure 2.4). A keyhole pattern mask is used to allow vapor deposition only on a specific area on both sides of the crystal. The mass active area only includes the gold pad which is 0.28cm<sup>2</sup>, whereas the electrochemically active area, 0.34cm<sup>2</sup>, includes the flag area within the o-ring. Silver paint is applied to the exposed flags for better contact with the clips from the oscillator circuit.

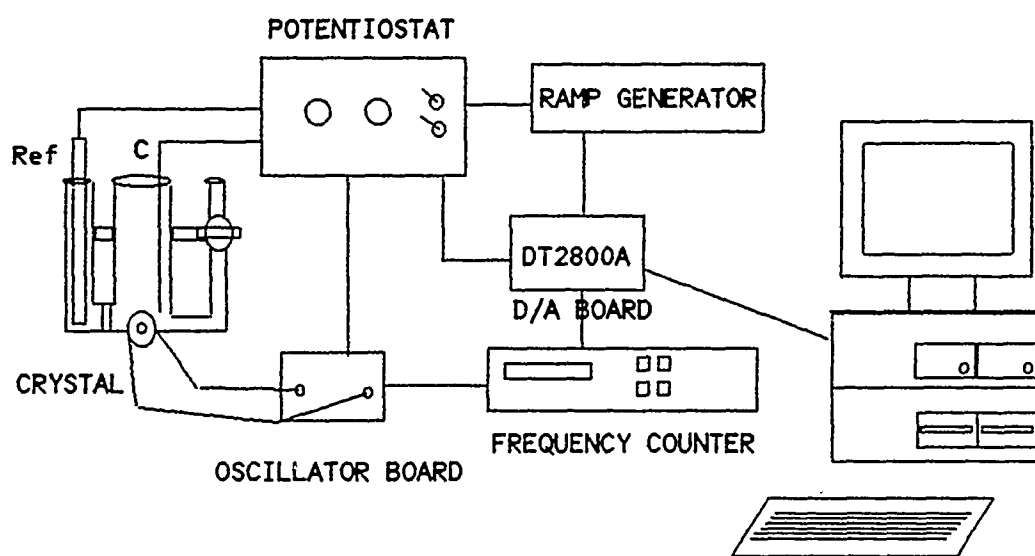


Figure 2.3 EQCM setup for data collection

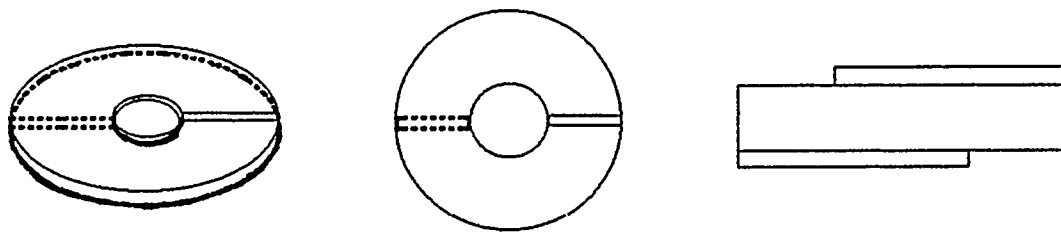


Figure 2.4 Examples of the AT cut crystals used by this laboratory. Shown are various views of a crystal.

## CHAPTER III

# ELECTROCHEMICAL AND QUARTZ CRYSTAL MICROBALANCE STUDIES OF FERROCENE AND COBALTICINIUM DERIVATIVES: ION AND SOLVENT TRANSPORT PROPERTIES

### Introduction

One of the important areas in electrochemistry and certainly in modified electrodes is the ability to form organized molecular assemblies which can perform some desired function whether it be electrocatalysis, electrosynthesis, passivation of the surface or a simple study of the monolayer's physical and chemical properties. Ferrocene has been used as a redox species for various modified electrodes over a number of years. There generally have been three classes of ferrocene monolayers used where the ferrocene is part of the layer and not a separate molecule. These are a) in physisorbed monolayers and multilayers, b) in chemisorbed monolayers and multilayers, and c) in polymer coatings.

Facci and coworkers<sup>33</sup> used Langmuir-Blodgett films of ferrocenyl surfactants to assemble monolayers on gold and platinum electrodes on the precept that modification of the

electrode surface with L-B films may introduce large scale order to allow for control over structural arrangement of the redox monolayers. Their monolayers were ordered head down on the surface of the electrode. Buttry and coworkers<sup>9b, 18</sup> took a different approach in that they relied on a self-assembly of the ferrocenyl surfactant molecules on the surface, but came up with the same packing density as Facci and coworkers. This was indicative of the lack of need to use Langmuir-Blodgett techniques, since self-assembly was just as effective but simpler to do.

Majda and coworkers<sup>34</sup> used self-assembly techniques to produce their monolayers on microporous aluminum oxide films on gold. The aluminum oxide film would have gold vapor deposited on one side then the surfactant ferrocene molecule would associate with the octadecyltrichlorosilane attached by silanes in the micropores. This allowed for the study of lateral electron transport from the ferrocenyl surfactants close to the surface to ones further up the pore.

In the area of chemisorption, Murray and coworkers<sup>35</sup> and Wrighton and coworkers<sup>36</sup> covalently attached molecules to the electrode surface by way of bond formation. This greatly added to stability of the monolayers and increased the utility of the surfaces. They both used silane chemistry to attach the molecules to the surface. Murray also found that multilayer formation greatly increased the stability of the ferricinium species. The drawback to this technique is

that the surface coverage is dependent not on molecular size but instead on availability of binding sites on the electrode surface.

Finally, polymerization techniques were used to immobilize ferrocene molecules to the surface. Murray and coworkers<sup>37</sup> bound molecules to metal oxide surfaces by silane chemistry. However, there are instances where the silanes can also polymerize to each other while attached to the electrode surface, giving added strength and durability. These systems are excellent for forming monolayers, and exhibit good thermal, chemical and mechanical stability but the high reactivity of  $-\text{SiCl}_3$ 's limits the chemistry of surfaces created when these silanes are attached to silicon.<sup>38</sup>

For the above reasons and because of the organosulfur chemistry mentioned in chapter I, this laboratory became interested in self-assembly of monolayers using thiols or disulfides as an anchor to the electrode surface. The importance of these sulfur linkages lies in their ability to self-assemble onto gold and silver electrodes with high surface coverages and yet remain relatively unreactive to the chemistry occurring at the surface. In this chapter several metallocene disulfides were synthesized for self-assembly of monolayers onto a gold electrode. These are the first examples of redox couples attached to the electrode surface by a disulfide to form a monolayer.

Various supporting electrolytes were examined for anion transport and several solvents were investigated also.

## Experimental

Figure 3.1 shows the structures of the redox molecules synthesized in this work. Compounds I and II are made by adding ferrocene monocarboxylic acid to benzene and adding phosphorous trichloride, in slight excess, to form the acid chloride. The reaction is allowed to reflux continuously for 24 hours. The acid chloride of the ferrocene is isolated by evaporation (rotavaporation) of the benzene and volatile by-products. It is then added in excess to 4-aminophenyldisulfide or 4-hydroxyphenyldisulfide in methylene chloride to ensure that both sides of the disulfide are reacted. The desired product, compound I or II, is collected as a precipitate or oil, respectively.

The structure and purity of compound I were determined by  $^1\text{H}$  NMR: 9.58 s(1), amide proton; 7.79 d(2), 7.52 d(2), phenyl protons; 5.02 d(2), 4.46 d(2), substituted cyclopentadienyl ring; 4.21 m(5), unsubstituted cyclopentadienyl ring; (DMSO- $d_6$ ). The structure and purity of compound II were determined by  $^1\text{H}$  NMR: 7.62 d(2), 7.21 d(2), phenyl protons; 5.01 d(2), 4.56 d(2), substituted cyclopentadienyl ring; 4.35 m(5), unsubstituted cyclopentadienyl ring; ( $\text{CDCl}_3$ - $d_6$ ).

Compound III is made by adding cobalticinium hexafluorophosphate to THF on a vacuum line. The solution is

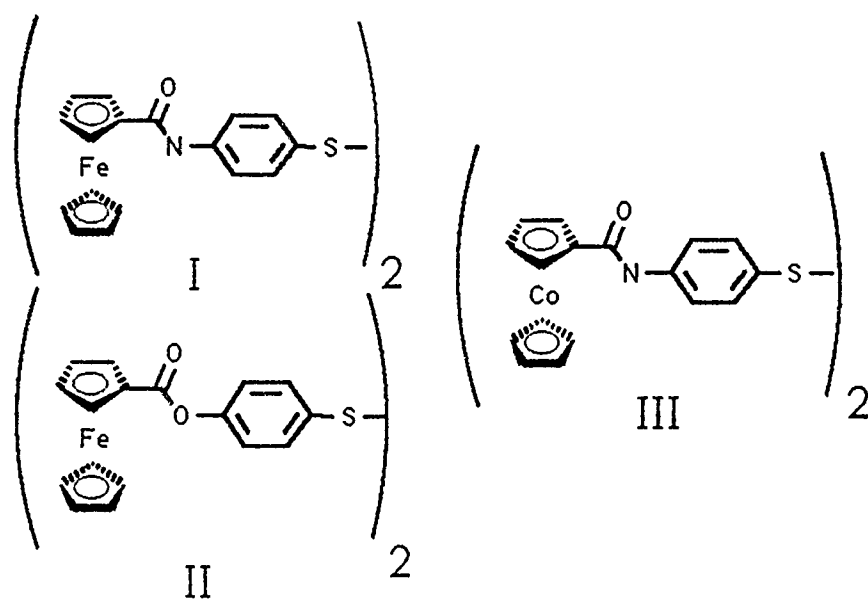


Figure 3.1 I=Ferrocenamide phenyl disulfide, II=Ferrocene ester phenyl disulfide, III=Cobaltcincinamide phenyl disulfide

then cooled to  $-78^{\circ}\text{C}$  and a slight excess of methyllithium is added to monomethylate one ring<sup>39</sup> (stirred six hours). The resulting cobaltocene derivative is dried and put in a glove box. 5-10 fold excess trityl tetrafluoroborate is added as an endo hydride extractor. The mixture is put back on the vacuum line and methylene chloride is added. This is allowed to react for 24 hours. The monomethyl cobaltocene is then dried and exposed to air, which will slowly oxidize it back to the cobalticinium derivative. The cobaltocene derivative is oxidized according to the procedure in Sheats and coworkers<sup>40</sup>. The monocarboxylic acid is isolated. Since the cobalt is in its highest oxidation state, excess thionyl chloride can be used by itself to make the acid chloride. The acid chloride is isolated and compound III is then made the same way as compounds I and II. The structure and purity of compound III were determined by  $^1\text{H}$  NMR: 10.09 s(1), amide proton; 7.84 d(2), 7.58 d(2), phenyl protons; 6.55 d(2), 6.09 d(2), substituted cyclopentadienyl ring; 6.04 m(5), unsubstituted cyclopentadienyl ring; (acetone- $\text{d}_6$ ).

The coating of the crystals to form the monolayer was done as follows. For the ferrocene or cobalticinium derivatives, they were dissolved in acetone. This solution is used to coat the electroactive area (gold pad and flag) of the crystal. The crystal was in contact with the coating solution for one hour. The crystals are then rinsed with

acetone and fitted to the modified electrochemical H-cell for performing EQCM work.

The charge, which is related to the coverage, is calculated by the cut and weigh method. As will be indicated later, this method had to be used because of the capacitive background currents, since they change with the surface coverage. Normally, the collected data, i.e., the cyclic voltammogram, can have its background subtracted and its charge calculated by the appropriate computer algorithms; however, this is only appropriate when the background does not change over the course of the experiment. Once the charge is known, the frequency change is measured and converted into grams of mass sensed per  $\text{cm}^2$ . The charge is converted into a surface coverage of moles per  $\text{cm}^2$ , then it is divided into the grams of mass sensed per  $\text{cm}^2$  to give grams of mass sensed per mole of compound on the surface. This is the grams per mole referred to later in this study.

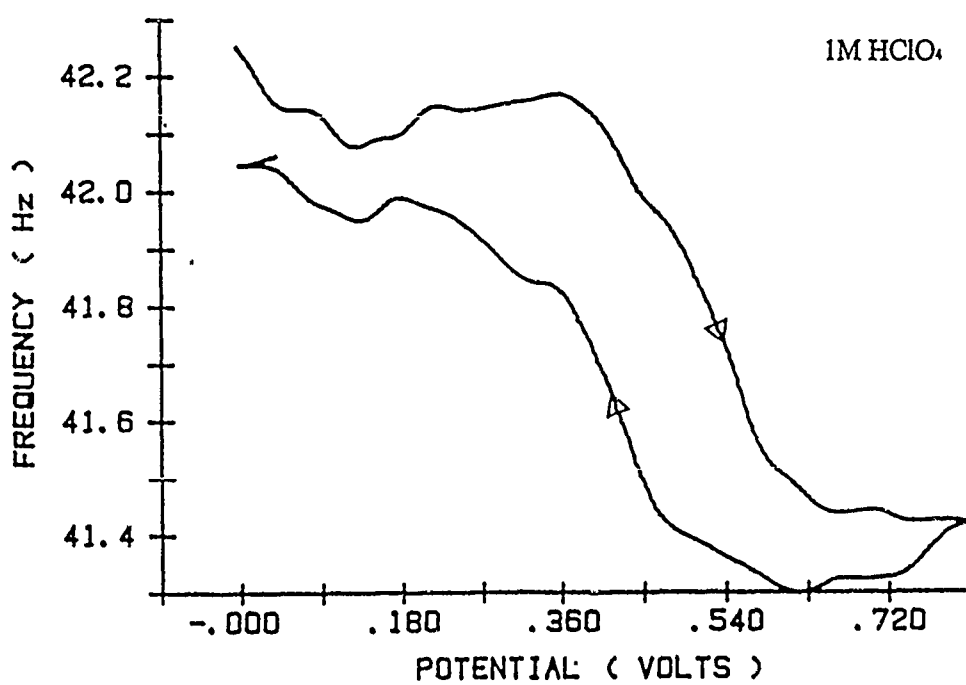
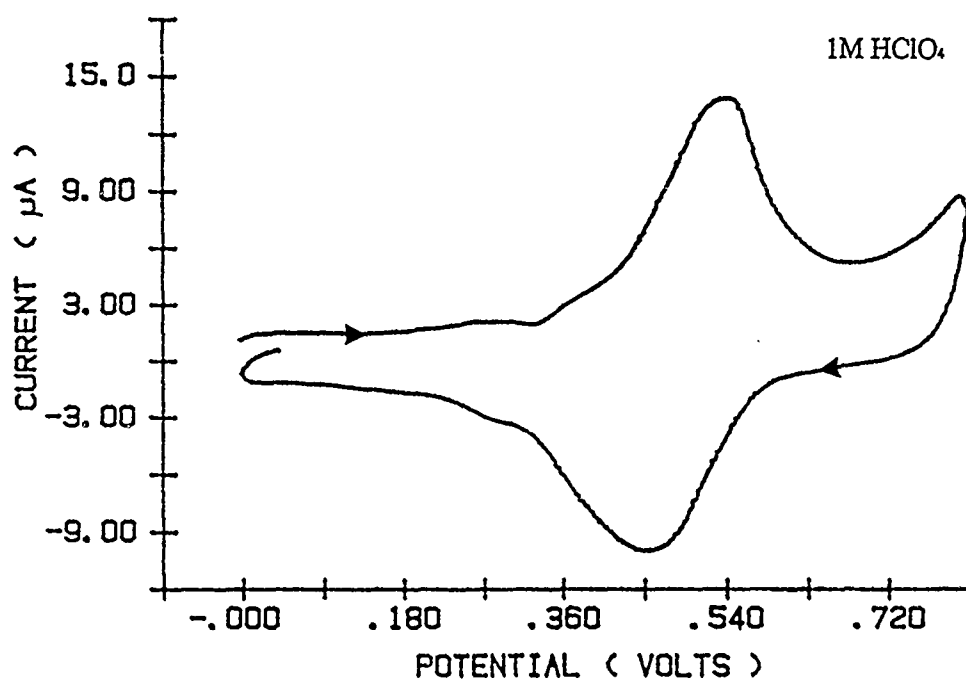
The equipment set up for the collection of data has been previously discussed in the experimental section of chapter II. The electrochemical cell is a modified H-cell where the reference electrode is separated from the working and counter electrodes by a fritted glass junction. The surface roughness of the vapor deposited gold electrodes was calculated, from lead UPD experiments, to be 1.1.

## Results and Discussion

All the disulfide compounds spontaneously assemble by chemisorption on the gold surface to form a very stable and closely packed monolayer. It is thought that lateral transport<sup>1f,41</sup> takes place in these monolayers allowing for higher packing density and hence higher coverages. This allows for increased interaction between molecules attached to the surface. All of this contributes to a more robust system with which to work than previous self assembled electrode systems, i.e., surfactants. Added to this is the advantage of having a probe attached to or in the monolayer. This will enable one to report on the intermolecular interactions and ion and solvent transport in a monolayer. The voltammograms are well behaved (reproducible, no unexpected distortions of the wave), and have the typical surface wave characteristics<sup>43</sup>. Coupled with the frequency data from the EQCM, they supply important information about solvent and ion transport, surface coverage, stability of the monolayer, intermolecular interactions, and electron transfer mechanisms.

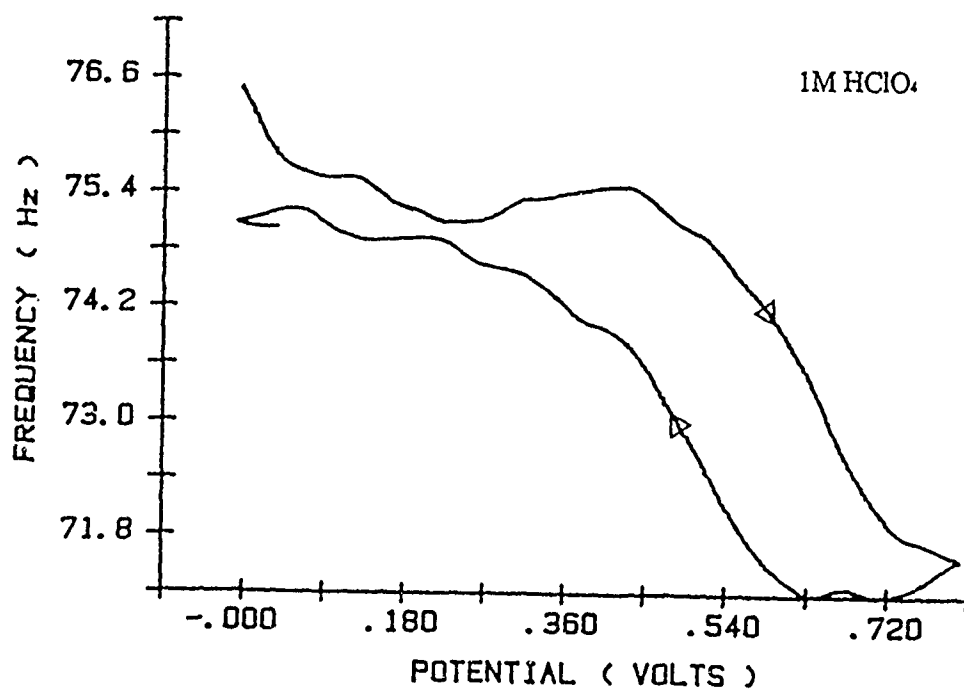
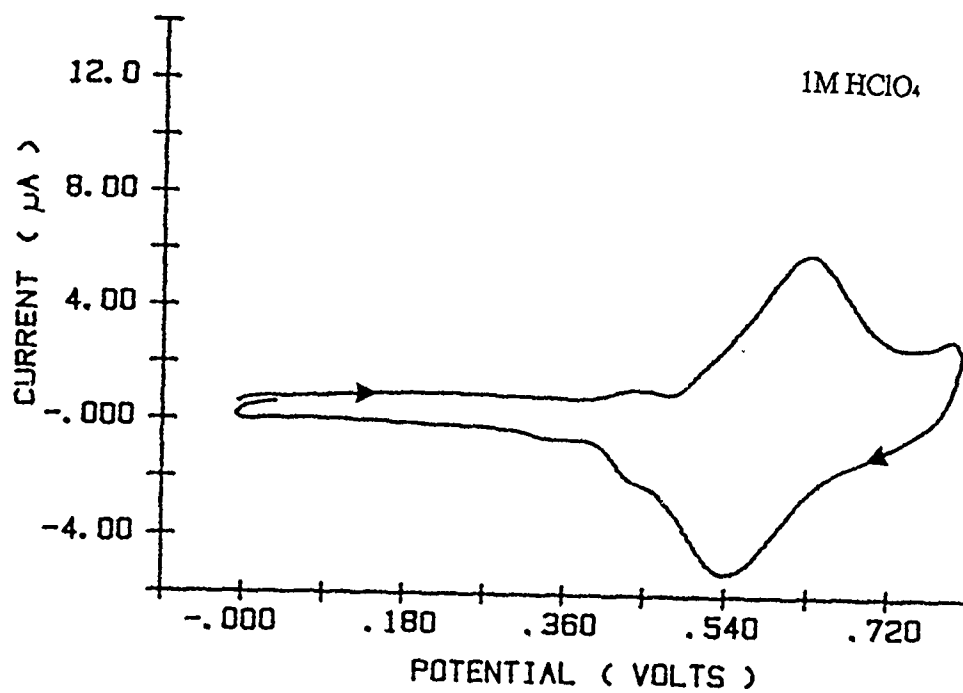
The molecules whose data will be discussed are ferrocenamide phenyl disulfide (I), ferrocene ester phenyl disulfide (II), and cobalticenamide phenyl disulfide (III). Figures 3.2 and 3.3 show the voltammograms and frequency data for ferrocenamide phenyl disulfide and ferrocene ester

Figure 3.2 Ferrocenamide phenyl disulfide in 1M HClO<sub>4</sub> with a scan rate of 100mV per second versus SSCE.



FERROCENAMIDE PHENYL DISULFIDE

Figure 3.3 Ferrocene ester phenyl disulfide in 1M HClO<sub>4</sub> with a scan rate of 100mV per second versus SSCE.



FERROCENE ESTER PHENYL DISULFIDE

phenyl disulfide, respectively. The frequency decrease indicates that upon oxidation of the ferrocene molecule there is a corresponding transport of anions and/or solvent into the monolayer to maintain charge neutrality. The reverse is true of the ferrocinium molecule when it is reduced and this causes the frequency to increase back to its original value.

The calculated charge, from compound I's voltammogram in figure 3.2, is  $27\mu\text{C}$  per  $\text{cm}^2$  which is in good agreement with the calculated charge for the ferrocene molecules in an upright but tilted position on the surface with the ferrocene part extended away and on its side (sort of like a flag in a stiff breeze on a bent over flagpole). This amounts to a surface coverage of  $2.8 \times 10^{-10}$  moles per  $\text{cm}^2$ . As can be seen from the frequency plot, there is a  $0.75\text{Hz}$  per mole of  $e^-$ 's change over the course of the potential scan. This amounts to an effective mass change sensed by the EQCM of 47 grams per mole which is less than can be accounted for solely by transport of  $\text{ClO}_4^-$  anions. The data in table 3.1 shows the calculated grams per mole of mass sensed by the EQCM for two different coverages of I on the surface. Note that as coverage (charge) increases the change in frequency decreases and, therefore, the grams per mole decreases. Figure 3.4 best illustrates what is thought to be occurring. On the left, two different monolayer coverages are displayed. The top right shows the lower monolayer coverage

## Effect of Surface Coverage on Molecular Weight

Charge, $\mu\text{C}$	$\Delta F$ , hz	MW
10.08	.442	25.42
5.147	3.65	411.0

Table 3.1 Demonstration of changes in mass sensed by the crystal from changes in the surface coverage of Ferrocenamido phenyl disulfide in .1M NaCl supporting electrolyte.

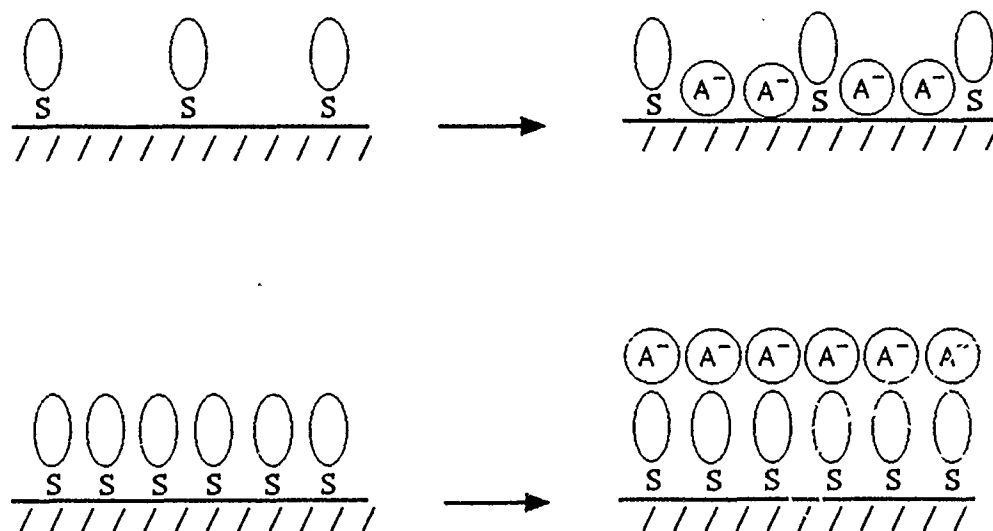
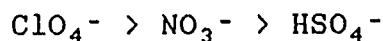


Figure 3.4 Graphic explanation of results depicted in Table 3.1. Shown is Ferrocenamide phenyl disulfide bound to the surface in varying coverages.

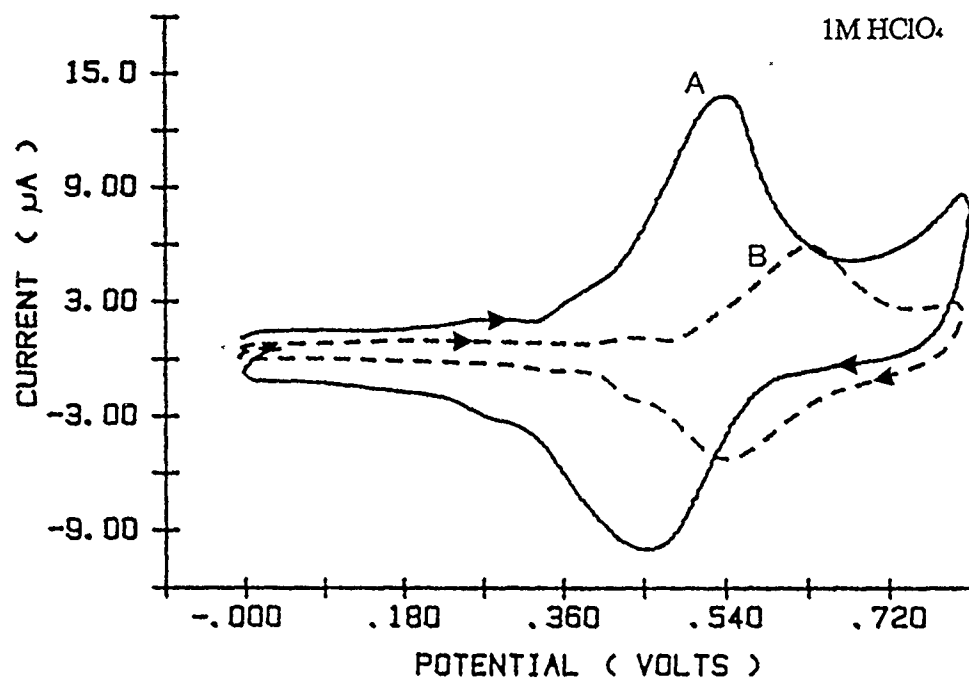
with the bulk anions and solvent on the surface of the electrode. This lower coverage monolayer has many defects in it and large amounts of bulk anions and solvent incorporate into the monolayer in these defects or areas of no coverage. The lower right shows the higher coverage with the bulk anions and solvent as the outer layer. This would mean that as the coverage increased, the bulk anions and solvent would be forced to remain outside of the monolayer thereby lessening the amount of mass that the crystal would sense.

Figure 3.5 shows a large difference in the redox potentials of compounds I and II in relation to each other. This may be due to the ester group being more electron withdrawing which would make the ferrocene group harder to oxidize. The difference in charge is just because the two are different coverages. Compounds I and II were also compared with different anions. Use was made of perchloric acid, nitric acid, and sulfuric acid. As shown in figure 3.6, compound I has an interesting trend with varying the anion type within the monolayer. The redox potential shifts more positive as the acid is changed from perchloric to nitric to sulfuric. The observed potential shifts are attributed to ion pairing effects between the ferrocene and the anion. The strength of the ion pairing, with respect to anions used in these experiments, has the following trend:



Compound II shows the same results with the above acids.

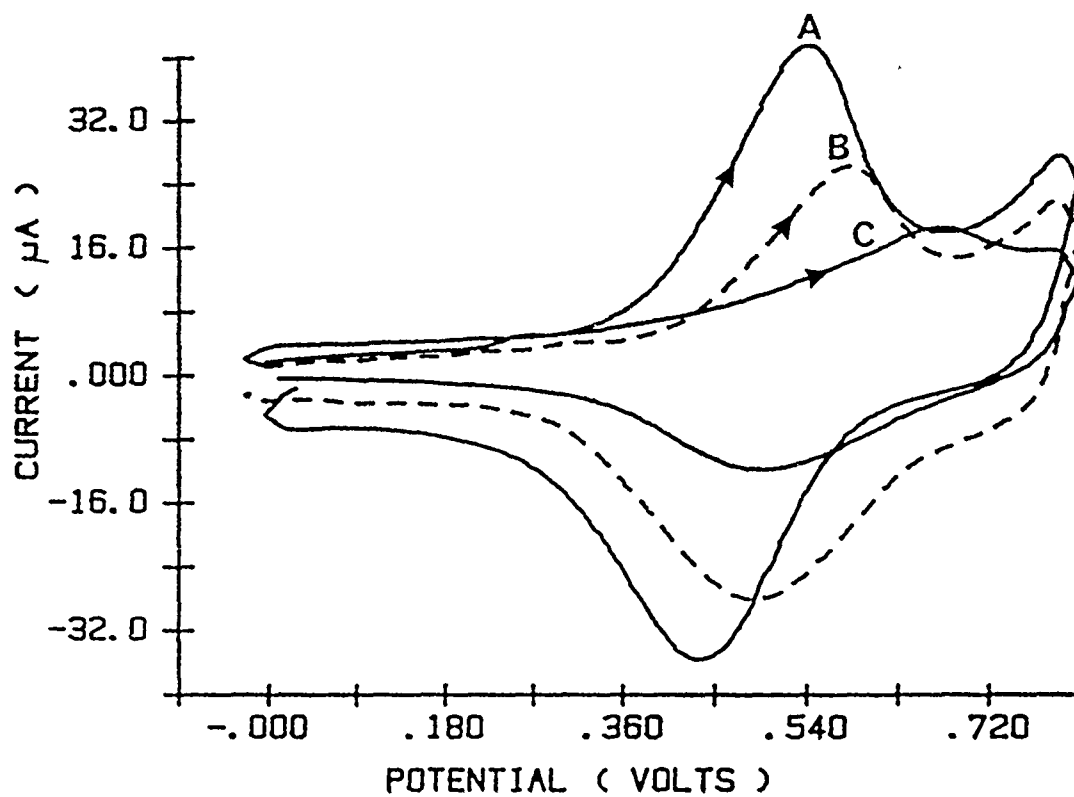
Figure 3.5 Voltammograms of Ferrocenamide phenyl disulfide and Ferrocene ester phenyl disulfide from two different coatings are superimposed on each other. Both were done in 1M HClO<sub>4</sub> versus SSCE.



A FERROCENAMIDE PHENYL DISULFIDE

B FERROCENE ESTER PHENYL DISULFIDE

Figure 3.6 Voltammograms of Ferrocenamide phenyl disulfide in:  
A) 1M HClO<sub>4</sub>, B) 1M HNO<sub>3</sub>, and C) 1M H<sub>2</sub>SO<sub>4</sub> versus SSCE.



FERROCENAMIDE PHENYL DISULFIDE IN:

A 1M  $\text{HClO}_4$

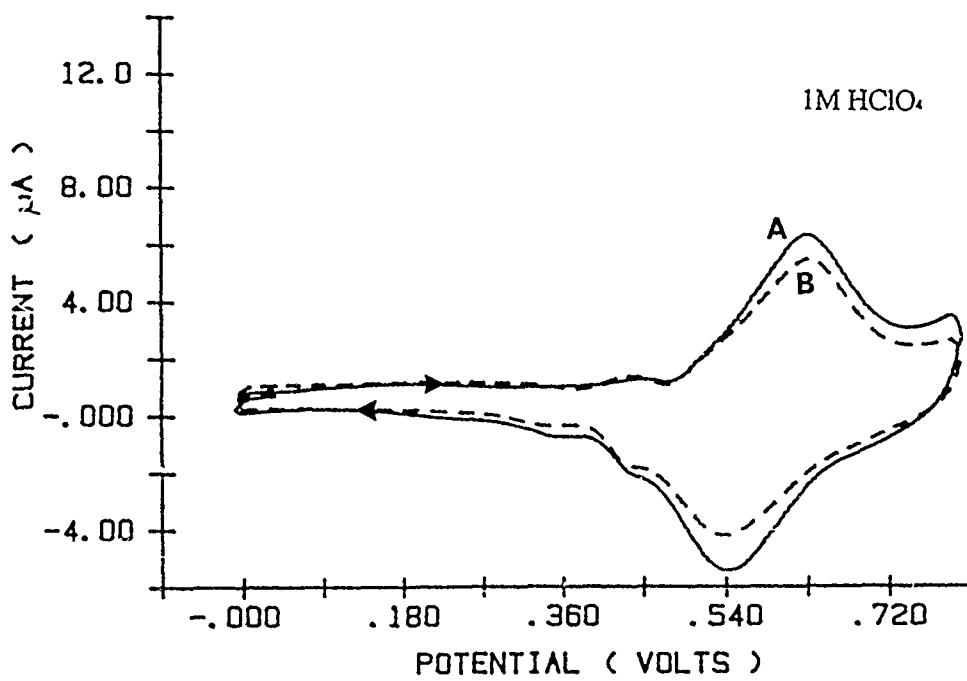
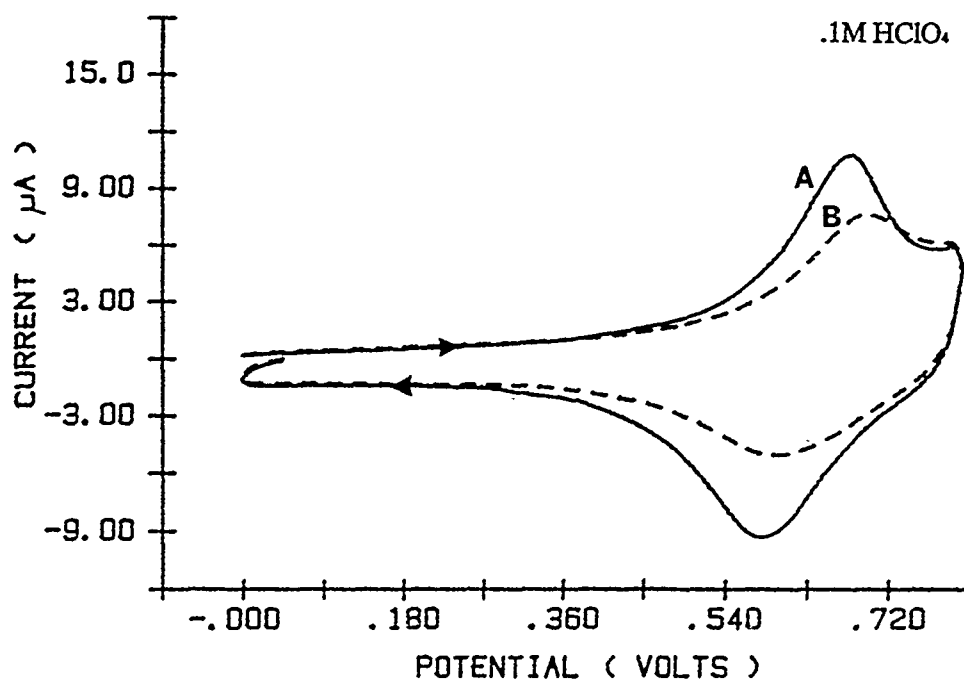
B 1M  $\text{HNO}_3$

C 1M  $\text{H}_2\text{SO}_4$

Uniquely, compound II can easily be hydrolyzed unlike compounds I and III, because of the presence of an ester bond that can be hydrolyzed in acidic water. As can be seen in figure 3.7, where scans were taken at time  $t=0$  (first scan) and at  $t=70\text{mins}$  ( $1\text{M HClO}_4$ ) and  $t=7\text{hrs}$  ( $.1\text{M HClO}_4$ ), there is a corresponding loss in charge of the faradaic current. If the capacitive current is examined, no change in current is demonstrated. This indicates that the ferrocene is lost but there is still a disulfide moiety on the surface. This is known by looking at changes in the capacitive current. When an adsorbate binds to the surface, in this case a disulfide molecule, the dielectric constant at the surface changes<sup>42</sup>. This causes a change in the capacitive current. In the case of all disulfide and thiol compounds that this laboratory has tested, the capacitive current decreases when the compounds adsorb to the surface. Therefore, if loss of faradaic current were due to loss of adsorbate from the surface, the capacitive current would increase. In these experiments there was no observable change in the capacitive currents during hydrolysis. Loss of faradaic current was believed to be due to cleavage of ester bond. Compound I did not experience any loss under the same conditions. The loss was greater in  $1\text{M}$  acid than in  $.1\text{M}$  acid, which would tend to suggest that the hydrolysis rate is affected by acid concentration.

Nonaqueous solvents were tried as well. Acetonitrile,

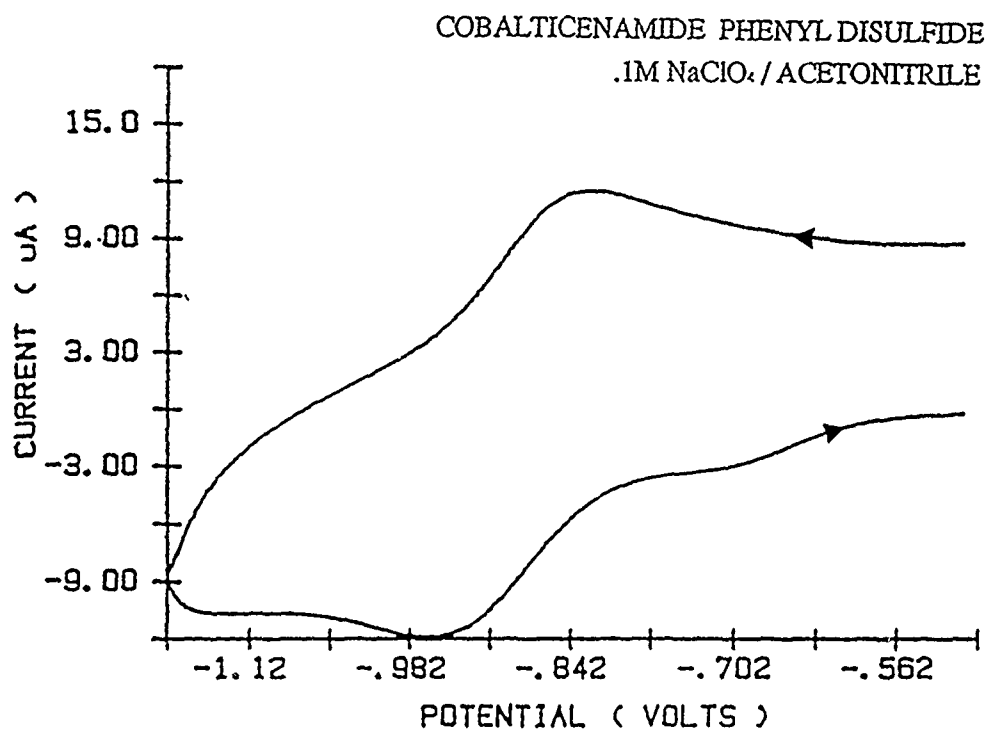
Figure 3.7 Study of hydrolysis of the ester bond. Voltammograms of Ferrocene ester phenyl disulfide in .1M HClO<sub>4</sub> and 1M HClO<sub>4</sub> versus SSCE. A) t=0 (first scan)  
B) t=7hrs (.1M HClO<sub>4</sub>) t=70mins (1M HClO<sub>4</sub>)



FERROCENE ESTER PHENYL DISULFIDE

dichloromethane, dimethylsulfoxide, and tetrahydrofuran were all used without success. It turns out that compounds I, II, and III are solvated by the nonaqueous solvent and get washed off the surface. Figure 3.8 shows cobalticinamide phenyl disulfide (III) in acetonitrile. The response was only observed for one scan because by the next scan the cited dissolution of the film from the surface or competitive adsorption of acetonitrile displacing the disulfide had occurred. The acetonitrile must solvate the molecule enough that it washes away from the surface. Mercaptoalkanes have the advantage of close association between the alkane chains so, if the sulfur gold bond breaks, it is still close enough to the surface to reform. The conjugated compounds I, II, and III do not have that close association therefore nothing holds them close to the surface when the bond breaks to allow time for reforming.

Figure 3.8 Voltammogram of Cobalticinamide phenyl disulfide in .1M NaClO<sub>4</sub> and acetonitrile versus silver as a pseudo reference electrode.



## Conclusions

From the proceeding discussion, one can see that the EQCM is a powerful tool in the study of anion and solvent transport. By changing the supporting electrolyte, it was demonstrated that different anions have a profound influence on voltammetric waveshapes and their  $E_0$ 's. Also shown was that by slightly changing substituents in a molecule, such as in the case of the ferrocenes, one can change the character of the voltammogram. Finally, it was found that the dielectric constant at the surface changed by adsorption, and this was used to monitor the hydrolysis of an ester bond. This proved very important, since the loss of the redox species from the surface does not tell how the loss occurred.

The data from the nonaqueous electrolytes indicated that the compounds examined in this chapter are not stable enough in nonaqueous solvents. Therefore, efforts are underway to explore other redox couples attached to electrodes using disulfides and thiols. Synthetically, the self-assembling systems are quite flexible. There are numerous ways to change the molecules to allow control over their tendencies for adsorption. For the case of introducing instability, the best examples are the organometallic compounds in nonaqueous medium depicted earlier in this report. An opposite change would be the addition of alkane

chains to increase stability in nonaqueous as well as aqueous media. Finally, to tighten up the monolayers, space filling moieties could be added or possibly chiral groups and other functional groups would be useful for other electrosynthetic applications.

There are many areas which can be studied using redox species such as those described above. A number of these areas are already being pursued with promising results. Ease of synthesis and modification, ability to self assemble, and good electrochemistry all go a long way into making these systems very useful in the study of electrode surface modifications.

## CHAPTER IV

### ELECTROCHEMICAL AND QUARTZ CRYSTAL MICROBALANCE STUDIES OF VILOGEN DERIVATIVES: ION AND SOLVENT TRANSPORT PROPERTIES

#### Introduction

Modified electrodes are very attractive for many applications such as electrochemical sensors<sup>26</sup>, electrochemical synthesis<sup>50</sup>, photochemical applications<sup>5c, 14a</sup>, and electrocatalysis<sup>37b, 51</sup>. There are many different ways to modify an electrode. Modification layers can either contain a redox couple or lack one and the modification can be by either physisorption or chemisorption. The nature of the above is only limited by one's imagination. This chapter is concerned more with chemisorbed monolayers containing redox couples.

There are many different ways to chemisorb a redox couple to the surface of an electrode. Silanes<sup>1b, 4, 5, 15</sup>, cyano groups<sup>24</sup>, acid chlorides<sup>17b, 22</sup>, cyanuric attachments<sup>52</sup>, etc., have all played a major role in modifying electrodes but they lack a high surface coverage. Organosulfur compounds on gold have a high surface coverage due to their high packing density and self assembly making them easy to attach to the surface.

Just as there have been different ways to attach redox

couples to the surface, there have been many different redox couples used. It is beneficial to have a redox couple which does not undergo degradation due to changing electrode conditions. Ferrocene is a very commonly used modifier, but it has a degradation problem with the oxidized ferricinium ion. Viologens, on the other hand, do not have this problem. They are very attractive because they can be cycled many times without experiencing degradation. Viologens also can be quite stable in many solvents and their electrochemistry is well characterized. The two redox couples (+2/+1, +1/0) are both accessible and reversible in a number of solvents. Synthetic attachment to the bipyridyl group is also relatively simple.

Reported herein is an electrode modification scheme which takes advantage of the above mentioned characteristics. Viologens have been utilized as redox couples which are attached to the surface of gold electrodes by way of a thiol linkage. The electrochemical behavior of these films was monitored using the Electrochemical Quartz Crystal Microbalance (EQCM).

## Experimental

Figure 4.1 shows the structures of the redox molecules synthesized in this work. Compounds I, II, IV, V, and VI are made similarly to the procedure of Donohue<sup>18</sup> by adding a 1:0.8 equivalent ratio of 4,4'-bipyridyl and 1-bromodecane or 1-bromooctadecane to acetone and refluxing for 12 hours. Isolation of the monoalkylviologen is accomplished by use of a Soxhlet extractor with petroleum ether. This is then added to acetonitrile with excess 1,10-dibromodecane. This is refluxed then for four hours and then isolated as the dialkylviologen (it usually precipitates, otherwise rotavap down and wash with pentane or ether to get rid of starting material). The dialkylviologen is added with 3-5 fold excess thiourea to water (may have to add alcohol to the water for the more insoluble species, but do not add more than 50% or the thiourea solubility will be hampered) and isolated as the isothiuronium salt (by precipitation or rotavap down), which is very stable. To make the thiol, the isothiuronium salt is added to water and then enough base is added to make the free base<sup>53</sup> which decomposes in the presence of water and heat to the mercaptan. Avoid addition of too much base or the dialkylviologen will reduce and precipitate. This part of the reaction can take up to several hours. Next, the reaction is stirred for four hours refluxing under argon (argon is used to avoid oxidation by air to the disulfide in



the presence of alkali), then the Na-salt is precipitated with excess base (this reduces the bipyridyl ring system and gets rid of any left over thiourea). Finally, the solid is filtered and redissolved in 1% HCl to protonate it.

The structure and purity of the above compounds were determined by  $^1\text{H}$  NMR.  $\text{C}_{10}\text{VC}_{10}\text{SCNHNH}_2\text{-HBr}$ : 9.44 d(4), 8.85 d(4) bipyridyl; 8.9 d(4) amines; 4.72 t(4) N-methylenes next to pyridyls; 3.15 t(2) S-methylene; 1.98 m(4) methylenes next to N-methylenes; 1.57 m(2) methylene next to S-methylene; 1.30 broad m(26) rest of methylenes; 0.86 t(3) methyl; (DMSO).  $\text{C}_{10}\text{VC}_{10}\text{SH}$ : 9.44 d(4), 8.85 D(4) bipyridyl; 4.72 t(4) N-methylenes next to pyridyls; 2.68 t(2) S-methylene; 1.98 m(4) methylenes next to N-methylenes; 1.60 m(2) methylene next to S-methylene; 1.26 broad m(26) rest of methylenes; 0.86 t(3) methyl; (DMSO).  $\text{C}_{18}\text{VC}_{10}\text{SCNHNH}_2\text{-HBr}$ : 9.44 d(4), 8.85 d(4) bipyridyl; 9.00 d(4) amines; 4.72 t(4) N-methylenes next to pyridyls; 3.15 t(2) S-methylene; 1.98 m(4) methylenes next to N-methylenes; 1.58 m(2) methylene next to S-methylene; 1.28 broad m(42) rest of methylenes; 0.86 t(3) methyl; (DMSO).  $\text{C}_{18}\text{VC}_{10}\text{SH}$ : same as  $\text{C}_{10}\text{VC}_{10}\text{SH}$ .  $\text{C}_{10}\text{VC}_3\text{SCNHNH}_2\text{-HBr}$ : 9.44 d(4), 8.85 D(4) bipyridyl; 9.07 d(4) amines; 4.80 t(2), 4.70 t(2) N-methylenes next to pyridyls; 3.42 m(2) methylene between the N-methylene and S-methylene; 2.37 m(2), 1.98 m(2) methylenes next to N-methylenes; 1.28 broad m(14) rest of methylenes; 0.86 t(3) methyl; (DMSO).  $\text{C}_{10}\text{VC}_{16}\text{SCNHNH}_2\text{-HBr}$ : 9.44 d(4), 8.85 d(4) bipyridyl; 9.08

d(2), 8.95 d(2) amines; 4.72 t(4) N-methylenes next to pyridyls; 3.15 t(2) S-methylene; 2.00 m(4) methylenes next to N-methylenes; 1.60 m(2) methylene next to S-methylene; 1.30 broad m(38) rest of methylenes; 0.86 t(3) methyl; (DMSO). C1VC12SCNHNH2-HBr: 9.44 d(4), 8.85 d(4) bipyridyl; 9.04 d(2), 8.92 d(2) amines; 4.72 t(5) N-methylene nad N-methyl next to pyridyls; 3.15 t(2) S-methylene; 1.98 m(2) methylene next to N-methylene; 1.58 m(2) methylene next to S-methylene; 1.30 broad m(38) rest of methylenes (DMSO).

The compound 9 or 10-bromoheneicosane is made by dissolving  $\text{HBr}_{(g)}$  in ethyl ether then adding 9-cis-heneicosene to brominate the double bond. The solution is then evaporated to remove the solvent leaving the oil. It is important to then add dichloromethane to redissolve the oil. This is followed by extraction with water, drying with  $\text{MgSO}_4$ , filtering, and evaporating off the dichloromethane. Compound III is then made by using the 9/10-bromoheneicosane and following the same procedure as for the other compounds above. It will be necessary to add alcohol to the thiourea step because this dialkylviologen is not very soluble in water alone. The structure and purity of the above compound were determined by  $^1\text{H}$  NMR.

9-cis-Heneicosene: 5.35 m(2)  $-\text{CH}=\text{CH}-$ ; 2.02 m(4) methylenes next to vinyl group; 1.30 m(30) rest of methylenes; 0.89 t(6) methyls; ( $\text{CDCl}_3$ ). 9/10-Bromoheneicosane: 4.03 m(1)  $-\text{CHBr}$ ; 1.78 m(4) methylenes next to  $-\text{CHBr}$ ; 1.30 m(30) rest

of methylenes; 0.89 t(6) methyls; (CDCl<sub>3</sub>).  
C9C11VC10SCNHNH<sub>2</sub>-HBr: 9.57 d(2), 9.48 d(2), 8.89 d(4)  
bipyridyl; 9.08 broad s(2), 8.98 broad s(2) amines; 4.90  
t(1), 4.74 t(4) N-methylenes next to pyridyls; 3.15 t(2)  
S-methylene; 2.03 m(6) methylenes next to N-methylenes; 1.58  
m(2) methylene next to S-methylene; 1.28 broad m(42) rest of  
methylenes; 0.86 t(6) methyls; (DMSO).

Concerning the coating of the viologen derivatives, they were dissolved in water and a portion of this solution is transferred to an electrochemical cell (modified H type) which contains the desired supporting electrolyte, for example, 0.1M NaCl. The thiol/supporting electrolyte solution is purged with argon. A bias potential, ca. 0.0V (versus SSCE), is applied to allow the coating process to take place on the Au surface. After coating, the cell is rinsed and new electrolyte is used. The crystal is then monitored by cyclic voltammetry until the cyclic voltammograms show no change. Following this, the crystals are rinsed in dichloromethane to remove the weakly bound layer of material, leaving a monolayer as determined by charge calculations. NaOH is added to the cell to shift the electrochemical window to view the viologen's voltammetry.

The coating procedure for the more insoluble viologens varies from the above procedures. Usually this entails dissolving the viologen in ethanol and coating the crystal for an hour, then washing in 200 proof ethanol. This

procedure is repeated for as long as it takes to set up a good monolayer (usually about four times). After rinsing and attaching the crystal to the H-cell, the charge is monitored to determine if a monolayer is present.

The same method as reported in chapter III was used for the charge calculation and the calculation of surface coverage to get the grams per mole mass sensed. The system used for data collection has been described previously in chapter II.

## Results and Discussion

Compounds I, II, III, IV, V, and VI have alkane chains that associate together to help stabilize the layer on the surface even in nonaqueous solvents unlike the previously reported conjugated compounds in chapter III. Changing the supporting electrolyte can have a dramatic effect on the cyclic voltammetry<sup>54</sup> of these compounds. Several different supporting electrolytes have been investigated with this in mind.

### C10VC10SH

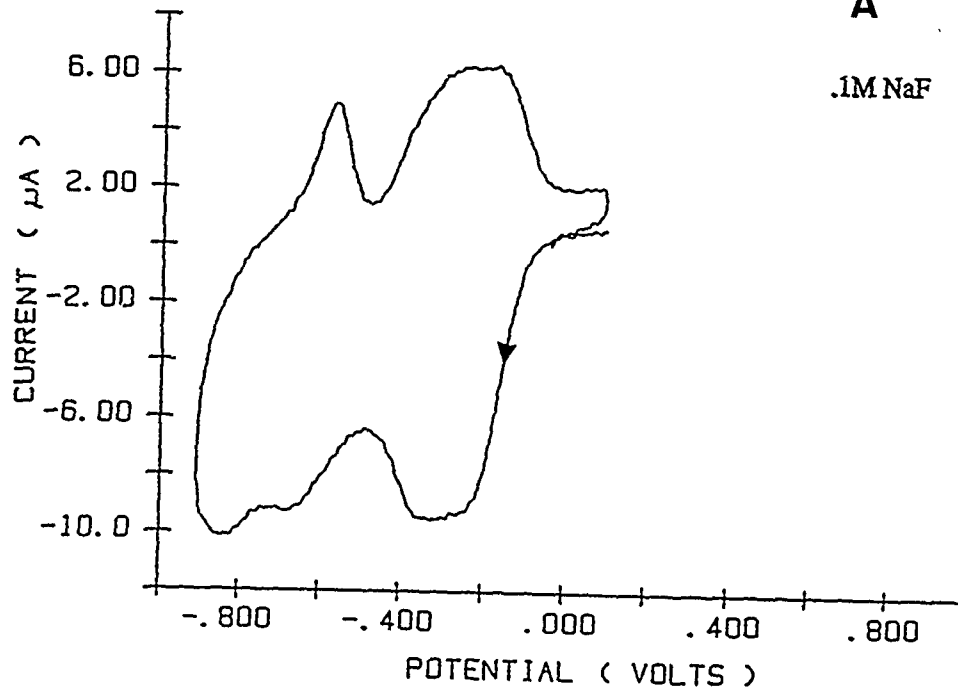
The first compound to be covered is compound I (C10VC10SH). Figure 4.2 illustrates current and frequency of compound I during cyclic voltammetry in .1M NaF<sub>(aq)</sub>. This dialkylviologen has well behaved voltammetry in that the redox events expected to occur have taken place without any extraneous abnormalities. As can be seen from the frequency plot, as the viologen is reduced the frequency increases indicating expulsion of anions and solvent. The voltammogram shows broadening in both the oxidative and reductive regions which can be rationalized in the cartoon in figure 4.3. The illustration shows two of the dialkylviologens bound to the surface with the accompanying anions. The circles indicate the hydration shells which are tightly bound to the

Figure 4.2 a) Voltammogram of N-(n-Decyl)-N'-(10-Mercaptodecyl)-4,4'-Bipyridinium Dichloride (C10VC10SH) in 0.1M NaF with a scan rate of 100mV/sec versus SSCE. b) Frequency data.

C10VC10SH

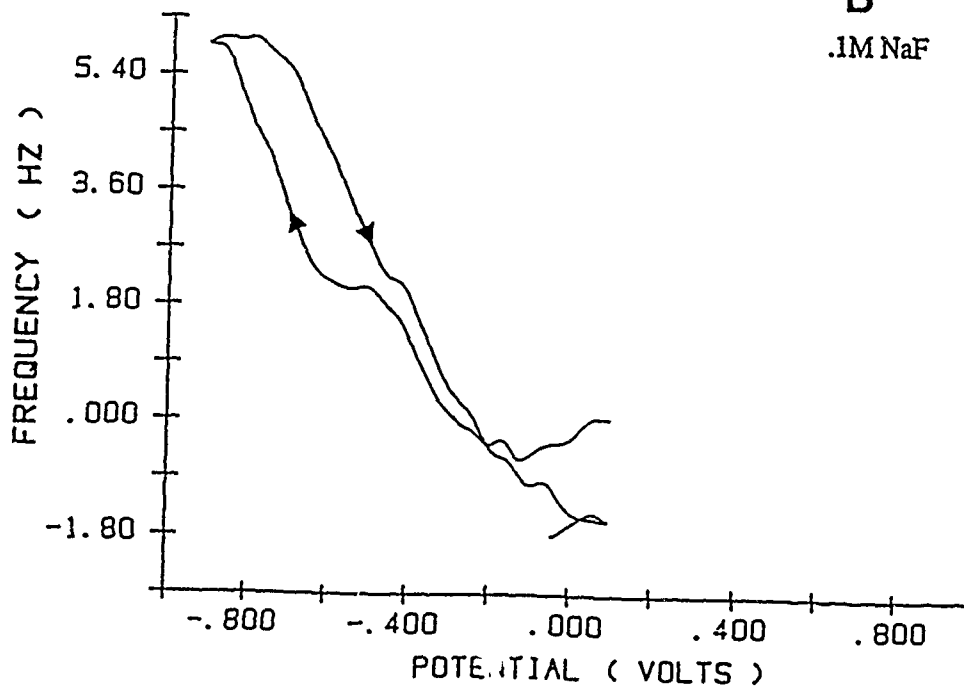
A

.1M NaF



B

.1M NaF



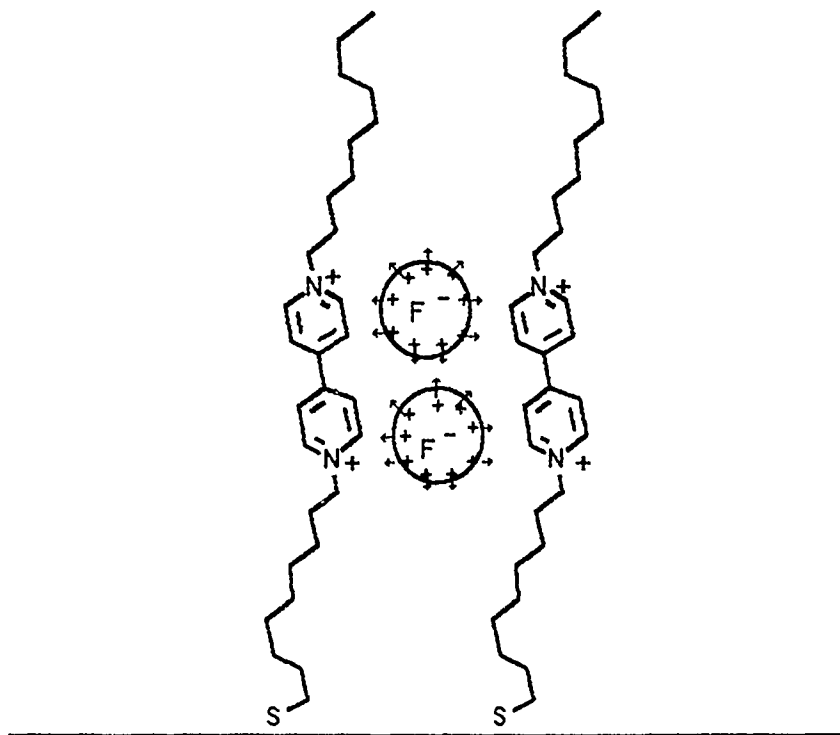
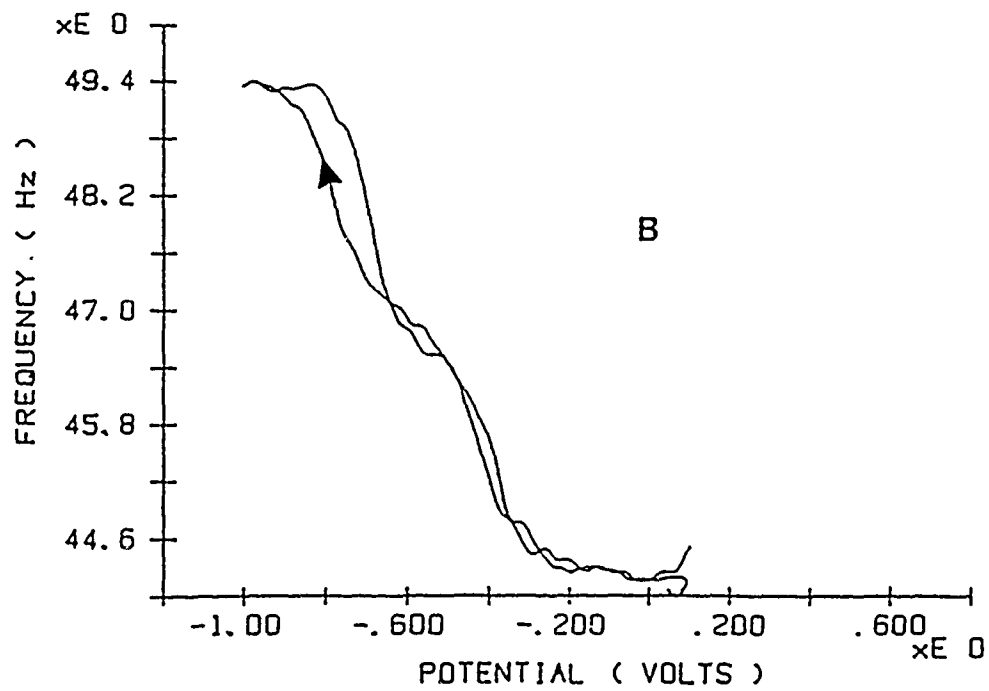
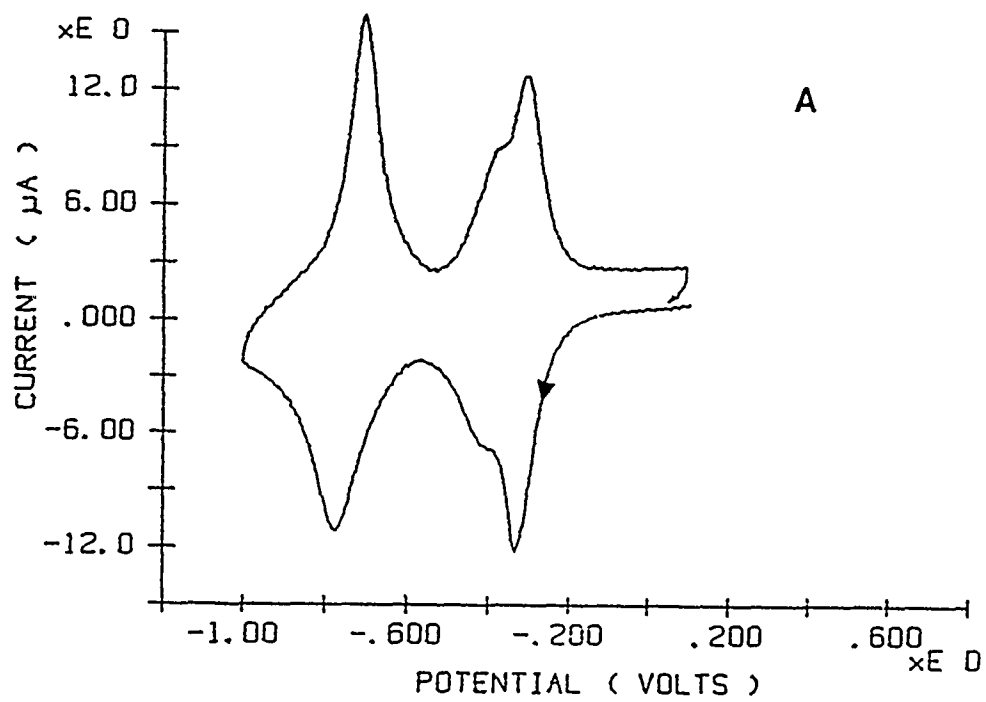


Figure 4.3 Graphic depiction of solvent-separated ion-pair of (C10VC10SH) in NaF supporting electrolyte.

fluorides<sup>55</sup>. Since the waters are held so tightly, there is no shielding of the charges on the viologen from each other due to dielectric saturation of the hydration sphere<sup>56</sup>, thereby causing broadening of the wave. The positions of the formal potentials on the potential axis are much more positive than those for methylviologen<sup>57</sup> in solution, which is indicative of stabilization of the cation radical over the dication in these monolayers. This is most likely due to strong intermolecular interactions among the cation radical viologen molecules.

The second supporting electrolyte used was 0.1M NaCl. Figure 4.4 shows the voltammogram and frequency data on the monolayer of compound I. The first thing that is noticed is that the voltammogram of the chloride is not as broad as the voltammogram of the fluoride. This is probable because some shielding of the charge is taking place making the peak less broad. What is more noticeable in the voltammogram of the chloride than the fluoride (although it exists in the case of the fluoride too) is the double peak in the first redox couple. This is present in the fluoride but because it is so broad, it is harder to see. None of the other anions tested displayed this split peak in the first redox couple. Not much is known yet about this phenomenon. However, Matsuda et al<sup>58</sup> have recently indicated that a negative interaction energy, such as what one could get from the interaction of the dicationic viologen and the cationic radical viologen,

Figure 4.4 a) Voltammogram of N-(n-Decyl)-N'-(10-Mercaptodecyl)-4,4'-Bipyridinium Dichloride (C10VC10SH) in 0.1M NaCl with a scan rate of 100mV/sec versus SSCE. b) Frequency data.



would give two peaks centered on where there would normally be one. If this is taken further, as the anions are changed from fluoride (the least shielding and therefore giving the largest negative interaction energy due to repulsion,  $>200\text{mV} = E_{f_{whh}}$ , the full width at half height of the current peak) through chloride, nitrate, bromide, etc. to perchlorate (which has the largest shielding and a positive interaction energy due to ion pairing; reducing repulsion,  $100\text{mV} = E_{f_{whh}}$ ), it would seem that the experimental results match what is expected from the theory<sup>58</sup>. Other possibilities include, but are not limited to, effects specific to different crystal faces (and perhaps different geometrical arrangements of the adsorbates), or dimerization processes. These features are not present in the second wave (corresponding to the reversible reduction from the cation radical to the neutral form) under any of the conditions which have been investigated. Much more experimentation needs to be done in this area before any concrete conclusions can be drawn.

The calculated charge from I's voltammogram is  $41\mu\text{C}$  per  $\text{cm}^2$ . This amounts to a surface coverage of  $4.2 \times 10^{-10}$  moles per  $\text{cm}^2$  which gives a molecular area of  $39 \text{ \AA}^2$  per molecule. This is in good agreement with the calculated value of  $38 \text{ \AA}^2$  per molecule for a hexagonal close packed arrangement of viologens oriented perpendicular to the gold surface<sup>59</sup>, and from molecular modeling. In this case, the

area per molecule is determined by that of the viologen moiety because it is considerably larger than is the projected area for a perpendicularly oriented alkane chain (ca. 20 Å<sup>2</sup> per molecule). Thus, both the experimental observation of the achievement of saturation coverage and the geometrical constraints of the molecule support the view that this coverage is the saturation coverage.

For monolayer systems, it has generally been found that a linear relationship exists between mass changes at the electrode surface and the EQCM frequency change during a redox process, thereby allowing the direct calculation of the mass change associated with the redox process<sup>9b,27</sup>. As can be seen from the frequency plot in figure 4.4, there is a 5.1 Hz per 2 moles of electrons change over the course of the potential scan. This amounts to an effective mass change sensed by the EQCM of 106 g mole<sup>-1</sup> which is more than anion transport can account for. Therefore, it seems likely that solvent is being transported across the bilayer-like layer as well. The data thus imply that about 4.0 molecules of H<sub>2</sub>O are lost from the monolayer for every Cl<sup>-</sup> lost during the reduction, and that these compositional changes are reversible on the cyclic voltammetric time scale. Alternative explanations involving mixed transport of solvent, anions, and cations within the monolayer are possible, but mixed transport usually causes the net mass change to be smaller than that predicted for the

unidirectional transport case, not larger.

The effect of surface coverage on mass was also examined with the  $\text{Cl}^-$  and compound I. Shown in table 4.1 is how varying the surface coverage affects the grams per mole measured with the EQCM. The surface coverage increases down the table. At low surface coverage the change in frequency is lower but the grams per mole is higher. As the coverage increases the grams per mole decreases. This is the same effect seen with the organometallic compounds reported earlier in chapter II, and the explanation would be the same. That is, as the surface coverage increases the amount of solvent and anions in the layer decreases since the number of defects and their size decreases. The interesting thing to note is that after a monolayer of coverage the grams per mole can further decrease until a stable double monolayer is formed. This second monolayer, which is not anchored to the gold surface, is very stable and it takes washing the crystal with dichloromethane to remove it. It displays the same characteristics as the single monolayer as relating to anions and solvent transport but it has a lower grams per mole than a single monolayer. This is probably due to intercalation of the second layer into the first one as shown in figure 4.5. In undergoing the intercalation, the two monolayers are thought to be expelling anions and solvent further to give a lower grams per mole sensed by the EQCM.

## Effect Surface Coverage on Mass

Charge, $\mu\text{C}/\text{cm}^2$	$\Delta F$ , hz	Grams/Mole
11.7	0.9	131
18.8	1.25	113
45.0 <sup>a</sup>	2.55	96
73.0 <sup>b</sup>	2.8	65
75.5 <sup>b</sup>	2.85	64

a Represents one monolayer coverage.

b Represents two monolayers coverage.

Table 4.1 Effects of varying surface coverage of the monolayer  
in .1M NaCl.

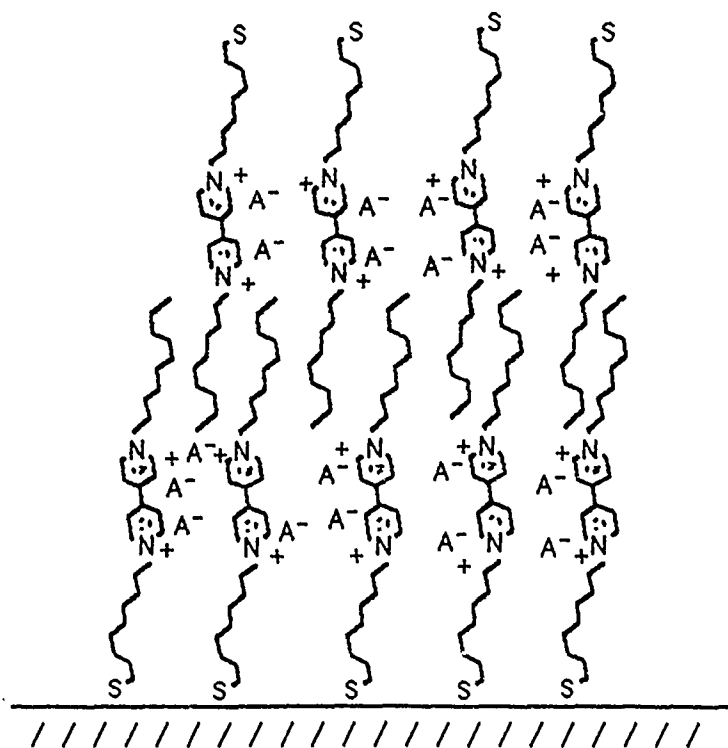
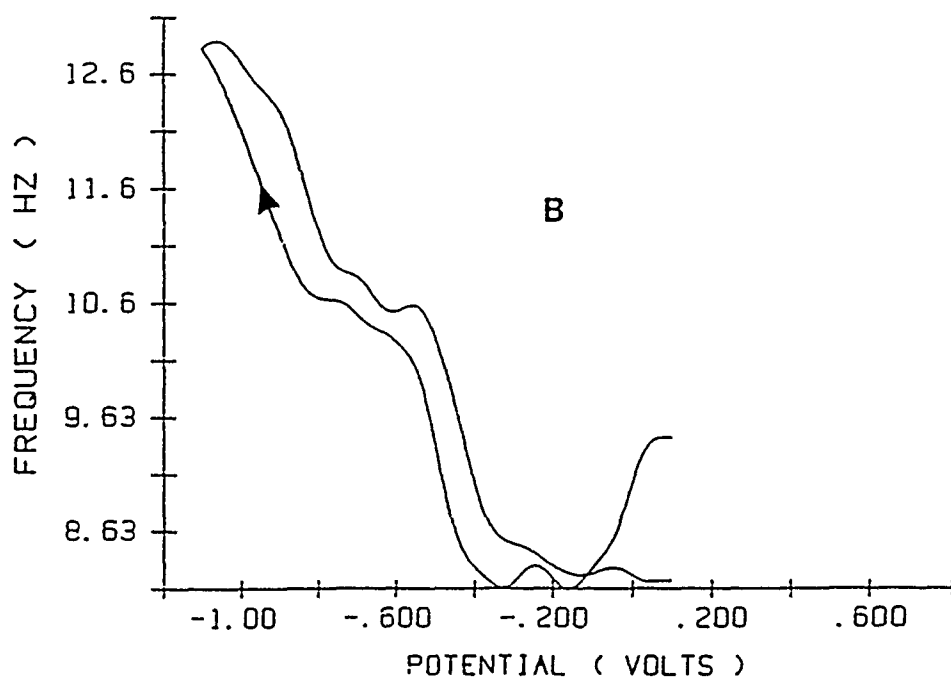
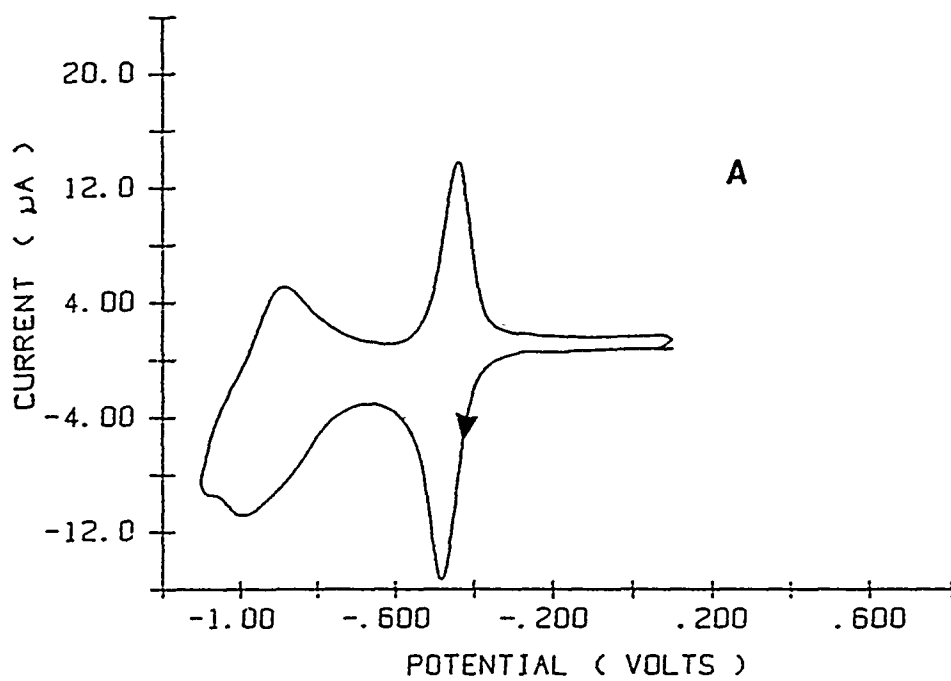


Figure 4.5 Graphic depiction of intercalation of second layer into the monolayer to form a stable bilayer.

The next anion tested on compound I is perchlorate. As can be seen in figure 4.6, the first redox couple is very sharp in appearance and is not split. The second redox couple is broad. Both redox processes are shifted more negative in potential (e.g. from ca.  $-0.35$  V in  $\text{Cl}^-$  to ca.  $-0.5$  V in  $\text{ClO}_4^-$  for the first reduction wave), and the frequency change is of about the same magnitude as in the  $\text{Cl}^-$  case, indicating that little, if any, solvent is transferred during the redox process in  $\text{ClO}_4^-$  (which has a molar mass of  $99 \text{ g mole}^{-1}$ ). Also, the double layer charging current in the  $\text{ClO}_4^-$  cyclic voltammogram is more than a factor of two smaller than that in the  $\text{Cl}^-$  case, indicating a layer which is less "leaky" towards the penetration of supporting electrolyte than is the layer in  $\text{Cl}^-$  solution<sup>2b</sup>.

These data indicate that  $\text{ClO}_4^-$  causes the monolayer to be much more compact than does  $\text{Cl}^-$ , containing less solvent and being less permeable to the supporting electrolyte. Thus, the lower solvent content of the  $\text{ClO}_4^-$  monolayers would be the cause of the smaller amount of expelled solvent during the transition from the relatively hydrophilic dicationic state to the relatively hydrophobic cation radical state. This difference between the  $\text{Cl}^-$  and  $\text{ClO}_4^-$  cases is probably due to the presence of specific interactions between the  $\text{ClO}_4^-$  anions and the positively charged viologen moieties, which do not exist (or are of greatly reduced magnitude) in the  $\text{Cl}^-$  case. This behavior is

Figure 4.6 a) Voltammogram of N-(n-Decyl)-N'-(10-Mercaptodecyl)-4,4'-Bipyridinium Dichloride (C10VC10SH) in 0.1M NaClO<sub>4</sub> with a scan rate of 100mV/sec versus SSCE. b) Frequency data.



reminiscent of observations of anion transport in thin films of poly(vinylferrocene), in which  $\text{ClO}_4^-$  was transported with almost no associated solvent, while more hydrophilic anions, such as  $\text{NO}_3^-$  and  $\text{Cl}^-$ , were transported with large amounts of solvent<sup>47,54b</sup>. Therefore, the sharpness of the first redox couple waveshape is probably due to ion-pairing taking place between the  $\text{ClO}_4^-$  and the dialkylviologen as shown in figure 4.7. The  $\text{ClO}_4^-$  ion-pairs with the cationic viologen which effectively shields the cationic charges from each other. This causes the peaks to get narrower.

A study of the voltammetric waveshape as a function of temperature was undertaken with the anions:  $\text{ClO}_4^-$ ,  $\text{NO}_3^-$ ,  $\text{Cl}^-$ , and compound I to gain further insight into the nature of the above mentioned ionic interactions. Table 4.2 lists the temperature data from the nitrate and perchlorate only since the chloride anion provides the same information as the nitrate anion. The temperature range used was 27°C to 60°C using a water jacketed electrochemical H-cell. In examining the data, it can be seen in the perchlorate case that as the temperature is increased the peak current increases, and the full width at half height of the current peak ( $E_{f_{whh}}$ ) decreases. This is the direct opposite to the normal  $kT$  broadening usually observed for current-potential plots when nothing else is occurring.<sup>43</sup> This peak sharpening with increasing temperature can be interpreted<sup>50</sup> as being due to an attractive interaction between the redox groups

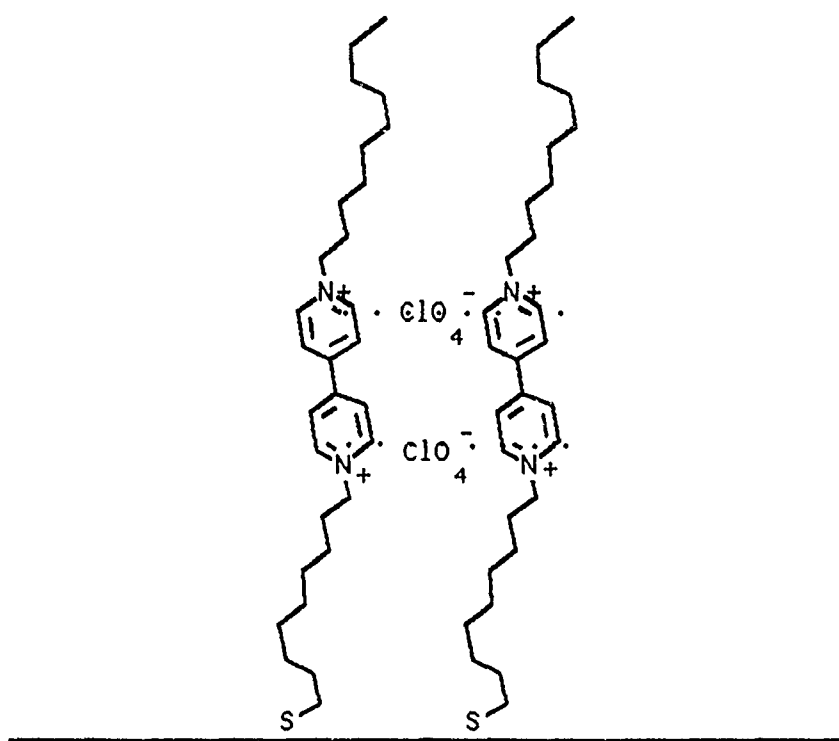


Figure 4.7 Graphic depiction of contact ion-pair of (C10VC10SH) in NaClO<sub>4</sub> supporting electrolyte.

Temperature Effects on Peak Shape  
in

TEMPERATURE, C	NaNO <sub>3</sub> E <sub>F<sub>WHH</sub></sub> , mV	NaClO <sub>4</sub> E <sub>F<sub>WHH</sub></sub> , mV
27	116	109
40	125	—
50	140	105
60	147	86

Table 4.2 Effects of varying temperature on the monolayer in .1M NaClO<sub>4</sub> in relation to the E<sub>f<sub>whh</sub></sub> of the current peak.

within the monolayer which increases in importance as temperature is increased. Two possible explanations for this decrease in  $E_{f_{whh}}$  are: 1) some type of ion pairing between the anions within the monolayer and the positively charged viologen sites is taking place, and 2) hydrophobic interactions between the alkyl chains of neighboring molecules is occurring, either of which might serve to mediate attractions between the redox groups.

In order to rule out the second possibility, a study of the temperature dependence of the waveshape for the first redox couple for the  $\text{NO}_3^-$  case was performed. Nitrate was used instead of chloride to avoid the occurrence of the double wave for the first reduction process. The EQCM data for nitrate showed some degree of solvent transport just as in the chloride case. Table 4.2 shows the nitrate results. The first reduction wave broadens as temperature is increased, instead of sharpening as in the  $\text{ClO}_4^-$  case. The behavior in  $\text{Cl}^-$  is qualitatively similar to that for  $\text{NO}_3^-$ . On the basis of these data, it appears that the mediation of attractions between the redox groups by virtue of the hydrophobic interaction between adjacent alkyl chains is ruled out, because these should be independent of the anion used. The implication here is that specific interactions, probably of the ion pair type, between the dicationic viologen sites and the anions within the monolayer are responsible for the waveshape and the apparent redox

potential in the voltammetry of this system. It should be noted here that ion pairing between dicationic viologen derivatives bearing long alkyl chains and either tetraphenylborate or tetrakis[3,5-bis(trifluoromethyl)phenyl]borate anions in Langmuir-Blodgett films has been previously observed, both in the solid state<sup>61</sup> and in solutions of low dielectric constant solvents, such as dimethoxyethane, dichloromethane, and methanol<sup>62</sup>. Charge transfer ion pairs are also known to exist between viologens and multivalent anions in aqueous solutions<sup>63</sup>. Thus, ample precedent exists for the proposed existence of ion pairs within the sulfur anchored viologen monolayers described here. A possible implication of these results is that the effective dielectric constant within the monolayer is sufficiently small to allow for ion pairing.

The determination of the amount of mass transport occurring during the redox event, which were discussed previously with the chloride anion, was also done for the other anions. Shown in table 4.3 are three representative anions and their effect on the grams per mole mass sensed by the EQCM. All have about the same surface coverage within experimental error. There is a big difference in the grams per mole sensed, but since the coverages are about the same then the same number of anions must be present. Therefore, the discrepancy must be in the number of solvent molecules which is incorporated in with the anions. It turns out that

## Mass Effects of Differing Anions

ANION	CHARGE, $\mu\text{C}/\text{cm}^2$	$\Delta F$ , HZ	GRAMS/MOLE	# OF WATERS
$\text{F}^-$	40.7	3.25	136	6.5
$\text{ClO}_4^-$	45.7	2.25	84	0
$\text{Br}^-$	36.4	3.0	140	3.3

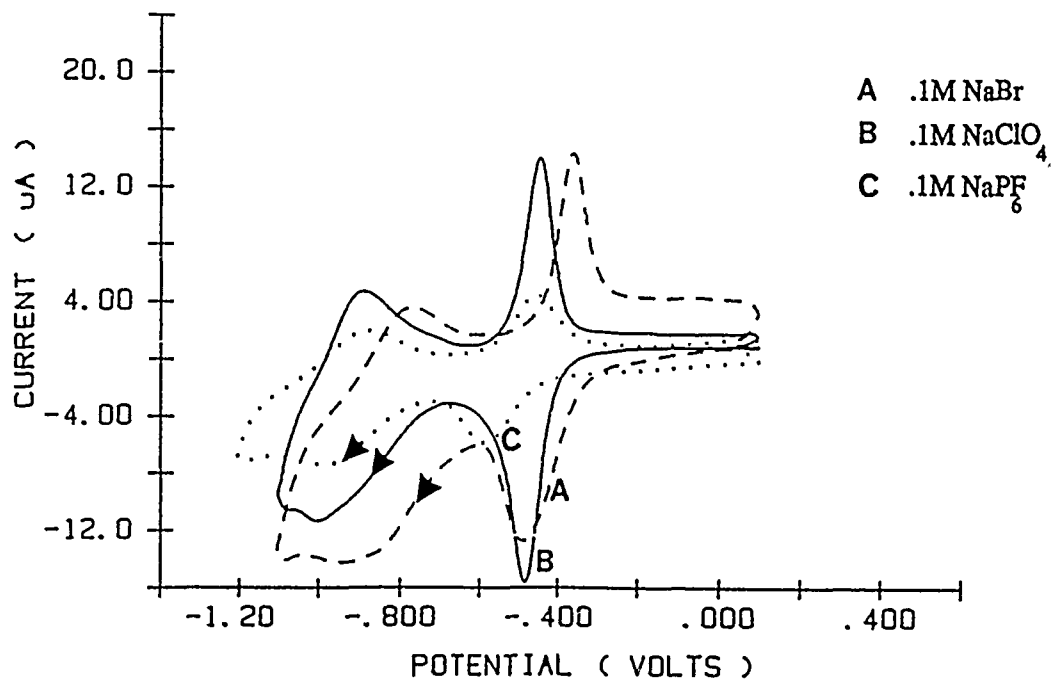
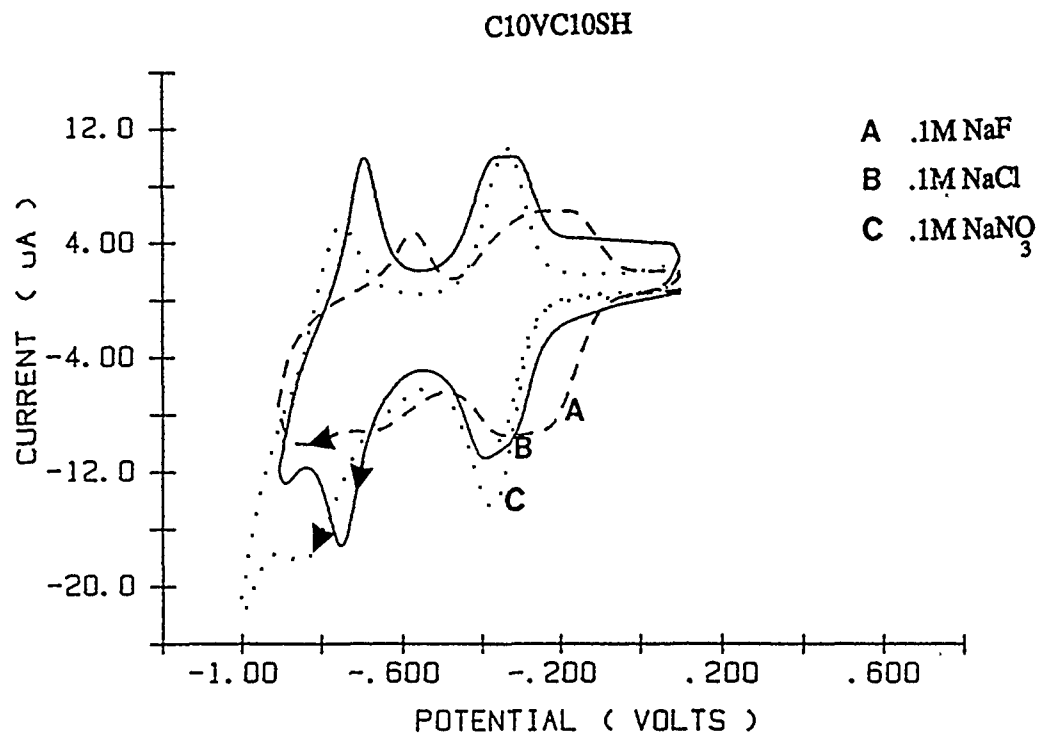
Table 4.3 Effects of differing the anion used as the supporting electrolyte with C10VC10SH.

fluoride has about twice as many waters as bromide and perchlorate has virtually none. Data from the chloride shown earlier gives chloride slightly more water than bromide. This is what one would expect from a system such as this where the anion that has the strongest affinity for water also causes the most hydration of the monolayer. Perchlorate, which is known for its ion pairing, shows virtually no water. Water would not be expected to associate with the more hydrophobic perchlorate.

For purposes of comparison of anion effects, all the anions tried so far are shown in figure 4.8 except for two, which will be discussed later. If just the top half is looked at first, one sees some shifts in redox potential caused by differences in the attractive interactions within the monolayer, such as ion pairing and inadequate shielding of the cationic charges when comparing fluoride, chloride and nitrate. This inadequate shielding is a result of the water in the hydration shells of the anions not being able to realign their dipoles. Also shown is the double peak in the first redox couple for the fluoride, and chloride but not the nitrate.

The bottom half of the figure is actually a more complicated set. The bromide salt of the C10VC10SH is the only one of the three ion pairs which is soluble in aqueous solution; serving thus as a coating source. In spite of its solubility, the peak characteristics, for the bromide case,

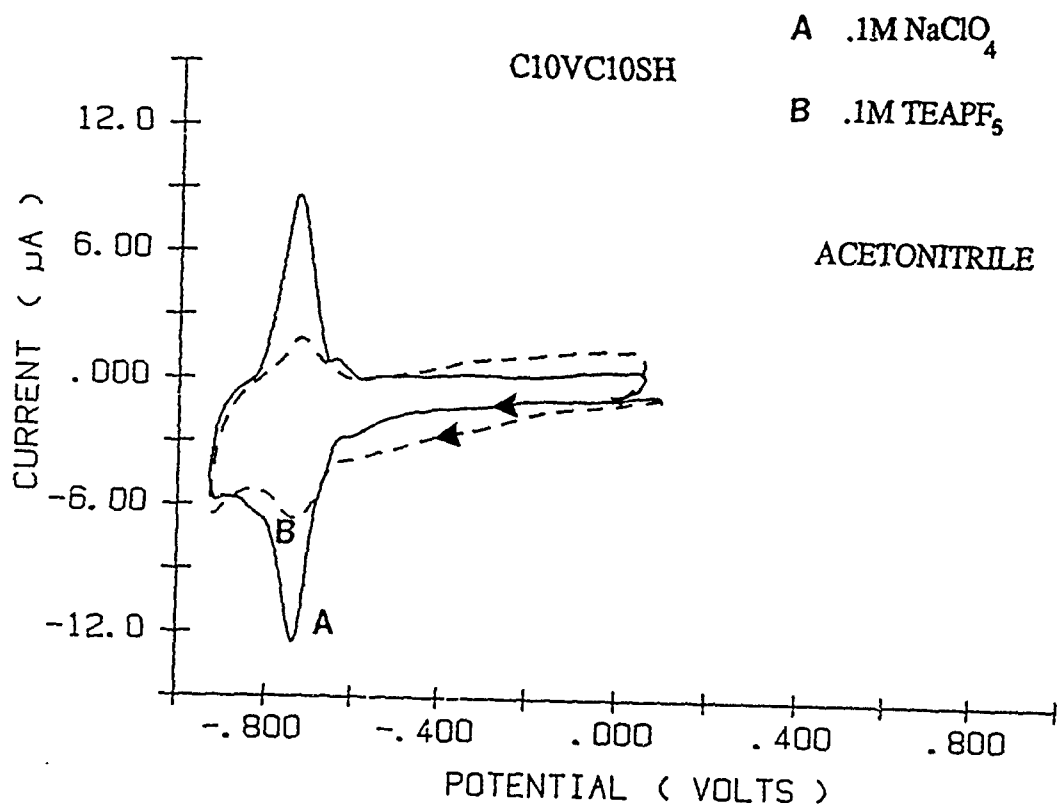
Figure 4.8 Voltammogram of N-(n-Decyl)-N'-(10-Mercaptodecyl)-4,4'-Bipyridinium Dichloride (C10VC10SH) in all the 0.1M supporting electrolytes with a scan rate of 100mV/sec versus SSCE.



resemble the perchlorate case. In looking at this bottom group, the second redox couple is broadened (all three) and shifted negative (except the bromide). This is generally due to the stabilization of the radical cation by these ion pairing anions relative to the other anions. The first redox couple's oxidative and reductive peaks are less reversible which may be a kinetic effect due to steric congestion within the monolayer and the less soluble nature of the monolayer with these anions.

Most of the studies presented thus far involved aqueous solutions of supporting electrolytes. To gain further knowledge about these systems, a few experiments in non-aqueous media were undertaken. Two anions were tested on C10VC10SH, i.e.,  $\text{ClO}_4^-$  and  $\text{PF}_6^-$ . Figure 4.9 shows the voltammograms of the two anions mentioned in acetonitrile. The formal potentials are quite similar and both waves are quite reversible. The difference in charge is just due to different coverages. Note the difference in capacitive current. The largest capacitive current is from the lowest coverage which is what would be expected from data presented earlier on coverage effects. Only the first redox couple is shown due to the interference of water reduction, since the second redox couple is where the reduction of water in acetonitrile take place. The reference used in these voltammograms with acetonitrile is a  $\text{Ag}/\text{AgClO}_4$  luggin capillary reference electrode. To compare this voltammogram

Figure 4.9 Voltammogram of N-(n-Decyl)-N'-(10-Mercaptodecyl)-4,4'-Bipyridinium Dichloride (C10VC10SH) in 0.1M NaClO<sub>4</sub> or 0.1M TEAPF<sub>6</sub> in acetonitrile with a scan rate of 100mV/sec versus SSCE.

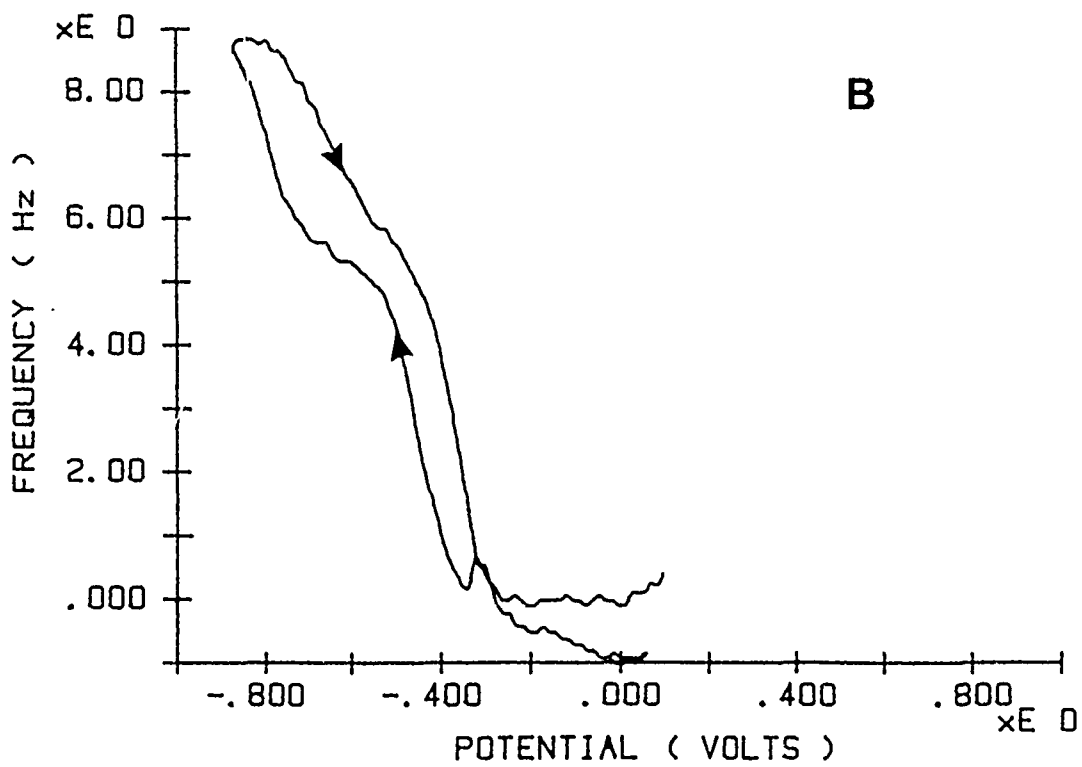
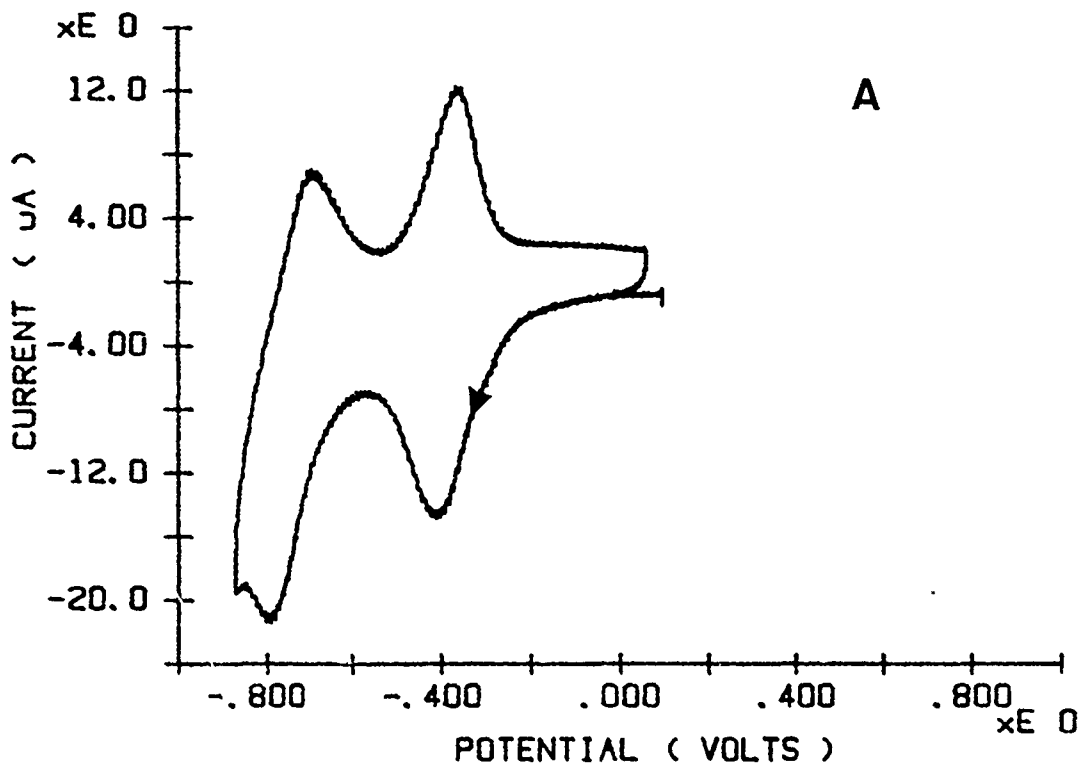


with the SSCE voltammograms from the aqueous experiment, 0.35V must be added to the acetonitrile voltammogram. Compound I in acetonitrile is easier to reduce when comparing it to the same anion used in water. This is because of less ion pairing and increased solvation in acetonitrile than water. Also, some loss is experienced in acetonitrile with the viologens as well, although, the loss is not as rapid as with the organometallic compounds mentioned earlier. This is because of the association possible between the alkane chains. Since there still is some loss, it might be due to something inherent with acetonitrile like competitive adsorption with the thiols on the gold surface.<sup>72</sup>

#### C18VC10SH

The second compound examined is C18VC10SH (compound II). The purpose of making this compound was to examine the result of increasing the outer chain length. The first supporting electrolyte used was 0.1M NaCl (see figure 4.10). The calculated charge from compound II's voltammogram is 40  $\mu\text{C}$  per  $\text{cm}^2$  which gives a molecular area of 39  $\text{\AA}^2$  per molecule. This is the same area obtained from compound I, which is in good agreement with the calculated value of 38  $\text{\AA}^2$  per molecule.<sup>59</sup> Therefore, saturation coverage is assumed for compound II using the same reasoning as for compound I.

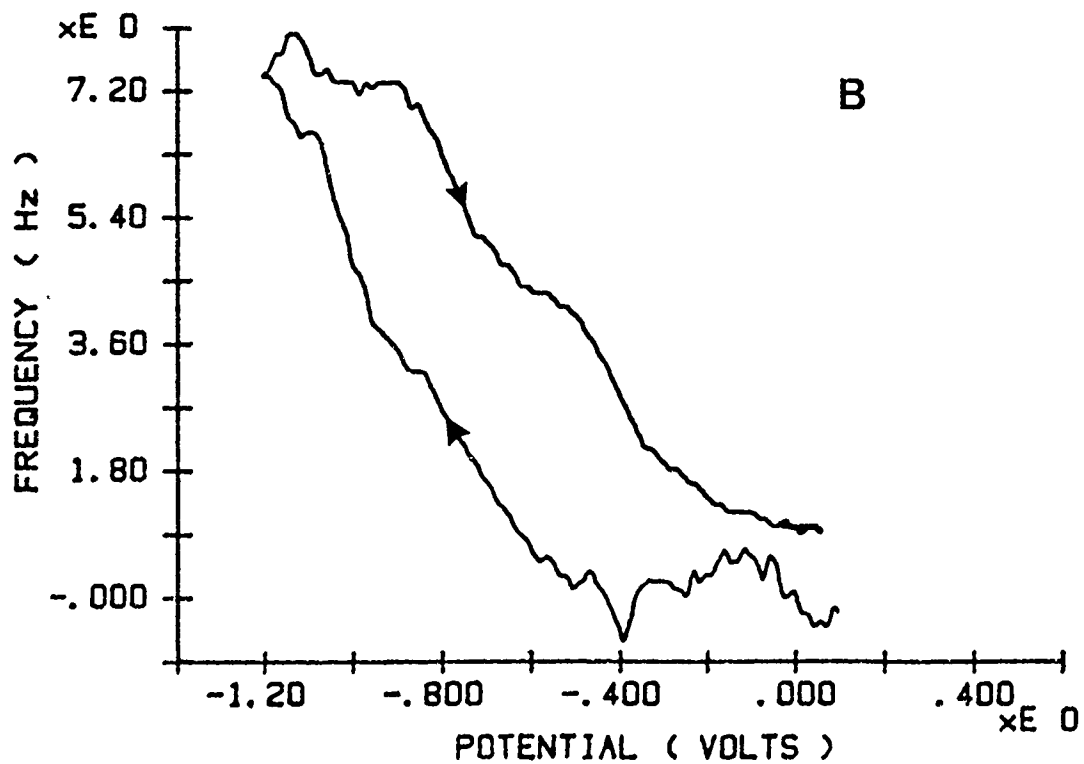
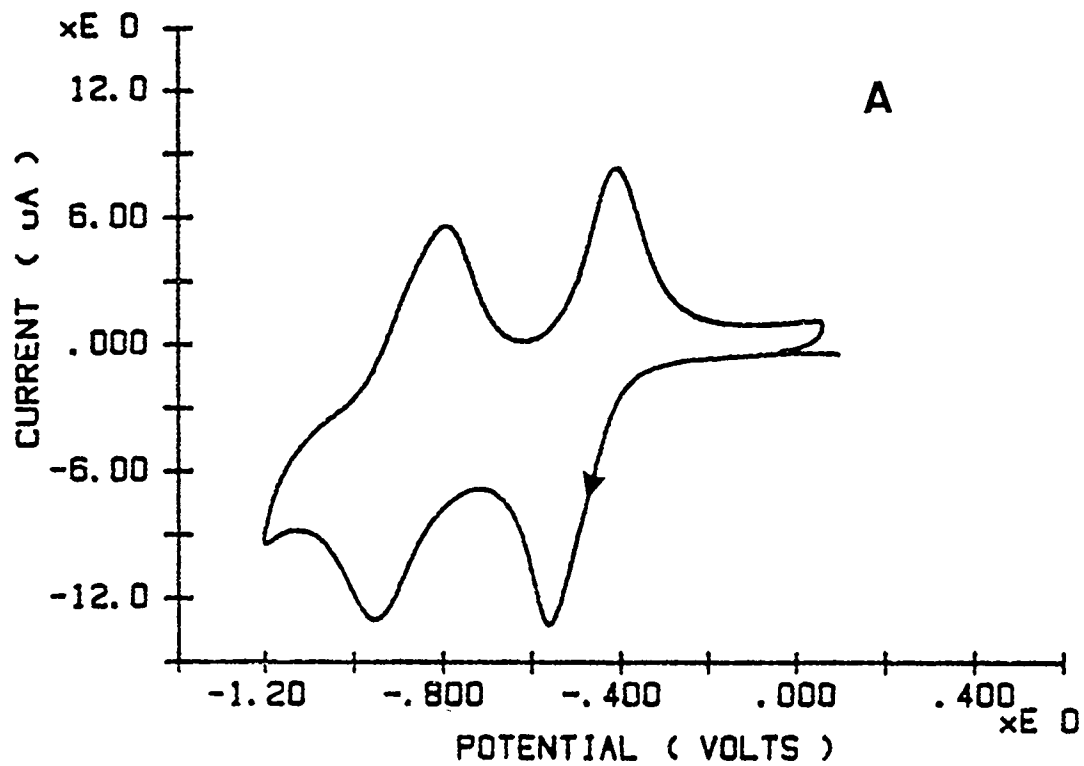
Figure 4.10 a) Voltammogram of N-(n-Octadecyl)-N'-(10-Mercapto decyl)-4,4'-Bipyridinium Dichloride (C18VC10SH) in 0.1M NaCl with a scan rate of 100mV/sec versus SSCE. b) Frequency data.



The frequency plot in figure 4.10 indicates a frequency change of 8.7 Hz per 2 moles of electrons over the course of the potential scan. This amounts to an effective mass change sensed by the EQCM of  $187 \text{ g mole}^{-1}$  which is more than anion transport can account for. Therefore, as in the case of C10VC10SH, solvent is being transported in and out of the layer as well. About  $\sim 8$  molecules of  $\text{H}_2\text{O}$  are lost from the monolayer for every  $\text{Cl}^-$  lost during the reduction process. The mass change is reversible upon reoxidation. This is twice the water transport seen in the C10VC10SH case, The increased solvent transport may be due to the ability of the larger layer (compound II is longer than compound I) to allow more solvent in from larger defects in the layer.

The next anion tested on compound II is perchlorate. As can be seen in figure 4.11, the first redox potential is shifted more negative than in the case of the  $\text{Cl}^-$ . This is due to the previously mentioned ion-pairing in the  $\text{ClO}_4^-$  case. The second redox potential is also shifted more negative than in the  $\text{Cl}^-$  case. Note from the large peak separations of the anodic and cathodic waves that the redox processes seem to be becoming quasi reversible. This is probably indicative of slowed anion transport through the outer layer of the insoluble monolayer. This effect is not as large in the C10VC10SH case as it is in the C18VC10SH case. Therefore, the kinetics for anion transport with

Figure 4.11 a) Voltammogram of N-(n-Octadecyl)-N'-(10-Mercapto decyl)-4,4'-Bipyridinium Dichloride (C18VC10SH) in 0.1M NaClO<sub>4</sub> with a scan rate of 100mV/sec versus SSCE. b) Frequency data.



compound II and slower than for compound I, probably because the outer alkyl chain is twice as large.

The frequency change for the  $\text{ClO}_4^-$  case of compound II is about the same as for compound I, about 5 Hz per 2 moles of electrons. This illustrates that no solvent is transported in and out of the monolayer when  $\text{ClO}_4^-$  is the counterion. Also, the double layer charging in figure 4.11 is smaller than in figure 4.10, as previously shown with compound I. This indicates that the monolayer with  $\text{ClO}_4^-$  is less "leaky" towards penetration of supporting electrolyte than the monolayer with  $\text{Cl}^-$  as the counterion. Therefore, these data indicate that, as with compound I, compound II, with  $\text{ClO}_4^-$  as the counterion, is a much more compact monolayer than with  $\text{Cl}^-$ . The data also suggests that ion-pairing is occurring in the  $\text{ClO}_4^-$  case and not in the  $\text{Cl}^-$  case

In comparing other anion effects with compound II, the data indicate the same trends as in the case of compound I. That is, that the monolayer with  $\text{F}^-$  as the counterion has the most positive formal potential. The order going more negative is  $\text{Cl}^-$ ,  $\text{Br}^-$ , then  $\text{ClO}_4^-$  counterion. Also, monolayers with  $\text{F}^-$  as the counterion have a larger solvent transport than the other counterions, in the same order as above.

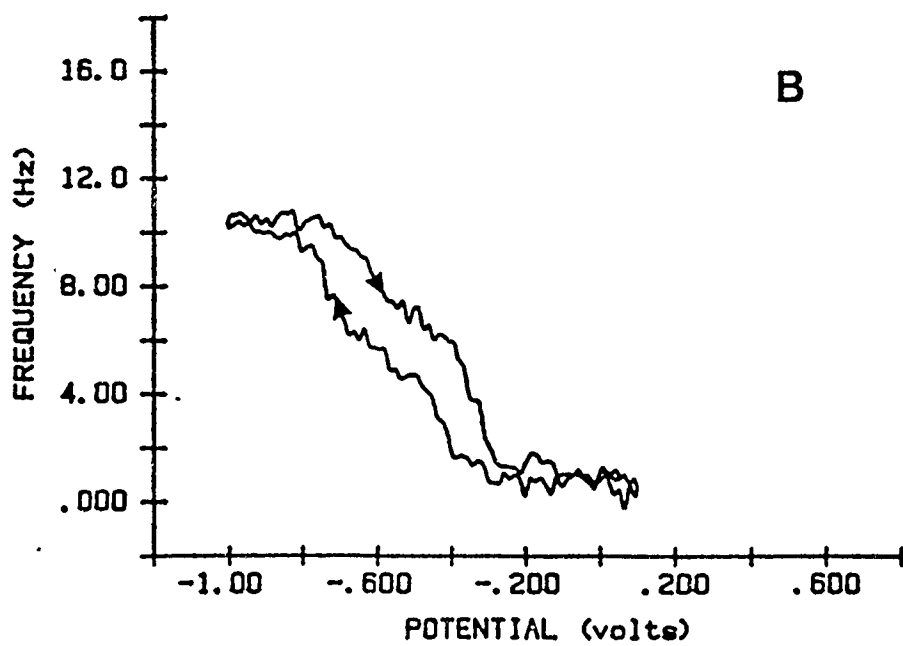
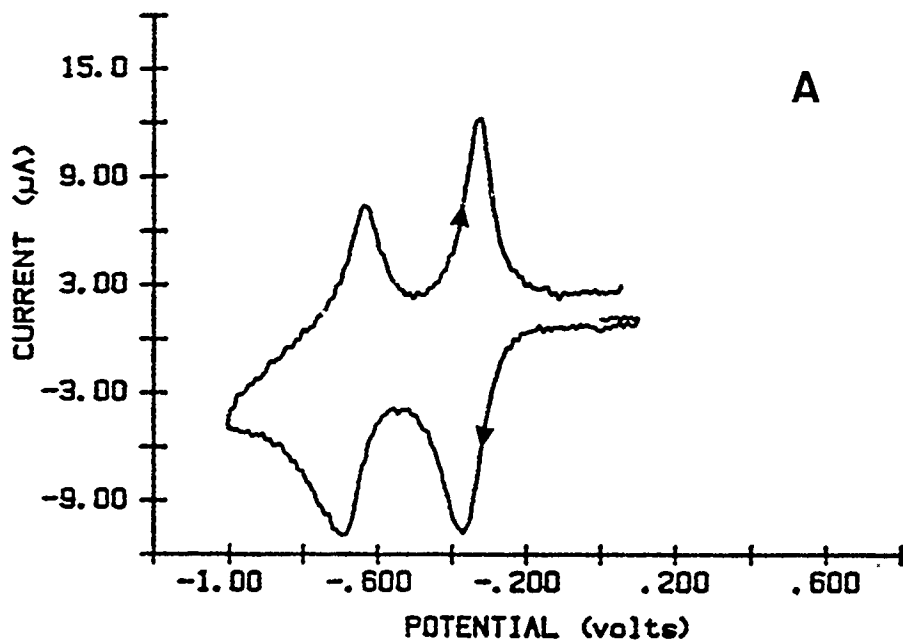
C9C11VC10SH

The third compound examined is C9C11VC10SH (compound III). This compound is unique because of its having two alkyl chains in the outer part of the monolayer towards the solution and one alkyl chain down towards the electrode. This compound was constructed to allow for tightening up the outer half of the monolayer by inducing more order to get a closer packing. The area of the outer chain is actually a little larger than the bipyridyl group and associated anions, so the size of the outer chains should determine the surface coverage if the system is close-packed. Alkyl chains are ca. 18-20 Å<sup>2</sup>, so two alkyl chains are ca. 36-40 Å<sup>2</sup>. This is close to the experimental range below.

The first supporting electrolyte used was 0.1M NaCl (see figure 4.12). The calculated charge from compound III's voltammogram is 40 μC per cm<sup>2</sup>. This amounts to a surface coverage of 4.1x10<sup>-10</sup> moles per cm<sup>2</sup> which gives a molecular area of 39 Å<sup>2</sup> per molecule. This is consistent with what has been previously determined for the other compounds, but the outer chains are responsible unlike the other compounds.

The frequency plot in figure 4.12 indicates that there is a 9.2 Hz per 2 moles of electrons change over the course of the potential scan. This amounts to an effective mass change sensed by the EQCM of 198 g mole<sup>-1</sup>. For every Cl<sup>-</sup> anion transported 9 molecules of water are also transported across the monolayer. This is reversible on the voltammetric

Figure 4.12 a) Voltammogram of N-(10 Heneicosyl)-N'-(10-Mercapto decyl)-4,4'-Bipyridinium Dichloride (C9C11VC10SH) in 0.1M NaCl with a scan rate of 100mV/sec versus SSCE. b) Frequency data.



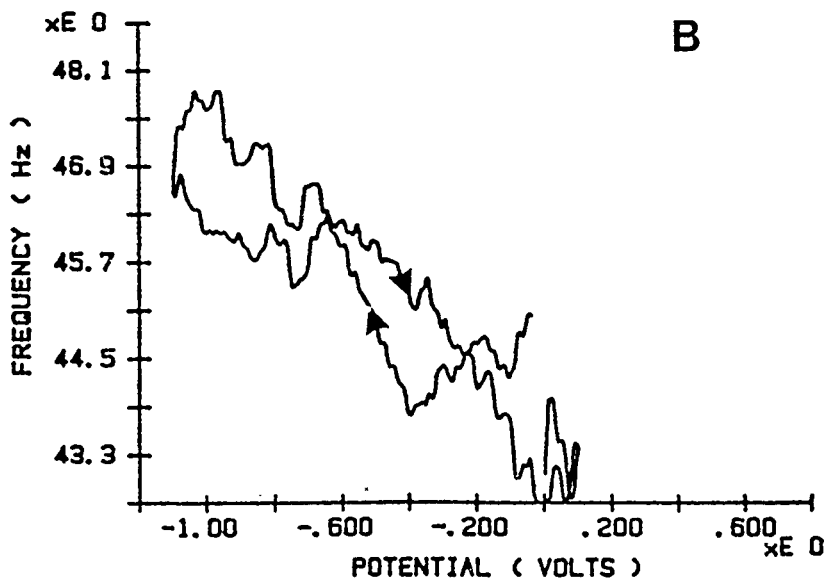
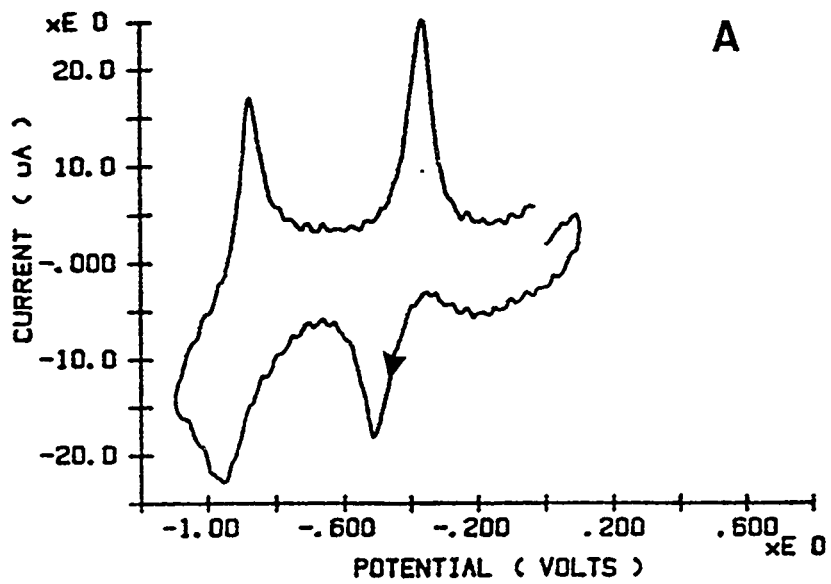
time scale.

The next anion examined was perchlorate. As can be seen in figure 4.13, the two redox potentials are shifted more negative than in the  $\text{Cl}^-$  case. These are the same results as seen with the first two compounds examined. Notice also that the  $\text{ClO}_4^-$  has a large  $\Delta E_p$  (131 mV). This is much larger than the  $\Delta E_p$  (29 mV) for compound I and about the same as for compound II. This is probably due to the kinetics of the first redox event slowing down the rate, again because the anions and solvent are having difficulty getting across ~~the lightly congested outer part of the~~ layer.

In examining the frequency data for the voltammogram in figure 4.13, one can see that the frequency change is on the same order of magnitude as the previous compounds, about 5 Hz per 2 moles of electrons. This is because all of the compounds have relatively the same surface coverages, and, since  $\text{ClO}_4^-$  does not transport water with it, they should all have frequencies proportional to the charges from those surface coverages. This is due to the need for maintaining charge neutrality in the monolayer.

The  $\text{Cl}^-$  waveshapes in figure 4.12 are not as narrow as the  $\text{ClO}_4^-$  waveshapes in figure 4.13. This is consistent with the  $\text{Cl}^-$  and  $\text{ClO}_4^-$  data from compounds I and II. Therefore, ion-pairing seems to be present in the C9C11VC10SH case with  $\text{ClO}_4^-$  and not with  $\text{Cl}^-$ .

Figure 4.13 a) Voltammogram of N-(10 Heneicosyl)-N'-(10-Mercapto decyl)-4,4'-Bipyridinium Dichloride (C9C11VC10SH) in 0.1M NaClO<sub>4</sub> with a scan rate of 100mV/sec versus SSCE. b) Frequency data.



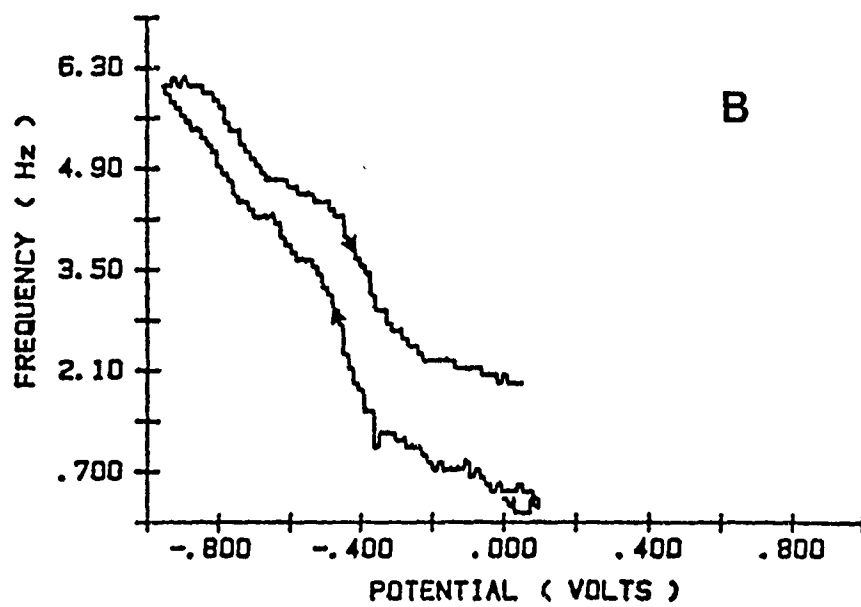
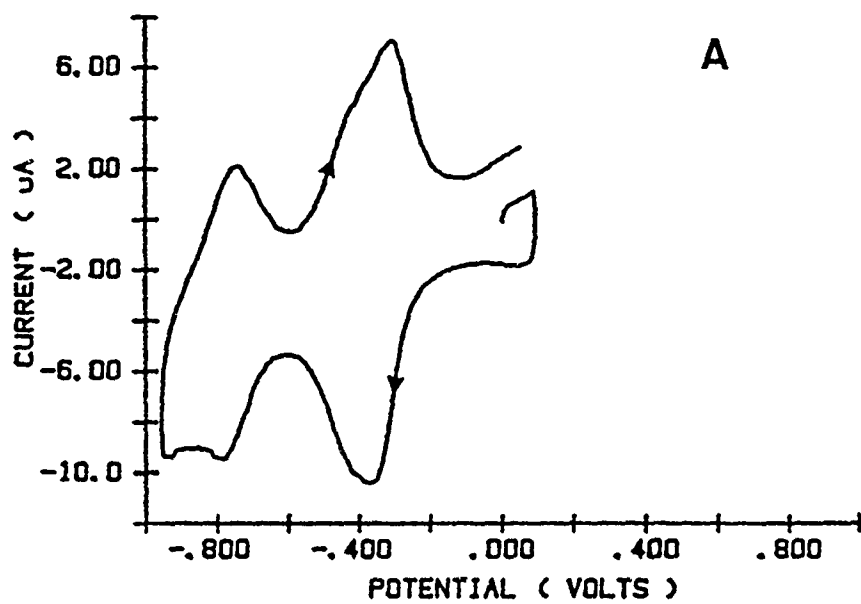
C10VC3SH

Compound V was made to examine what would happen to the redox response of the monolayer if the bipyridyl were placed closer to the electrode surface. The hope was that this compound would help tell whether the free methyl alkyl viologen would adsorb head up or head down<sup>13</sup>. The purpose was to determine if ease of electron transfer to the bipyridyl or anion transport kinetics was the main driving force in determining the redox response of the monolayer.

The first electrolyte used was 0.1M NaCl. The voltammetry in this medium is depicted in figure 4.14. The first thing that is noticeable is that the first redox wave is larger than the second. This may be due to the viologen mostly collapsing to the surface after the first reduction. During the second reduction, the wave shifts and broadens because the anions are trapped outside the layer. Since there is no longer any charge compensating effect, the viologen no longer feels the full driving force of the applied potential. The rest of the bipyridyls then do not reduce<sup>64</sup>.

In examining just the first redox event, the second aspect noticed is that the wave has a shoulder. This was also seen in compound I with Cl<sup>-</sup> and F<sup>-</sup> counterions. It is still not understood why there is a shoulder occurring and

Figure 4.14 a) Voltammogram of N-(n-Decyl)-N'-(3-Mercaptopropyl)-4,4'-Bipyridinium Dichloride (C10VC3SH) in 0.1M NaCl with a scan rate of 100mV/sec versus SSCE. b) Frequency data.



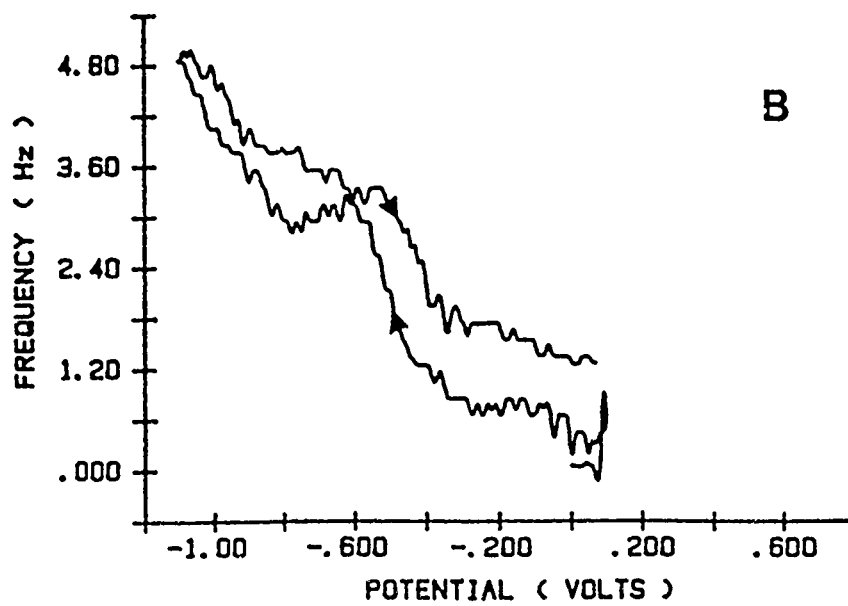
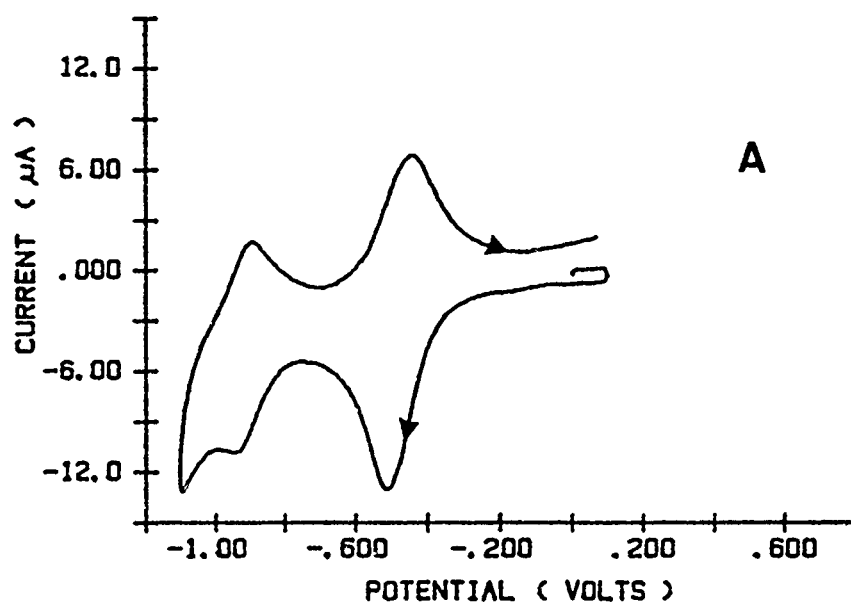
only with the two compounds that have a decyl chain as the outer part of the monolayer.

The frequency data (see figure 4.14) show that most of the solvent transport takes place during the first redox event, and that the overall frequency change is about 5 Hz per 2 moles of electrons. Thus, the magnitude of the frequency change is comparable to C10VC10SH. This is reversible, but shows some hysteresis indicative of slower transport. This slower transport is not present in C10VC10SH with Cl<sup>-</sup> as the counterion.

The next anion examined is ClO<sub>4</sub><sup>-</sup> (see figure 4.15). The same effect is observed with the first redox wave being larger than the second. This is not something that only happens in the Cl<sup>-</sup> case. The potential of these redox events is shifted more negative as in all other compounds when comparing Cl<sup>-</sup> and ClO<sub>4</sub><sup>-</sup> results. The double wave in the first redox couple is gone which is similar to the results of compound I. The ion-pairing effect of ClO<sub>4</sub><sup>-</sup> is noticed by the sharper peak currents, and the capacitive current is smaller than the capacitive current in the Cl<sup>-</sup> case. This indicates that the ClO<sub>4</sub><sup>-</sup> counterion monolayer is more tightly packed and less leaky to solvent and anion transport.

As in all ClO<sub>4</sub><sup>-</sup> compounds examined, the frequency change is comparable, so there is no water being transported. The  $\Delta E_p$  for the ClO<sub>4</sub><sup>-</sup> case versus the Cl<sup>-</sup> case

Figure 4.15 a) Voltammogram of N-(n-Decyl)-N'-(3-Mercaptopropyl)-4,4'-Bipyridinium Dichloride (C10VC3SH) in 0.1M NaClO<sub>4</sub> with a scan rate of 100mV/sec versus SSCE. b) Frequency data.



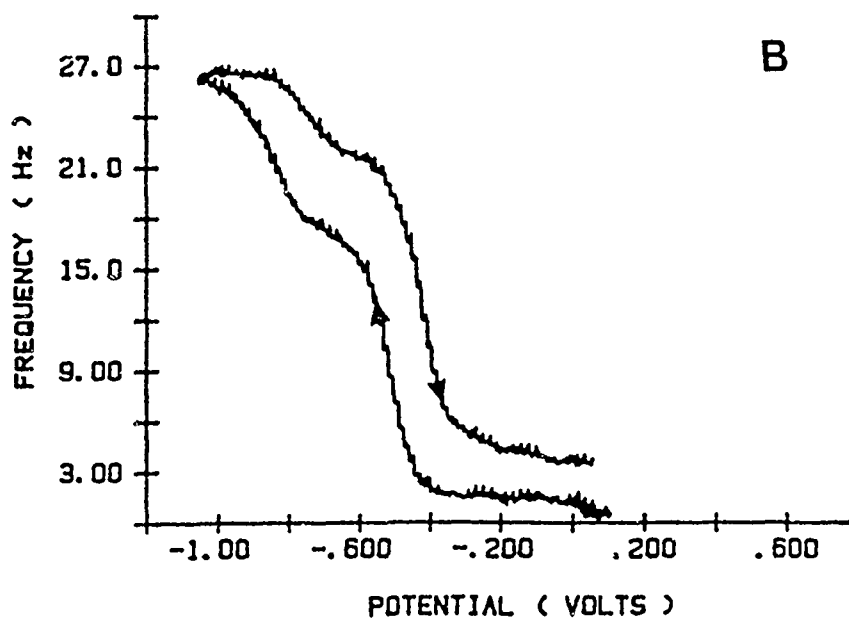
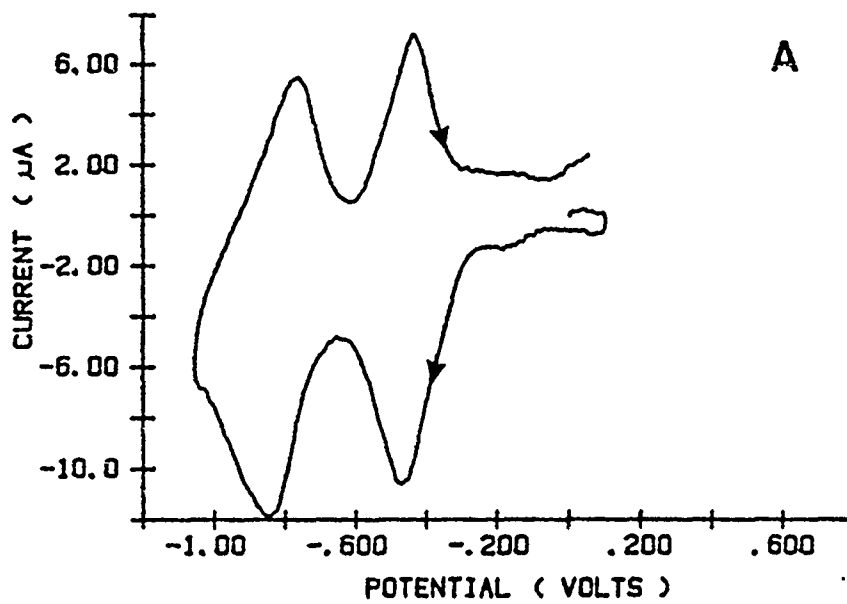
is indicative of the more tightly packed nature of the  $\text{ClO}_4^-$  monolayers compared to the  $\text{Cl}^-$  case. This means that there are kinetic limitations to the redox event in the  $\text{ClO}_4^-$  case.

#### C1VC12SH

Compound VI was synthesized to examine the effect of placing the bipyridyl near the monolayer/solution interface. This is called the head up configuration.

Figure 4.16 contains the voltammogram for C1VC12SH in 0.1M NaCl. In examining the voltammogram, a salient feature is that the waveshapes are very symmetrical and that both redox potentials are shifted more negative than any other compound examined in 0.1M NaCl. The C1VC12SH compounds voltammogram is closer to the formal potential for methyl viologen (first reduction  $E^f = -0.69$  Volts in 50mM NaCl)<sup>57</sup> than any other of the compounds. Since the voltammogram is very symmetric, there does not seem to be any kinetic problems with ion transport as experienced in the C10VC3SH case. The apparent reason that both redox potentials are shifted more negative is that the bipyridyl dication is highly solvated in this compound, so it is stabilized. This makes it harder to reduce to the cation radical. The frequency data also support this. Most of the solvent transport occurs during the first reduction process and not

Figure 4.16 a) Voltammogram of N-Methyl-N'-(12-Mercaptododecyl)-4,4'-Bipyridinium Dichloride (C<sub>1</sub>VC<sub>12</sub>SH) in 0.1M NaCl with a scan rate of 100mV/sec versus SSCE. b) Frequency data.



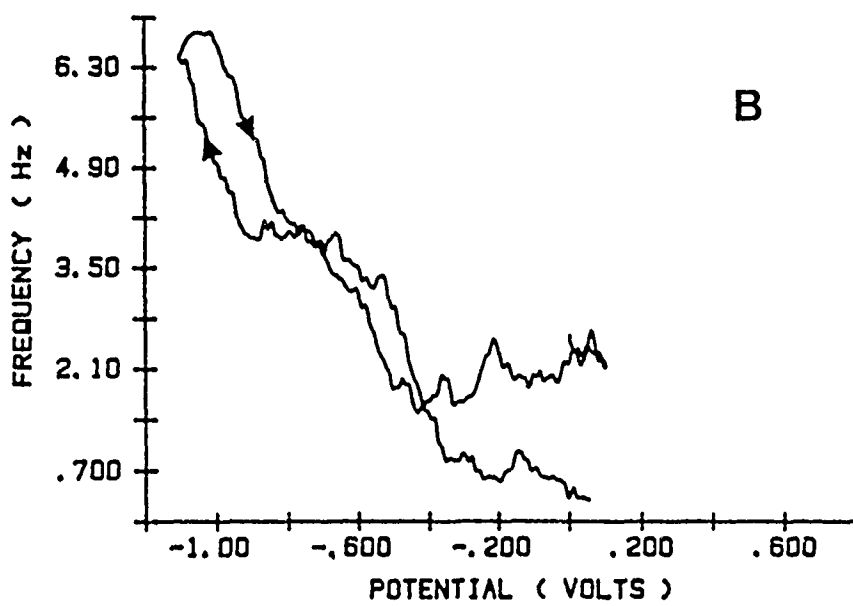
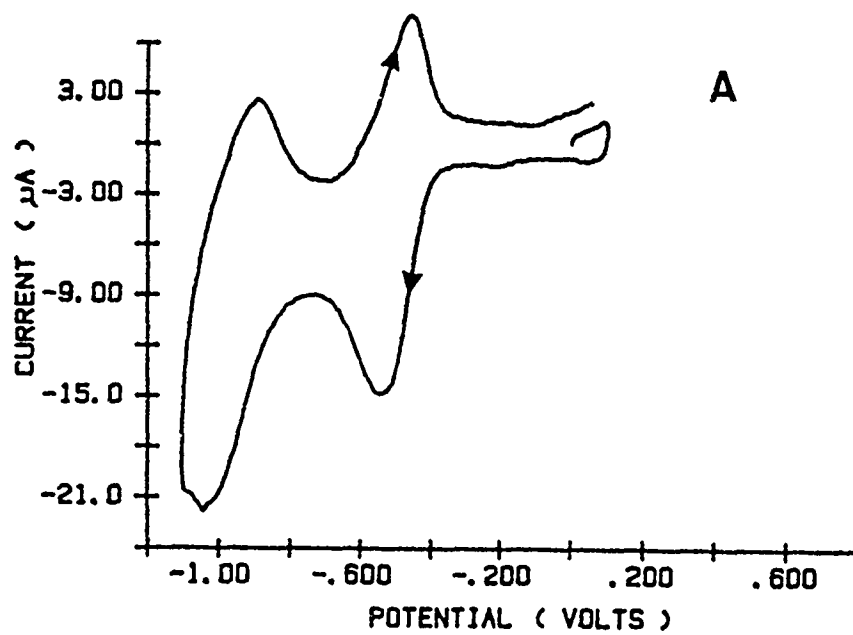
the second reduction process. This indicates that the cation radical is less solvated.

The next anion examined was perchlorate. Figure 4.17 shows that the  $\text{ClO}_4^-$  case is similar to the other compounds in that it is more negative than the  $\text{Cl}^-$  cases. This indicates that perchlorate probably does ion-pair with compound VI also. In examining the frequency change, one notes that it is on the same scale as the other compounds. The film is very hydrophobic so no water is being transported during the redox event. Having the bipyridyl group close to the solution/monolayer interface does not help in solvating the layer when  $\text{ClO}_4^-$  is the counterion. The capacitive current is indicative of the  $\text{ClO}_4^-$  monolayer being a more densely packed, less permeable film than in the  $\text{Cl}^-$  case. This goes along with previously mentioned behavior.

### ION SELECTIVITY

In describing the various anion effects on the different compounds, two anions were intentionally left out. This is because of their totally different effects from the previous anions. The two anions are  $\text{I}^-$  and tetrakis(p-sulfonatophenyl)porphyrin<sup>-4</sup>. What is unique about these anions is their size and their selectivity for the viologen monolayer over other anions. When in a solution of

Figure 4.17 a) Voltammogram of N-Methyl-N'-(12-Mercaptododecyl)-4,4'-Bipyridinium Dichloride (C1VC12SH) in 0.1M NaClO<sub>4</sub> with a scan rate of 100mV/sec versus SSCE. b) Frequency data.



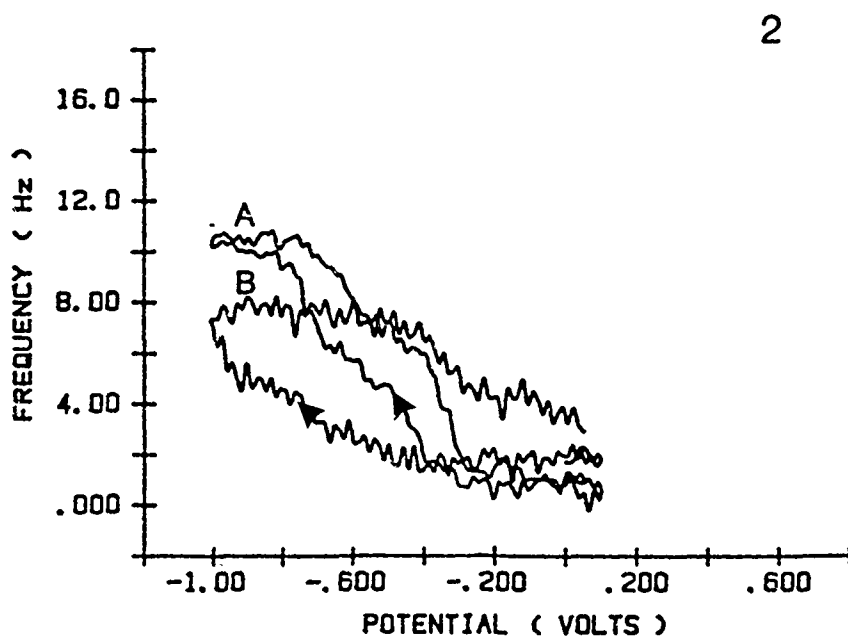
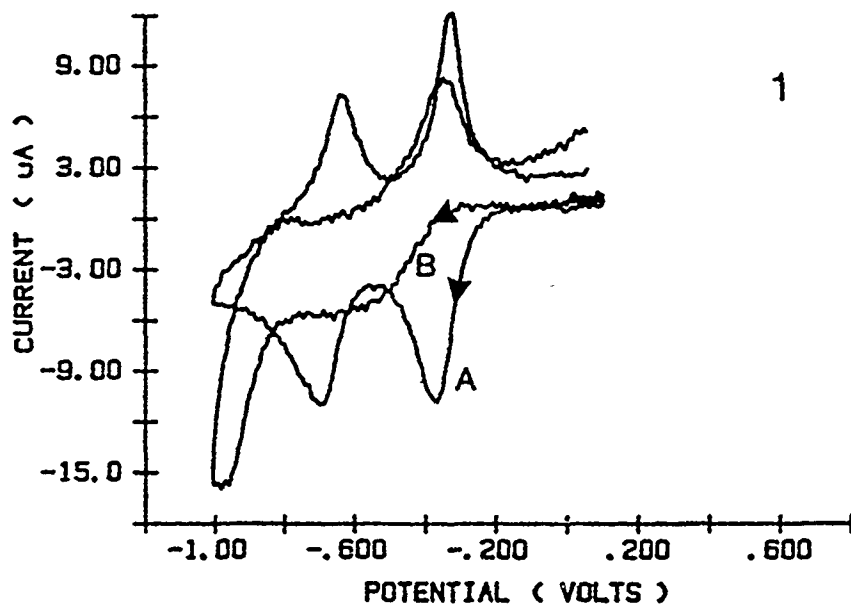
0.1M NaCl they both are favored to bind to the bipyridyl over the Cl<sup>-</sup> counterion even though the Cl<sup>-</sup> is present at a larger concentration.

Figure 4.18 shows a comparison of the behavior in 0.1M NaI and 0.1M NaCl. Notice that in NaCl the monolayer behaves normally as before, but when the monolayer is exposed to NaI something different occurs. The I<sup>-</sup> counterion, once in, does not want to come out. The monolayer does not have the redox waveshape normally expected, because the I<sup>-</sup> transport is inhibited. This could be because the I<sup>-</sup> binds to form a tight ion-pair within the monolayer or the monolayer packs tightly with I<sup>-</sup> which restricts the flow of anions and solvent. The frequency data do indicate that there is some mass flow but due to the broad nature of the wave, it is difficult to determine the charge with accuracy.

The high selectivity toward I<sup>-</sup> binding is evidenced by the following experiment. A small amount of I<sup>-</sup> remained in the cell following a change of supporting electrolyte to Cl<sup>-</sup>. The film had to be repeatedly cycled to get the I<sup>-</sup> to exchange with the Cl<sup>-</sup>. Once the cycling stopped, the small amount of I<sup>-</sup>, in the cell, found its way back into the monolayer even though the Cl<sup>-</sup> was so prevalent. This would seem to indicate a high selectivity for I<sup>-</sup> by the monolayer.

The next anion examined is tetrakis(p-sulfonatophenyl) porphyrin<sup>-4</sup> ( see figure 4.19). The monolayer was examined in 0.1M NaCl and it exhibited the normal electrochemistry.

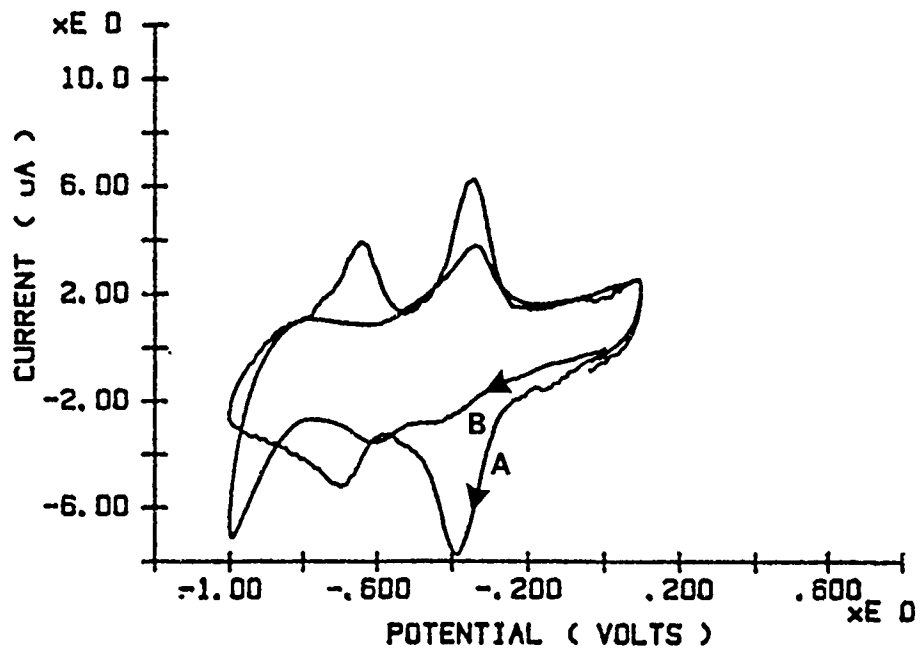
Figure 4.18 1) Voltammograms of N-(10-Heneicosyl)-N'-(10-Mercaptodecyl)-4,4'-Bipyridinium Dichloride (C9C11VC10SH) in a) 0.1M NaCl and in b) 0.1M NaI with a scan rate of 100mV/sec versus SSCE. 2) Frequency data.



a) C9C11VC10SH in .1M NaCl at 100mV/s versus SSCE

b) C9C11VC10SH in .1M NaI at 100mV/s versus SSCE

Figure 4.19 Voltammograms of N-(10-Heneicosyl)-N'-(10-Mercapto decyl)-4,4'-Bipyridinium Dichloride (C9C11VC10SH) in 0.1M NaCl with 0.1mM tetrakis(p-sulfonatophenyl)porphyrin with a scan rate of 100mV/sec versus SSCE. a) 0.1M NaCl b) 0.1M NaCl+0.01M porphyrin



About 1mg of the porphyrin was added to the cell for a concentration of .01M porphyrin. The chloride waveshapes disappeared and only the porphyrin waveshape remained. It looks very much like the waveshape for I<sup>-</sup>. The normal redox process is inhibited and the porphyrin transport is restricted even though the chloride is in greater concentration and four Cl<sup>-</sup>'s have to leave for every porphyrin that enters.

## Conclusion

In summary, one can see that the identity of the anion from the supporting electrolyte has a major influence on the voltammetry of the self assembling viologen redox monolayers described herein. Also, changing the structure of these monolayers has a profound effect on the ion and solvent transport across these redox monolayers. Table 4.4 contains summary data about both structural changes and transport properties.

One can see that ClVC12SH has the most negative  $E^f$  for  $Cl^-$ . This is expected since the bipyridyl is exposed to the solution monolayer interface allowing it to be highly solvated. This stabilizes the dication making it harder to reduce. The rest of the compounds have the bipyridyl buried deeply within the monolayer so it is exposed to a totally different environment. This caused the bipyridyl to be less solvated allowing it to be reduced more easily. Therefore, the  $Cl^-$  data shows that by changing the bipyridyls environment one can greatly effect its' electrochemical response to changing potential. There is some precedent for these environmental effects in the work of Kaifer and Bard<sup>73</sup>. They looked at the effect on the electrochemistry of viologen in the presence of liposomes and micelles, and found that the reduction potentials were influenced by the environment.

## Anion Effect on the Various Viologen Monolayers

	$\text{Cl}^-$		$\text{ClO}_4^-$	
	$E_0, \text{mV}$	$\Delta E_p, \text{mV}$	$E_0, \text{mV}$	$\Delta E_p, \text{mV}$
C1VC12SH	454	33	502	88
C10VC3SH	354	53	478	75
C10VC10SH	305	14	469	29
C18VC10SH	388	49	484	149
C9C11VC10SH	349	36	442	131

Table 4.4 Anion effects on various viologen monolayers in .1M NaCl and .1M NaClO<sub>4</sub>

In examining the  $\text{ClO}_4^-$  data, one can see a completely different result. All of the  $\text{ClO}_4^-$  cases are more negative than the  $\text{Cl}^-$  cases, and all the  $\text{ClO}_4^-$  frequencies are about the same. No solvent is transported in any of them. This is a result of the ion-pairing ability of  $\text{ClO}_4^-$ . Even the C1VC12SH compound has no solvent transport. This is due to the  $\text{ClO}_4^-$  compounds' insoluble nature. So even with the bipyridyl close to the surface, it is in an insoluble, more highly packed monolayer form. This does not allow for solvent transport.

It would seem that there are two effects that demonstratively influence the formal potentials of the redox processes. These are solvation of the bipyridyl and bipyridyl ion-pairing with the counterion. Also, there are several effects which influence the waveshape. Temperature generally broadens it, while ion-pairing sharpens it, and kinetic effects can cause quasi reversibility in these redox processes. Lastly, positioning of the bipyridyl in relationship to the electrode surface and the solution/monolayer interface have a profound influence on their electrochemistry. When the environment of the monolayer changes from the bipyridyl group at the solution/monolayer interface, C1VC12SH, to the bipyridyl group in the middle of the layer, C10VC10SH, there is a 150mV shift in the redox potential. When the anion is changed from fluoride to perchlorate, there is a 150mV shift

in the redox potential. At room temperature the thermal contribution to the peak potential,  $kT$ , is about 25mV. So, one can see that these potential changes are significant and they indicate that the environment at the electrode is quite different from that in the solution.

The self-assembled redox monolayers which we have presented here for the first time can be seen to be excellent systems with which to probe the detailed influence of structural variation on interfacial redox chemistry. The ease of synthesis of these molecules makes them good candidates for studies of the distance dependence of electron transfer, since the redox group may be placed a controllable distance from both the electrode surface and the monolayer/solution interface. Another especially attractive feature of these systems is that the transport of anions across the outer alkyl region of the monolayer serves as a good model for ion transport across bilayers.

## CHAPTER V

### ELECTROCHEMICAL AND QUARTZ CRYSTAL MICROBALANCE STUDIES OF VIOLOGEN DERIVATIVES: ELECTRON-MEDIATED EVENTS

#### Introduction

Monolayers play an important role in the study of redox electrocatalysis<sup>65</sup>. In electrocatalysis, the reduced redox molecule on the surface can reduce some solution phase species that can not get reduced on the bare electrode or reduce at a less favorable potential. Some reactions might be thermodynamically favorable but occur at a slow rate<sup>66</sup>. Others might occur at an acceptable rate but have a large overpotential<sup>37a,67</sup>. These reactions would benefit from having a catalyst. Many different types of molecules, or even the electrode itself, can be a catalyst in electrocatalysis<sup>68</sup>. What is needed in all cases is a lower activation energy pathway that will occur with a high current density. There are several important characteristics of electrocatalysts. These include: the mechanism of catalysis, stability, and the efficiency with which they exchange electrons with the electrode and with

solution phase species.

The main purpose of this part of the dissertation project is to study the fundamental properties which control electron transfer between the electrode and the monolayer, and between the monolayer and solution phase species. Both the distance dependence of the electron transfer rates and the permeability of the monolayer toward solution phase reactants influence the ability of the monolayer to mediate electron transfer between the electrode and the solution. In this study, both issues are addressed to some extent.

Viologens are known for their electrocatalytic properties concerning horse heart ferricytochrome C<sup>5b, 69</sup>. Viologens have also been used as electron transfer mediators for reduction of the spinach ferredoxin-TPN-reductase / triphosphopyridine nucleotide (TPN) system,<sup>70</sup> beef heart ferricytochrome C oxidase<sup>71</sup> and in the use of hydrogen as a reductant of myoglobin, and stellacyanin<sup>5b</sup>. The ferricytochrome C is of the class which has a positive overpotential, but can not get reduced at a gold electrode, because its metal center can not get close enough to the surface, unless there is some modification of the electrode to enable it to do so. This is an example of a species that is thermodynamically favorable, but not kinetically favorable. Use is made of the viologen to act

as an electron-mediator to the metal center of the metalloprotein.

The spinach ferredoxin-TPN-reductase / triphosphopyridine nucleotide (TPN) system is different than the ferricytochrome C system. Electrocatalysis is used to increase the rate of a reaction with the addition of spinach ferredoxin-TPN-reductase. The viologen needs the spinach ferredoxin-TPN-reductase to reduce the TPN at an adequate rate. The authors wanted to substitute an electrochemical route for the known photosynthetic route to help improve the overall rate.

An example of a solution species which has a large negative overpotential is dibromoalkanes. Metallotetraphenylporphyrins were used to electrocatalyze the reduction of a variety of dibromoalkanes<sup>67</sup>. The metallotetraphenylporphyrins are covalently bound to the surface of the electrode and mediate the electron transfer to allow the dibromoalkanes to be reduced at a much smaller negative overpotential. This is an example of the first type of reaction mentioned.

The initial electrocatalytic experiments planned for this study will be ones to test the electron transfer properties of the monolayer films. From the electrochemical and EQCM data collected already, it is known that electron transfer can occur from the electrode surface to the

dicationic bipyridyl which is ten methylene units away from the surface. The next step will be to test the "bimolecular" electron transfer from the reduced bipyridyl to some solution species. Again, the methylene chains will provide a spacer between the bipyridyl and the solution species. This spacer will vary from one to ten methylene units depending on whether compound VI or I and III are used. Compound III was made so as to bring more order to the outer layer to probe the influence of monolayer permeability on this electron transfer.. Compound VI was made to intentionally make it easier for the solution species to reach the bipyridyl for homogeneous electron transfer.

## Experimental

The experimental setup was described in chapter II. The synthesis of the compounds used for self-assembling the monolayers was described in chapter IV. The three compounds used in this study are C10VC10SH (compound I), C9C11VC10SH (compound III), and C1VC12SH (compound VI). All monolayers used in this chapter were self-assembled from 0.1M NaCl and saturation surface coverages were verified using charge calculations from the resulting cyclic voltammograms.

The three solution phase molecules that were used are hexaamineruthenium(III) chloride, hexaaminecobalt(III) chloride, and 1,3,6,8,10,13,16,19-octaazabicyclo [6.6.6] eicosanecobalt trichloride (cobalt(III) sepulchrates trichloride). All are from Aldrich Chemical Company. The  $E^f$ 's are -0.18V, -0.25V (irreversible), and -0.54V, respectively, in .1M HClO<sub>4</sub> verses SSCE.

The monolayers were self-assembled onto the EQCM electrode, then either 0.1M NaCl or 0.1M NaClO<sub>4</sub> was used as the supporting electrolyte during the electron-mediation experiments. One of the three above inorganic compounds was then added to the cell in concentrations ranging from 0.25mM to 1.0mM. All experiments were done with cyclic voltammetry.

## Results and Discussion

The well established reaction scheme for redox electrocatalysis is<sup>65</sup>:



in which  $\text{DAV}^{++}$  is the dialkylviologen dication,  $\text{DAV}^{+\cdot}$  is the dialkylviologen cation radical,  $\text{DAV}^{\circ}$  is the fully reduced dialkylviologen, SP is the solution species, and RSP is the reduced solution species. The second step is rate limiting, and the third step can be as well. This is confirmed by scan rate studies.

All the reactions are downhill with respect to the  $\text{V}^{++}/\text{V}^{+\cdot}$  reduction, since the viologen redox potentials have a greater negative overpotential than the ammine compounds. The exception is the cobalt sepulchrate compound, since it needs the  $\text{V}^{+\cdot}/\text{V}^{\circ}$  reduction to be mediated due to its larger negative overpotential than the  $\text{V}^{++}/\text{V}^{+\cdot}$  reduction.

### Hexaamineruthenium(III) chloride

The first compound investigated was hexaamineruthenium(III) chloride in 0.1M NaCl. The EQCM was coated with a monolayer of C10VC10SH. Figure 5.1 shows the cyclic voltammogram of C10VC10SH mediating the reduction of hexaamineruthenium(III) chloride. The voltammogram shows that the electron-mediation is occurring at the first redox potential and not the second. Since the first redox potential of the viologen is more negative than the formal potential of the ruthenium compound, the above result would be expected. By the time the potential scan reached the second redox potential of the viologen, all of the ruthenium within the diffusion layer is reduced. Therefore, the second waveshape appears normal. With C10VC10SH, the process appears to be reversible on the timescale of the experiment.

C9C11VC10SH was the next monolayer used as the electron-mediator. The EQCM was coated and put in a cell containing 0.1M NaCl as the supporting electrolyte. Figure 5.2 demonstrates the same behavior as found with C10VC10SH. The reduction only occurs at the first redox potential and it has the typical waveshape of an electron-mediated response. If the ruthenium compound were penetrating significantly into the outer layer of either monolayer, one

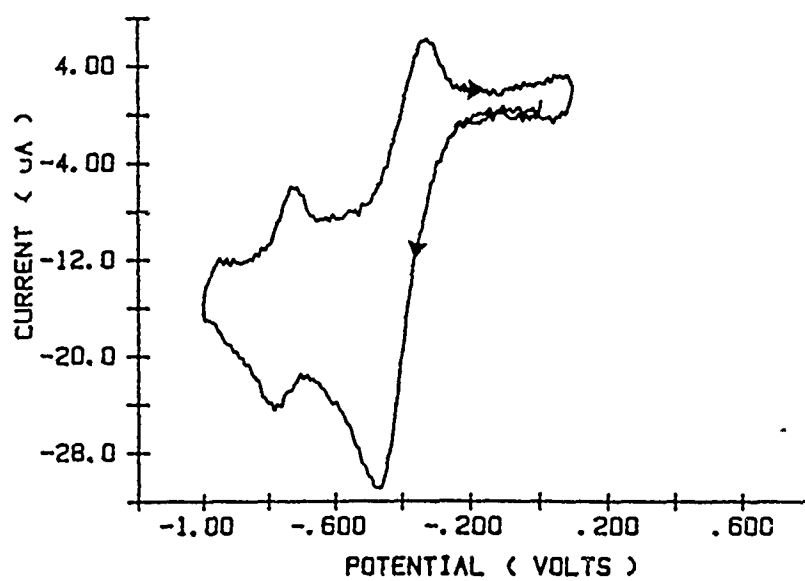


Figure 5.1 Voltammogram of C10VC10SH in 0.1M NaCl with 0.5mM Ru(NH<sub>3</sub>)<sub>6</sub>Cl<sub>3</sub>; scan rate is 100mV/sec versus SSCE.

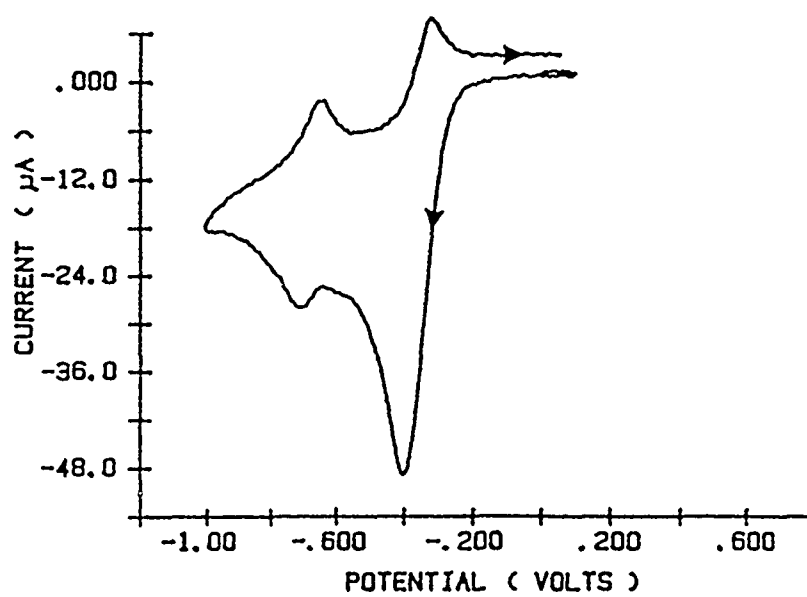


Figure 5.2 Voltammogram of C9C11VC10SH in 0.1M NaCl with 0.75mM  $\text{Ru}(\text{NH}_3)_6\text{Cl}_3$ ; scan rate is 100mV/sec versus SSCE.

would expect considerable differences between the responses of C10VC10SH and C9C11VC10SH. The fact that they are so similar argues for little permeation. The ruthenium mediation is scan rate dependent where most of it is stopped by 1600mV/sec. This seems to argue for mediation, because permeation to the electrode would not be stopped by changing the scan rate. Reduction due to straight permeation, without mediation, would just shift to more negative potentials.

The last compound used to produce a monolayer was C1VC12SH. This monolayer was also examined in 0.1M NaCl as the supporting electrolyte. The results, as shown in figure 5.3, were very similar to the results for C10VC10SH and C9C11VC10SH. It would seem that it does not matter if the bipyridyl is at the solution/monolayer interface or buried within the monolayer, or if the monolayer is constructed to restrict the flow of large ions. The mediation rate appears unaffected by all of these changes. The difference exists in the scan rate data from C9C11VC10SH and C1VC12SH. There is some scan rate dependence of hexaamineruthenium(III) chloride with C1VC12SH, but one can not completely shut down the electron transfer like in the C9C11VC10SH case. This is probably due to the bipyridyl being close to the solution/monolayer interface so no partial permeation is necessary.

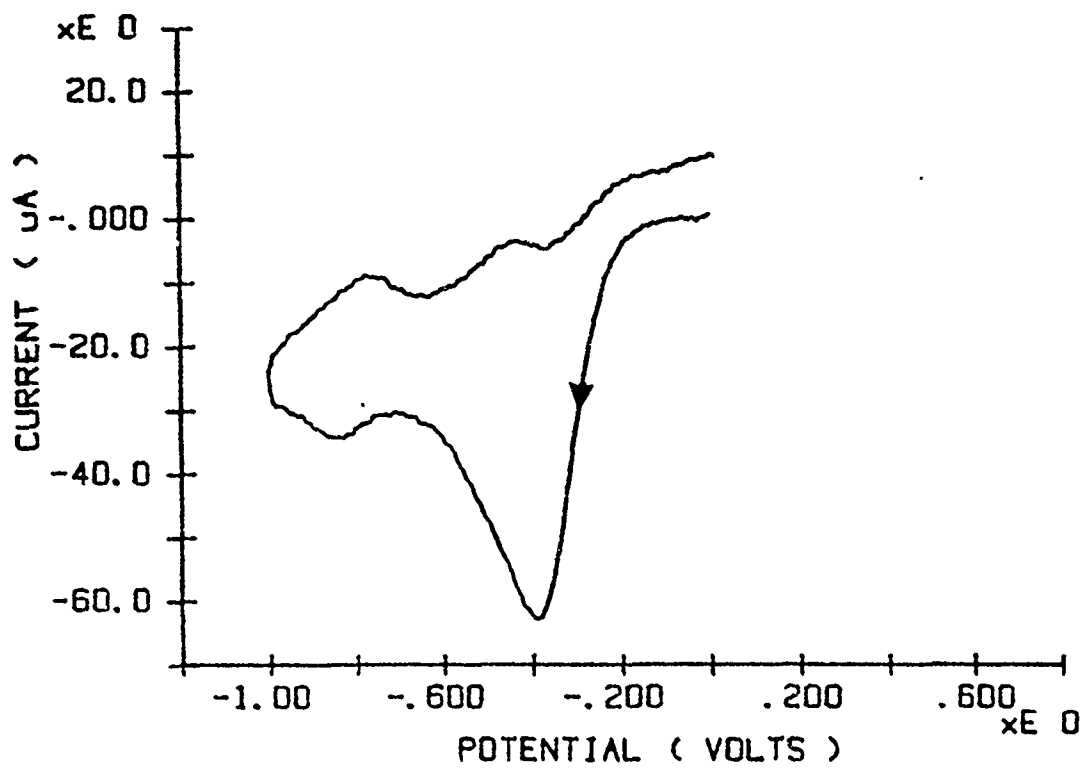


Figure 5.3 Voltammogram of C1VC12SH in 0.1M NaCl with 1.0mM  $\text{Ru}(\text{NH}_3)_6\text{Cl}_3$ ; scan rate is 100mV/sec versus SSCE.

Decanethiol was added to the C1VC12SH to tighten up the lower part of the monolayer. This was done to inhibit any permeation to the electrode surface. Previously, hexanethiol was added to a monolayer of C10VC10SH. This resulted in a more ordered monolayer which allowed for an increase in solvent transport, since more solvent could now exist in the vicinity of the bipyridyl group. The voltammetry was redone on the electron-mediation of hexaamineruthenium(III) chloride with C1VC12SH and no difference from the previous voltammogram was indicated. This seems to indicate that all of the reactions with hexaamineruthenium(III) chloride are diffusion-controlled and that no permeation to the electrode surface is occurring.

#### Hexaaminecobalt(III) chloride

The second solution species investigated is hexaaminecobalt(III) chloride. The first monolayer examined with it is C10VC10SH. Figure 5.4 illustrates the results obtained in 0.1M NaCl as the supporting electrolyte. The cobalt compound has an irreversible reduction potential at -0.25 volts. This is less negative than the first viologen reduction potential. Therefore, one would expect that the electron-mediation should occur at the first redox

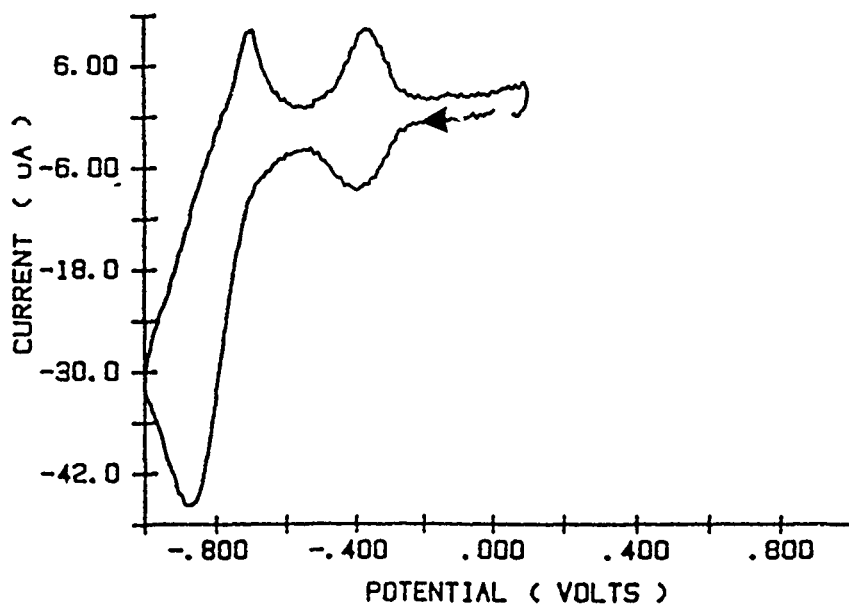


Figure 5.4 Voltammogram of C10VC10SH in 0.1M NaCl with 0.5mM  $\text{Co}(\text{NH}_3)_6\text{Cl}_3$ ; scan rate is 100mV/sec versus SSCE.

potential. This did not occur, and instead the cobalt reduction occurred at the second viologen redox potential. To understand why this would occur, one must look at the self-exchange rate constant for the cobalt compound. Hexaamminecobalt(III) chloride is known to have a very slow self-exchange rate.  $\text{Ru}(\text{NH}_3)_6^{74a}$  has a  $k_{\text{hom}} = 8.0 \times 10^2$  and  $\text{Co}(\text{NH}_3)_6^{74b}$  has a  $k_{\text{hom}} < 10^{-10}$ . Therefore,  $\text{Co}(\text{NH}_3)_6$  needs; a stronger driving force applied to get the electron-mediation to occur at an appreciable rate, there is a distance factor and the cobalt compound needs to get closer to the bipyridyl group than does the isostructural ruthenium compound, or the  $\text{Co}(\text{NH}_3)_6$  has too slow a rate and can never be mediated.

In examining the C9C11VC10SH results in figure 5.5, one sees the same results as for C10VC10SH. So this seems to indicate a lack of any additional perturbation on the cobalt electron-mediation caused by tightening the layer. Of course if the electron transfer occurred via some long range mechanism across the outer layer, then one would not expect any difference in the voltammograms.

C1VC12SH was examined next with the cobalt compound to see if easier access to the bipyridyl would change the potential of the electron-mediation. Figure 5.6 shows that this is not the case. The voltammogram looks quite similar to those for the other monolayers, therefore this would

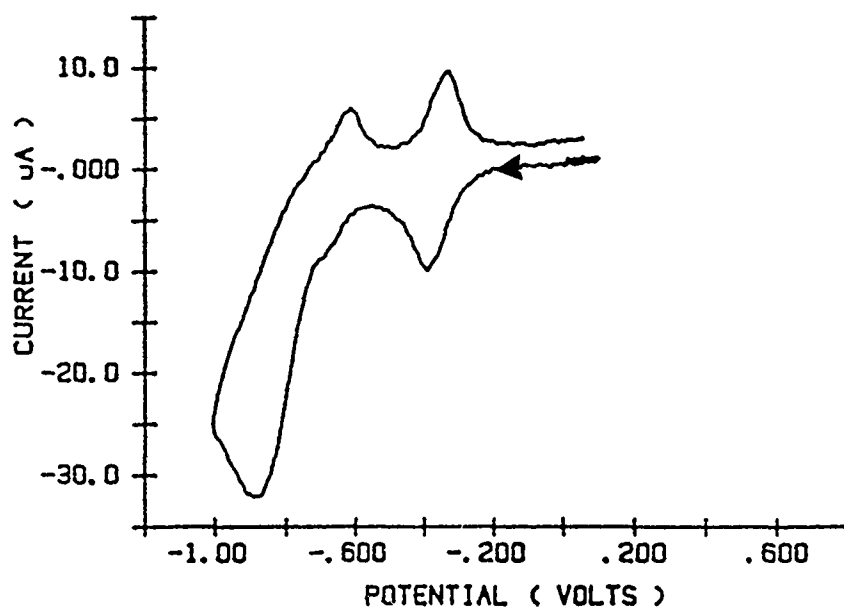


Figure 5.5 Voltammogram of C9C11VC10SH in 0.1M NaCl with 0.75mM  $\text{Co}(\text{NH}_3)_6\text{Cl}_3$ ; scan rate is 100mV/sec versus SSCE.

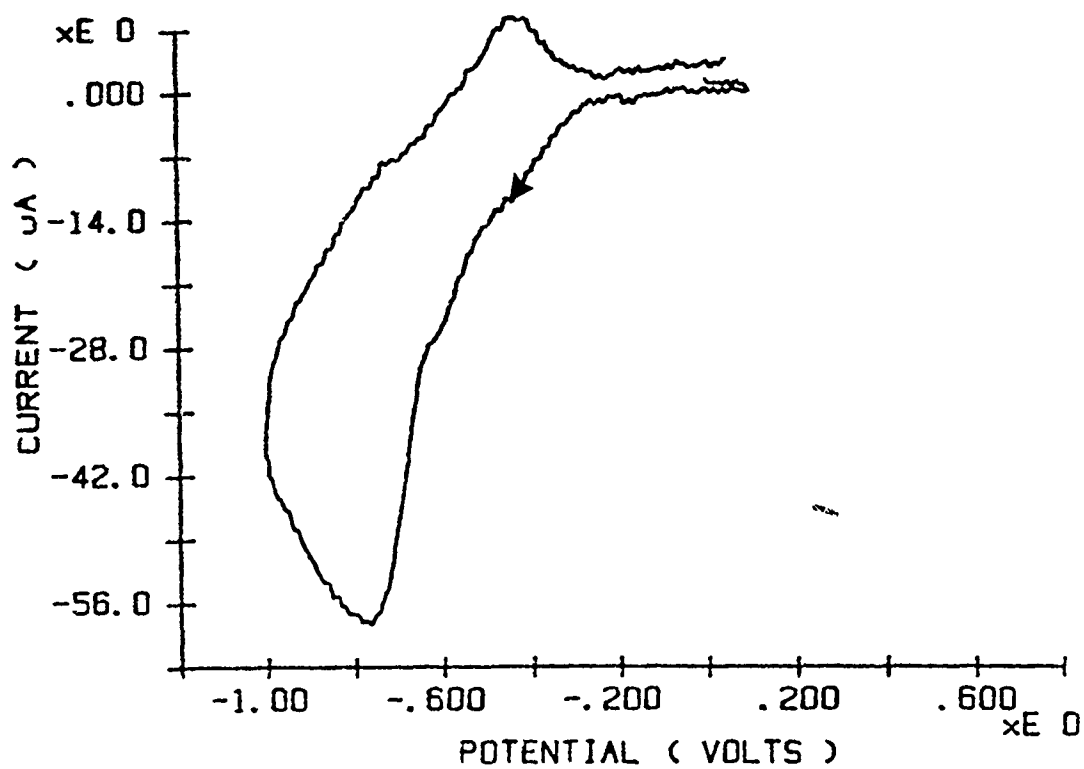


Figure 5.6 Voltammogram of C1VC12SH in 0.1M NaCl with 1.0mM  $\text{Co}(\text{NH}_3)_6\text{Cl}_3$ ; scan rate is 100mV/sec versus SSCE.

seem to rule out any distance effect problems the cobalt compound would have with the bipyridyl. It would seem that we are left with either the long range mechanism or that the electron-mediation is not taking place at all, but instead the cobalt is permeating through the layer and getting to the electron surface.

#### Cobalt(III) sepulchrates trichloride

The cobalt (III) sepulchrates trichloride is used so that if there is any problems with diffusion of the hexamine compounds into the outer layer of the viologen, its large size should prevent it from doing the same. The monolayer was C10VC10SH in 0.1M NaCl. Figure 5.7 shows the voltammetric results of the electron-mediation. The cobalt sepulchrates is mediated at the second redox potential of the viologen like the earlier cobalt compound. This was expected, since the formal potential of the cobalt sepulchrates is between the two redox potentials of the viologen monolayer. Therefore, as with the ruthenium compound earlier, the sepulchrates compound behaved normally.

C9C11VC10SH was examined next in 0.1M NaClO<sub>4</sub> as the supporting electrolyte. The voltammogram in figure 5.8 looks very similar to the voltammogram for C10VC10SH in

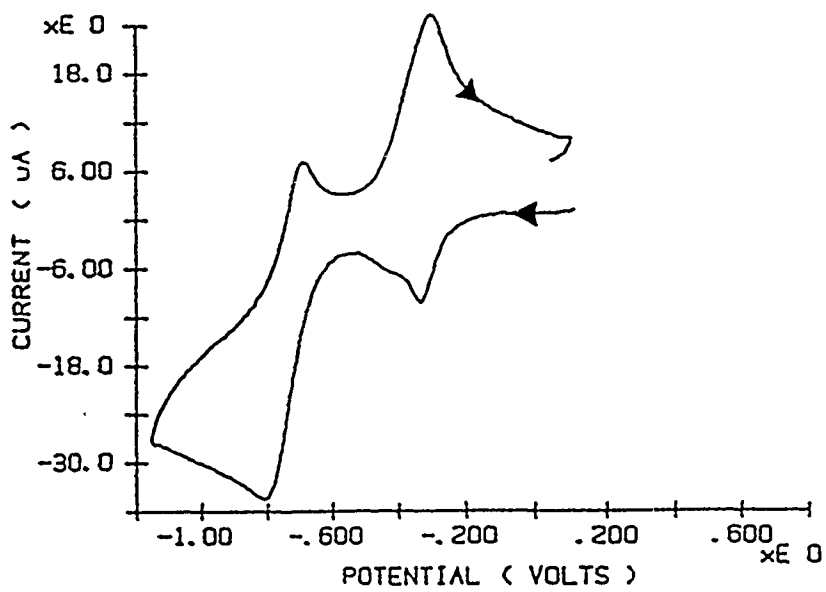


Figure 5.7 Voltammogram of C10VC10SH in 0.1M NaCl with 0.5mM CoSepCl<sub>3</sub>; scan rate is 100mV/sec versus SSCE.

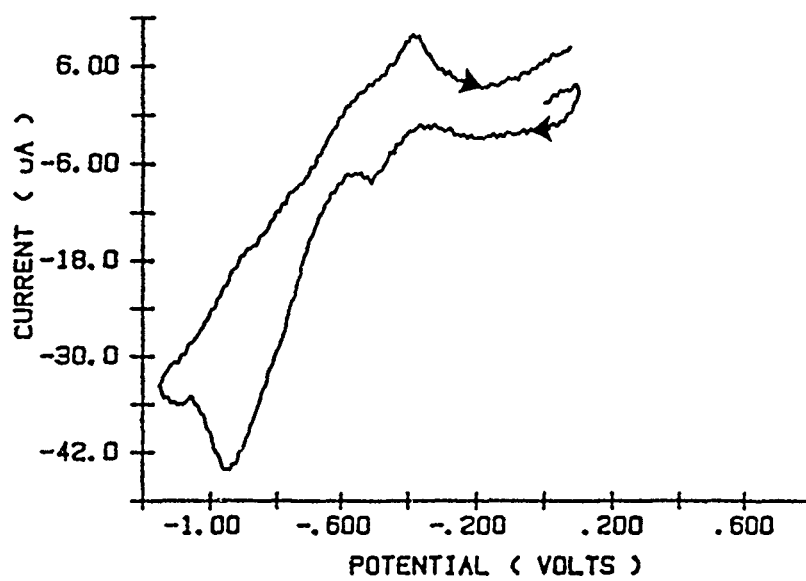


Figure 5.8 Voltammogram of C9C11VC10SH in 0.1M NaClO<sub>4</sub> with 0.75mM CoSepCl<sub>3</sub>; scan rate is 100mV/sec versus SSCE.

0.1M NaCl. It would seem that changing the monolayer to more tightly packed has made no difference in the voltammetric response. Changing the electrolyte to  $\text{ClO}_4^-$  (one that makes the monolayer more insoluble and, therefore, more collapsed), also has made no change. This would seem to indicate that the cobalt sepulchrate is not permeating through defects formed after reduction, because collapsing the film by changing the electrolyte did not effect the voltammetry. The reverse mediation ( $\text{Co}^{2+} + \text{V}^{2+} \rightarrow \text{Co}^{3+} + \text{V}^{+}$ ) is not apparent, as it is in the C10VC10SH with  $\text{Cl}^-$ .

#### Permeation Effects

Finally, consider all of the previous voltammograms of this electron-mediation. None of the eight figures shown in this chapter show any electrochemical response at the normal formal potentials for the three inorganic compounds whose mediation is being studied. Therefore, no permeation is taking place by the inorganic cations before the viologen monolayers are being reduced.

A permeation study was done with dimethylaminomethyl ferrocene. After a C10VC10SH monolayer was formed, this compound was added before and after hexaminecobalt(III) chloride was added for electron-mediation. Figure 5.9 shows

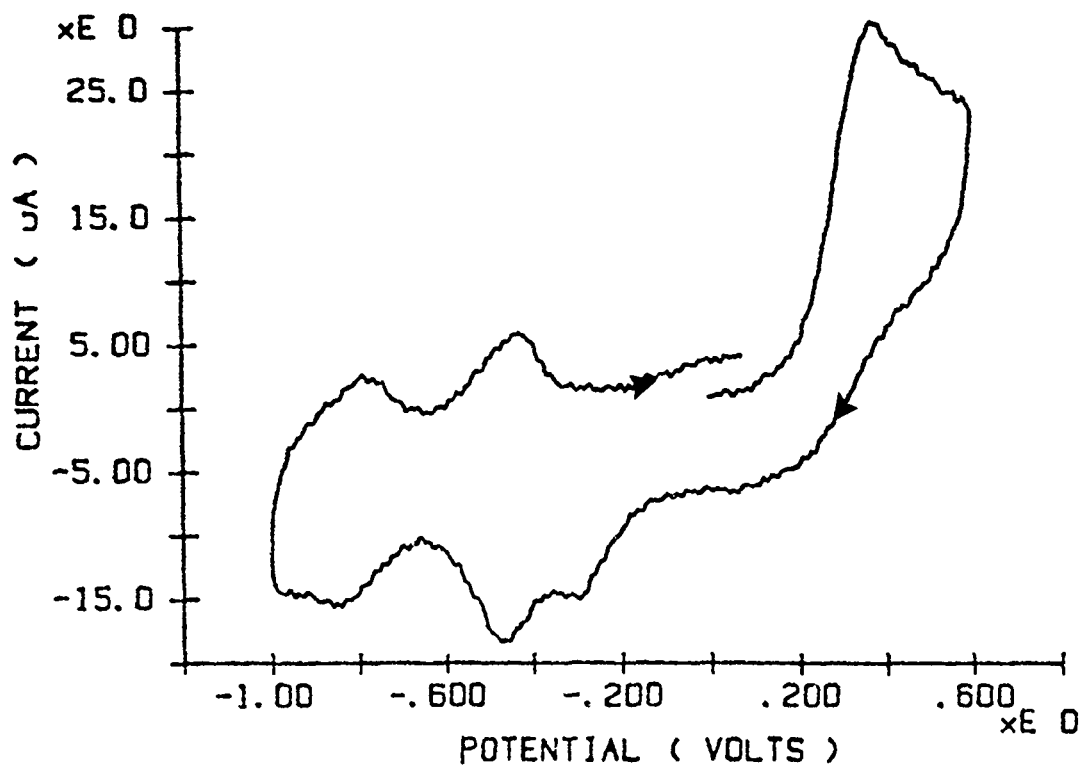


Figure 5.9 Voltammogram of  $\text{ClOVCIOSH}$  in  $0.1\text{M NaCl}$  with added dimethylaminomethylferrocene; scan rate is  $100\text{mV/sec}$  versus SSCE.

that the uncharged ferrocene compound permeated into the layer to the surface and was oxidized. The large response at the ferrocene/ferricinium wave indicates that neutral ferrocene freely permeates. Thus, there must be considerable free volume in the layer. The reduction of the ferrocene could not take place in the layer, though, since it now was charged. The reduction of the ferrocene had to be mediated by the bipyridyl. This seems to indicate that charged species would have a hard time getting into the layer, but not uncharged ones.

### Conclusion

In reviewing the data on the two ammine compounds, one must remember that they are isostructural. The only difference between them is the different metal center, yet they have completely different electrochemistry.

$\text{Ru}(\text{NH}_3)_6\text{Cl}_3$  is electron mediated, but  $\text{Co}(\text{NH}_3)_6\text{Cl}_3$  is not. Scan rate data indicates that the  $\text{Co}(\text{NH}_3)_6\text{Cl}_3$  permeates through the monolayer to be reduced at the electrode surface. Electrostatics keep the compounds from diffusing through the layer as long as the bipyridyls are still charged. Since  $\text{Co}(\text{NH}_3)_6\text{Cl}_3$  has too slow a self-exchange to cross react with the bipyridyl, it must wait until the viologen monolayer is reduced to  $\text{V}^0$  to overcome electrostatics problems. In the case of the C1VC12SH monolayer, it must be more permeable so  $\text{Co}(\text{NH}_3)_6\text{Cl}_3$  can get through during the  $\text{V}^{2+}/\text{V}^+$  reduction.

This illustrates that an electrode is not the same as a molecule with the same potential. For  $\text{Co}(\text{NH}_3)_6\text{Cl}_3$  to react with the viologen monolayer, a bimolecular reaction has to be able to take place. Not so with an electrode, it is always activated. If the viologen were not there,  $\text{Co}(\text{NH}_3)_6\text{Cl}_3$  would reduce on the bare electrode.

Viologen monolayers would seem to be good electron-mediators. The data suggest that electron-meditation is occurring and that it is possible to use monolayers for

this purpose. The results are somewhat ambiguous, in that the identity of the rate-limiting step for mediation is somewhat unclear. Rotating disk experiments will be done in the future to help elucidate this point.

## REFERENCES

(1) a) Wasserman, S. R.; Tao, Y.-T.; Whitesides, G. M. *Langmuir* 1989, 5, 1074-1087. b) Sagiv, J. *J. Am. Chem. Soc.* 1980, 102, 92-98. c) Tillman, N.; Ulman, A.; Penner, T. L. *Langmuir* 1989, 5, 101-111.

(2) a) Nuzzo, R. G.; Allara, D. L. *J. Am. Chem. Soc.* 1983, 105, 4481-4483. b) Porter, M. D.; Bright, T. B.; Allara, D. L.; Chidsey, C. E. D. *J. Am. Chem. Soc.* 1987, 109, 3559-3568. c) Nuzzo, R. G.; Fusco, F.; Allara, D. L. *J. Am. Chem. Soc.* 1987, 109, 2358-2368. d) Troughton, E. B.; Bain, C. D.; Whitesides, G. M.; Nuzzo, R. G.; Allara, D. L.; Porter, M. D. *Langmuir* 1988, 4, 365-385. e) Bain, C. D.; Troughton, E. B.; Tao, Y.-T.; Evall, J.; Whitesides, G. M.; Nuzzo, R. G. *J. Am. Chem. Soc.* 1989, 111, 321-35. f) Bain, C. D.; Evall, J.; Whitesides, G. M. *J. Am. Chem. Soc.* 1989, 111, 7155-7164.

(3) De Long, H. C.; Buttry, D. A., unpublished results.

(4) Fischer, A. B.; Wrighton, M. S.; Umana, M.;

Murray, R. W. *J. Am. Chem. Soc.* 1979, 101, 3442-3446.

(5) a) Wrighton, M. S.; Palazzotto, M. C.; Bocarsly, A. B.; Bolts, J. M.; Fischer, A. B.; Nadjro, L. *J. Am. Chem. Soc.* 1978, 100, 7264-7271. b) Bookbinder, D. C.; Lewis, N. S.; Wrighton, M. S. *J. Am. Chem. Soc.* 1981, 103, 7656-7659. c) Dominey, R. N.; Lewis, N. S.; Bruce, J. A.; Bookbinder, D. C.; Wrighton, M. S. *J. Am. Chem. Soc.* 1982, 104, 467-482. d) Simon, R. A.; Mallouk, T. E.; Daube, K. A.; Wrighton, M. S. *Inorg. Chem.* 1985, 24, 3119-3126.

(6) a) Langmuir, I. *J. Am. Chem. Soc.* 1917, 39, 1848-1906. b) Blodgett, K. B. *J. Am. Chem. Soc.* 1935, 57, 1007-1022. c) Blinov, L. M. *Russ. Chem. Rev.* 1988, 52, 713-735. d) Mohwald, H. *Angew. Chem. Int. Ed. Engl. Adv. Mater.* 1988, 27, 728-734.

(7) a) Maoz, R.; Sagiv, J. *J. Colloid Interface Sci.* 1984, 100, 465-496. b) Gun, J.; Iscovici, R.; Sagiv, J. *J. Colloid Interface Sci.* 1984, 101, 201-213. c) Gun, J.; Sagiv, J. *J. Colloid Interface Sci.* 1986, 112, 457-472. d) Maoz, R.; Sagiv, J. *Thin Solid Films* 1985, 132, 135-157. e) Cohen, S. R.; Norman, R.; Sagiv, J. *J. Phys. Chem.* 1986, 90, 3054-3056. f) Maoz, R.; Sagiv, J. *Langmuir* 1987, 3, 1045-1051.

(8) a) Nuzzo, R. G.; Zegarski, B. R.; Dubois, L. H. *J. Am. Chem. Soc.* 1987, 109, 733-40. b) Dubois, L. H.; Zegarski, B. R.; Nuzzo, R. G. *Proc. Natl. Acad. Sci. USA*

1987, 84, 4739-4742. c) Allara, D. L.; Hebard, A. F.; Padden, F. J.; Nuzzo, R. G.; Falcone, D. R. *J. Vac. Sci. Technol. A*, 1983, 1, 376-382. d) Strong, L.; Whitesides, G. M. *Langmuir* 1988, 4, 546-558. e) Bain, C. D.; Whitesides, G. M. *Science* 1988, 240, 62-63. f) Bain, C. D.; Whitesides, G. M. *J. Am. Chem. Soc.* 1988, 110, 3665-3666. g) Bain, C. D.; Whitesides, G. M. *Langmuir* 1989, 5, 1370-1378. h) Laibinis, P. E.; Hickman, J. J.; Wrighton, M. S.; Whitesides, G. M. *Science* 1989, 245, 845-847. i) Bain C. D.; Biebyck, H. A.; Whitesides, G. M. *Langmuir* 1989, 5, 723-727.

(9) a) Buttry, D. A.; Nordyke, L.; Donohue, J. In *Chemically Modified Surfaces in Science and Industry*; Leyden, D., Collins, W., Eds.; Gordon and Breach; New York, 1988; p377-391. b) Donohue, J. J.; Buttry, D. A. *Langmuir* 1989, 5, 671-678.

(10) Widrig, C. A.; Majda, M. *Langmuir* 1989, 5, 689-695.

(11) Fischer, A. B.; Kinney, J. B.; Stanley, R. H.; Wrighton, M. S. *J. Am. Chem. Soc.* 1979, 101, 6501-6506.

(12) Willman, K. W.; Murray, R. W. *J. Electroanal. Chem.* 1982, 133, 211-31.

(13) Widrig, C. A.; Majda, M. *Anal. Chem.* 1987, 59, 754-760.

(14) a) Bookbinder, D. C.; Bruce, J. A.; Dominey, R. N.; Lewis, N. S.; Wrighton, M. S. *Proc. Natl. Acad. Sci. USA*

1980, 77, 6280-6284. b) Bookbinder, D. C.; Wrighton, M. S. *J. Am. Chem. Soc.* 1980, 102, 5123-5125.

(15) a) Ghosh, P. K.; Spiro, T. G. *J. Am. Chem. Soc.* 1980, 102, 5543-5549. b) Ghosh, P. K.; Spiro, T. G. *J. Electrochem. Soc.* 1981, 128, 1281-1287.

(16) Abruña, H. D.; Meyer, T. J.; Murray, R. W. *Inorg. Chem.* 1979, 18, 3233-40.

(17) a) Koval, C. A.; Anson, F. C. *Anal. Chem.* 1978, 50, 223-229. b) Oyama, N.; Anson, F. C. *J. Am. Chem. Soc.* 1979, 101, 1634-1635.

(18) Donohue, J. J. Ph.D. Thesis, University of Wyoming, 1989.

(19) Weaver, M. J.; Li, T. T. *J. Phys. Chem.* 1986, 90, 3823-3829.

(20) Bunding Lee, K. A.; Mowry, R.; McLennan, G.; Finklea, H. O. *J. Electroanal. Chem.* 1988, 246, 217-224.

(21) a) Diem, T.; Czajka, B.; Weber, B.; Regen, S. L. *J. Am. Chem. Soc.* 1986, 108, 6094-6095. b) Fabianowski, W.; Coyle, L. C.; Weber, B. A.; Granata, R. D.; Castner, D. G.; Sadownik, A.; Regen, S. L. *Langmuir* 1989, 5, 35-41.

(22) a) Lennox, J. C.; Murray, R. W. *J. Am. Chem. Soc.* 1978, 100, 3710-3714. b) Jester, C. P.; Rocklin, R. D.; Murray, R. W. *J. Electrochem. Soc.* 1980, 127, 1979-1985. c) Rocklin, R. D.; Murray, R. W. *J. Phys. Chem.* 1981, 85, 2104-2112.

(23) a) Smith, D. F.; Willman, K.; Kuo, K.; Murray, R. W. *J. Electroanal. Chem.* 1979, 95, 217-227. b) Finklea, H. O.; Robinson, L. R.; Blackburn, A.; Richter, B.; Allara, D.; Bright, T. *Langmuir* 1986, 2, 239-244. c) Sabatini, E.; Rubinstein, I. *J. Phys. Chem.* 1987, 91, 6663-6669. d) Sabatini, E.; Rubinstein, I.; Maoz, R.; Sagiv, J. *J. Electroanal. Chem.* 1987, 219, 365-371.

(24) Hickman, J. J.; Zou, C.; Ofer, D.; Harvey, P. D.; Wrighton, M. S.; Laibinis, P. E.; Bain, C. D.; Whitesides, G. M. *J. Am. Chem. Soc.* 1989, 111, 7271-7272.

(25) Czanderna, A. W.; Lu, C. In *Applications of Piezoelectric Quartz Crystal Microbalances. Methods and Phenomena, Vol. 7*; Lu, C., Czanderna, A. W., Eds.; Elsevier: New York, 1984; p1.

(26) Janata, J. *Principles of Chemical Sensors*; Plenum Press: New York, 1989, p55.

(27) Buttry, D. A. In *Electroanalytical Chemistry*; Bard, A. J., Ed.; Marcel Dekker: New York, Vol. 17, in press.

(28) Sauerbrey, G. *Zeitschrift für Physik* 1959, 155, 206-22.

(29) Bruckenstein, S.; Shay, M. *J. Electroanal. Chem.* 1985, 188, 131-36.

(30) Deakin, M. R.; Li, T. T.; Melroy, O. R. *J. Electroanal. Chem.* 1988, 243, 343-50

(31) Melroy, O.; Kanazawa, K.; Gordon, J. G.; Buttry, D. *Langmuir* 1987, 2, 697-700.

(32) Deakin, M. R.; Melroy, O. R. *J. Electroanal. Chem.* 1988, 239, 321-31.

(33) a) Facci, J. S.; Falcigno, P. A.; Bold, J. M. *Langmuir* 1986, 2, 732-38. b) Facci, J. S. *Langmuir* 1987, 3, 525-30.

(34) a) Miller, C. J.; Widrig, C. A.; Charych, D. H.; Majda, M. J. *Phys. Chem.* 1988, 92, 1928-36. b) Gross, C. A.; Miller, C. J.; Majda, M. J. *Phys. Chem.* 1988, 92, 1937-42. c) Bourdillon, C.; Majda, M. J. *Am. Chem. Soc.* 1990, 112, 1795-99.

(35) Lenhard, J. R.; Murray, R. W. *J. Am. Chem. Soc.* 1978, 100, 7870-75.

(36) Fischer, A. B.; Bruce, J. A.; McKay, D. R.; Maciel, G. E.; Wrighton, M. S. *Inorg. Chem.* 1982, 21, 1766-71.

(37) a) Murray, R. W.; Ewing, A. G.; Durst, R. A. *Anal. Chem.* 1987, 59, 379A-90A. b) Murray, R. W. *Acc. Chem. Res.* 1980, 13, 134-41.

(38) Bain, C. D.; Whitesides, G. M. *Angew. Chem. Int. Ed. Engl. Adv. Mater.* 1989, 28, 506-12.

(39) Muir, N. E. *J Organometal. Chem.* 1981, 208, C9-C11.

(40) Sheats, J. E.; Rausch, M. D. *J. Org. Chem.* 1970,

35, 3245-3249.

(41) Bain, C. D.; Whitesides, G. M. *J. Am. Chem. Soc.* 1989, 111, 7164-7175.

(42) a) Antropov, L. *Theoretical Electrochemistry*; MIR Publishers: Moscow, 1972; p259-262. b) Goodisman, J. *Electrochemistry: theoretical foundations, quantum and statistical mechanics, thermodynamics, the solid state*; John Wiley & Sons: New York, 1987; p74-75. c) Schmickler, W. *Ber. Bunsenges. Phys. Chem.* 1988, 92, 1203-1209. d) Schuhmann, D. *Electrochim. Acta* 1989, 34, 1889-1893, and references therein.

(43) Bard, A. J.; Faulkner, L. R. *Electrochemical Methods*; John Wiley & Sons: New York, 1980, p.488-552.

(44) *Fundamentals of Quartz Crystal Oscillators*, AN200-2, Hewlett-Packard Co.

(45) Buttry, D. A. In *In situ Characterization of the Electrode Solution Interface*; Abruña, H., Ed.; VCH Verlag Chemical: New York, in press.

(46) Lu, L.; Lewis, O. *J. Appl. Phys.* 1972, 43, 4385-

(47) Varineau, P.; Buttry, D. A. *J. Phys. Chem.* 1987, 91, 1292-95.

(48) Borjas, R.; Buttry, D. A. *J. Electroanal. Chem.* 1990, 280, 73-90.

(49) Ostrom, G. S.; Buttry, D. A. *J. Electroanal. Chem.* 1989, 256, 411-31

(50) a) Watkins, B. F.; Behling, J. R.; Kariv, E.; Miller, L. L. *J. Am. Chem. Soc.* 1975, 97, 3549-. b) Firth, B. E.; Miller, L. L.; Mitani, M. Rogers, T. *J. Am. Chem. Soc.* 1976, 98, 8271-2.

(51) Evans, J. F.; Kuwana, T.; Henne, M. T.; Royer, G. P. *J. Electroanal. Chem.* 1977, 80, 409-16.

(52) Tse, D. C. S.; Kuwana, T.; Royer, G. J. *Electroanal. Chem.* 1979, 98, 345-53.

(53) a) Reid, E. E. *Organic Chemistry of Bivalent Sulfur, Vol I*; Chemical Publishing Co., Inc.: New York, 1958, p.32-35. b) Reid, E. E. *Organic Chemistry of Bivalent Sulfur, Vol V*; Chemical Publishing Co., Inc.: New York, 1958, p.33

(54) a) Kerr, J. B.; Miller, L.L.; Van De Mark, M. R. *J. Am. Chem. Soc.* 1980, 102, 3383-90. b) Varineau, P. T. Ph.D. Thesis, University of Wyoming, 1989.

(55) Marcus, Y. *Ion Solvation*; John Wiley & Sons Ltd; Chichester, 1985.

(56) Hogen-Esch, T. E.; Smid, J. *J. Am. Chem. Soc.* 1966, 88, 307-18.

(57) Kaifer, A. E.; Bard, A. J. *J. Phys. Chem.* 1985, 89, 4876-80.

(58) a) Matsuda, H.; Aoki, K. Tokuda, K. *J. Electroanal. Chem.* 1987, 217, 1-13. b) Matsuda, H.; Aoki, K. Tokuda, K. *J. Electroanal. Chem.* 1987, 217, 15-32.

(59) Kobayashi, K.; Fujisaki, F.; Yoshimine, T.; Niki, K. *Bull. Chem. Soc. Jpn.* 1986, 59, 3715-22.

(60) Brown, A. P.; Anson, F. C. *Anal. Chem.* 1977, 49, 1589-95.

(61) a) Nagamura, T.; Sakai, K.; Ogawa, T. *J. Chem. Soc., Chem. Commun.* 1988, 1035-37. b) Nagamura, T.; Sakai, K.; Ogawa, T. *Thin Solid Films* 1989, 179, 375-80.

(62) a) Nagamura, T.; Sakai, K. *Chem. Phys. Lett.* 1987, 141, 553-57. b) Nagamura, T.; Sakai, K. *Ber. Bunsen.-Ges. Phys. Chem.* 1988, 92, 707-10. c) Nagamura, T.; Sakai, K. *J. Chem. Soc., Faraday Trans.* 1988, 84, 3529-37.

(63) Prasad, D. R.; Hoffman, M. Z. *J. Phys. Chem.* 1984, 88, 5660-65.

(64) Feldberg, S. private communication.

(65) Andrieux, C. P.; Saveant, J. M. *J. Electroanal. Chem.* 1978, 93, 163-68.

(66) Faulkner, L. In *Chemical and Engineering News*; Heylin, M., Ed.; American Chemical Society; Washington, D.C., 1984; p.28-45.

(67) Murray, R. W.; Rocklin, R. D. *J. Phys. Chem.* 1981, 85, 2104-12.

(68) Yeager, E.; Scherson, D. In *Proceedings of the Symposium on Electrocatalysis*; O'Grady, W. E., Ross, P. N. Jr., Will, F. G., Eds.; The Electrochemical Society, Inc.; Pennington, New Jersey, 1982; p.1-14.

(69) a) Steckhan, E.; Kuwana, T. *Ber. Bunsenges. Phys. Chem.* 1974, 78, 253-259. b) Land, E. J.; Swallow, A. J. *Ber. Bunsenges. Phys. Chem.* 1975, 79, 436-437. c) Lewis, N. S.; Wrighton, M. S. *Science* 1981, 211, 944-947.

(70) Ito, M.; Kuwana, T. *J. Electroanal. Chem.* 1971, 32, 415-425 and references therein.

(71) a) Heineman, W. R.; Kuwana, T.; Hartzell, C. R. *Biochem. Biophys. Res. Comm.* 1972, 49, 1-8. b) Heineman, W. R.; Kuwana, T.; Hartzell, C. R. *Biochem. Biophys. Res. Comm.* 1973, 50, 892-900.

(72) Solomun, T.; Christmann, K.; Baumgärtel, H. *J. Phys. Chem.* 1989, 93, 7199-208.

(73) a) Kaifer, A. E.; Bard, A. J. *J. Phys. Chem.* 1985, 89, 4876-80. b) Kaifer, A. E. *J. Am. Chem. Soc.* 1986, 108, 6837-38.

(74) a) Meyer, T. J.; Taube, H. *Inorg. Chem.* 1968, 7, 2369-79. b) Stranks, D. R. *Disc. Faraday Soc.* 1960, 29, 73-79.